PHASE DISTORTION IN ENVELOPE ELIMINATION AND RESTORATION RADIO FREQUENCY POWER AMPLIFIERS

A Thesis
Presented to
The Academic Faculty

by

Pavlo Fedorenko

In Partial Fulfillment
of the Requirements for the Degree
Doctor of Philosophy in the
School of Electrical and Computer Engineering

Georgia Institute of Technology
August 2009

PHASE DISTORTION IN ENVELOPE ELIMINATION AND RESTORATION RADIO FREQUENCY POWER AMPLIFIERS

Approved by:

Professor John Papapolymerou,
Committee Chair
School of Electrical and Computer
Engineering
Georgia Institute of Technology

Professor J. Stevenson Kenney,
Advisor
School of Electrical and Computer
Engineering
Georgia Institute of Technology

Professor W. Marshall Leach
School of Electrical and Computer
Engineering
Georgia Institute of Technology

Professor Alan Doolittle
School of Electrical and Computer
Engineering
Georgia Institute of Technology

Dr. Douglas Teeter
Boston Design Center
RF Micro Devices

Date Approved: 19 June 2009

ACKNOWLEDGEMENTS

This work would not have been possible without the support of many people. While I cannot possibly list all of them on this page, I am very grateful to every one of them and want to express my appreciation for their help over the years.

First and foremost, I would like to thank my advisor and mentor Dr. J. Stevenson Kenney. Dr. Kenney patiently supported and guided me through my graduate studies. He ensured my professional development, and at the same time contributed to my growth as a person by profoundly solidifying the spirit of freedom, honesty, open collaboration and the utmost ethical behavior.

I am thankful to Dr. Doug Teeter and Fred Schindler for their ongoing research advice and mentorship over the last years. I would also like to thank Ginny Lacquio, Wilfer Hernandez, Susan Diola, Dave Widay, Nhak Chea and RFMD Corporation, who made this research possible. It has been an honor and a pleasure to work with RFMD on both research and production challenges.

My deep gratitude is extended to my families, both in Ukraine and in the United States. I owe much of my success to my parents, Borys and Galyna Fedorenko, who have instilled in me the desire to learn, help others and be the best person I can be.

Finally I would like to thank all of my friends, who stood by me in success and in failure. They have always ensured that while growing up, we never lost our easy-going spirit or took ourselves too seriously.

TABLE OF CONTENTS

LIST OF TABLES

LIST OF FIGURES

SUMMARY

The objective of this research is to analyze and improve linearity of envelope elimination and restoration (EER) radio frequency (RF) power amplifiers. Envelope elimination and restoration was compared to other efficiency enhancement techniques and determined to likely be the most suitable solution for implementation of multimode, multiband portable RF transmitters. Distortion, stemming from dynamic power-supply modulation of RF transistors in EER RF power amplifiers was identified as one of the key challenges to the development of commercially viable EER transmitters. This dissertation presents a study of phase distortion in RF power amplifiers (PAs) with emphasis on identification of the origins of phase distortion in EER RF power amplifiers. Circuit-level techniques for distortion mitigation are also presented.

Memory effects in conventional power amplifiers are investigated through the accurate measurement and analysis of phase asymmetry of out-of-band distortion components. Novel physically-based power amplifier model is developed for attributing measured memory effects to their physical origin. The amount of linearity correction, obtained through pre-distortion for a particular RF power amplifier, is then correlated to the behavior of the memory effects in the corresponding PA.

Heterojunction field-effect transistor and heterojunction bipolar transistor amplifiers are used for investigation of voltage-dependent phase distortion in handset EER RF PAs. The distortion is found to stem from vector addition of signals, generated in nonlinear circuit elements of the PA. Specifically, nonlinear base-collector capacitance and downconversion of distortion components from second harmonic frequency are

found to be the dominant sources of phase distortion.

Shorting of second harmonic is proposed as a way to reduce the distortion contribution of the downconverted signal. Phase distortion is reduced by 50%, however a slight degradation in the amplitude distortion is observed. Push-pull architecture is proposed for EER RF power amplifiers to cancel distortion components, generated in the nonlinear base-collector capacitance. Push-pull implementation enables a 67% reduction in phase distortion, accompanied by a 1-2 dB reduction in amplitude distortion in EER RF power amplifiers.

This work, combined with other studies in the field, will help advance the development of multimode, multiband portable RF transmitters, based on the envelope elimination and restoration architecture.

CHAPTER I

INTRODUCTION

It is impossible to imagine our everyday life without communication systems. Television and radio, cellular telephones and wireless internet changed our lives forever. Today, information flows more freely around the globe than ever before. Economies of scale and ongoing cost reduction of communication systems ensure that even the poorest regions of the world have access to the modern communication technology.

Significant decrease in form factor and cost, that enabled rapid and ubiquitous adoption of communication systems around the world, has been primarily achieved by continuous introduction of digital circuitry into communication systems. By replacing more and more analog and RF components that do not scale with Moore's law with digital circuits, engineers put communication technology on track to achieve higher performance with lower cost through integration [49].

Currently, RF power amplifiers pose the biggest challenge to even greater cost reduction and integration of the entire transmit chain. In addition to complicating integration, RF PAs are widely known to be responsible for the majority of power consumption in communication systems [56]. High power consumption of RF PAs can be explained by two factors: high RF output power required to ensure large spatial coverage of the RF system, and low PA efficiency due to significant linearity constraints. While nothing can be done to decrease requirements for high RF signal power at the antenna port, increasing efficiency of the RF PA is an ongoing research task both in academia and in industry.

In stationary systems, such as cellular base stations, low efficiency of RF PAs increases thermal stress and decreases systems' time to failure due to the large amount

of dissipated heat. Despite high penalties incurred for inefficient RF PAs in the stationary systems, battery-powered mobile devices suffer the most from the PAs' high power consumption. Inefficient operation of RF PAs greatly reduces battery life of cellular telephones and other handheld communication devices, which translates into shorter talk times and limited personal mobility.

1.1 Efficiency of RF Power Amplifiers

One of the most fundamental reasons for inefficient operation of linear RF power amplifiers lies in the fact that the supply voltage is kept at a constant level, whereas the signal envelope is varied. To avoid signal clipping and therefore the loss of information, the following condition needs to be true

$$V_{supply}(t) \geqslant V_{envelope}(t). \tag{1}$$

To comply with condition (1), voltage supply is set to the peak of the RF envelope. As can be seen in Figure 1(a), the white area between the power supply and the envelope of the RF signal represents the energy wasted as heat in the DC-to-RF conversion. This concept is nearly identical to that used for calculating efficiency in linear analog amplifiers [30].

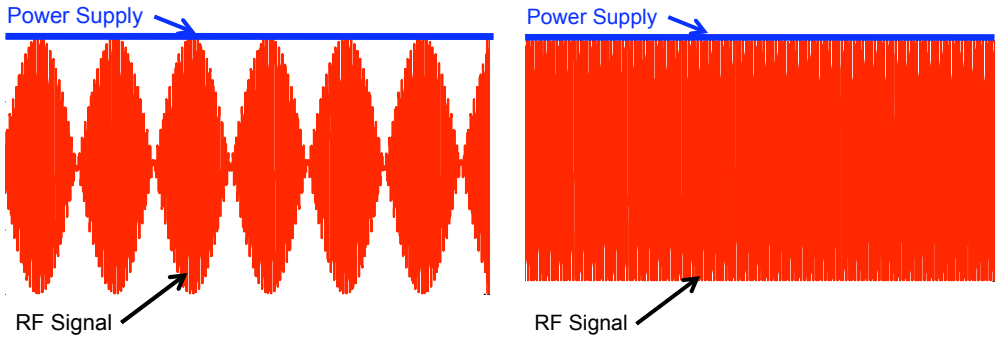

(a) Variable envelope RF signal. (b) Constant envelope RF signal.

Figure 1: Constant and variable envelope RF signals shown with constant power supply voltage.

One way to increase power efficiency of RF PAs is to use signals with information encoded in phase, not amplitude. This way any distortion applied to the amplitude of the signal will not degrade the quality of transmission. Constant-envelope signals enable power amplifiers to transfer significantly larger portion of DC energy to the RF signal. As can be seen in Figure 1(b), there is barely any white area between the power supply and the RF signal, therefore much less energy is wasted as heat.

Global system for mobile communications (GSM) is one of the ubiquitous standards employing constant envelope signals [57]. Encoding information purely into phase enables the signal to have peak-to-average power ratio (PAPR) of 0 dB. This, in turn, allows the use of deeply compressed power amplifiers in the transmit chain, resulting in significantly higher efficiency.

Due to substantial license costs and general crowding of the RF spectrum, there is continuous pressure to transmit more information using limited bandwidth. To achieve this task, information is encoded in both phase and amplitude of the signal. As a result, peak-to-average power ratio increases due to the trade-off between spectral and power efficiency. For example, modern modulation schemes, such as the worldwide interoperability for microwave access (WiMAX) standard, employ signals with high PAPR to enhance spectral efficiency for high-speed data transmission [15]. The use of signals with high peak-to-average power ratio, combined with stringent linearity requirements, in the form of adjacent channel power ratio (ACPR) or error-vector magnitude (EVM), results in low power amplifier efficiency, since PAs have to be operated at a significant power back-off from 1 dB compression point (P1dB) to meet the linearity requirements.

Table 1 shows a comparison of commercially available power amplifiers for GSM, wideband code division multiple access (WCDMA) and WiMAX technologies. The data was compiled using datasheets from RFMD, Triquint and Anadigics [3, 4, 58–60, 72]. All the amplifiers used for calculating the data in the table are implemented in

class AB architecture. Peak-to-average power ratios for WCDMA and WiMax signals are calculated using 0.1% point of complementary cumulative distribution function (CCDF). Peak power consumption levels are calculated. It should be noted that the average power consumption of the GSM system is significantly lower than the one quoted, because of time-division multiplexing used in GSM transmitters. In reality GSM transmitters are off for a significant porting of the frame, therefore output power averaged over time is significantly lower than the one quoted in Table 1.

Table 1: Industry averages of power amplifier efficiency under different signals of operation.

	GSM	WCDMA	WiMAX
Peak power consumption	6 W	1.5 W	1.6 W
Peak power dissipation	2.7 W	0.8 W	1.3 W
Peak RF power output	3.3 W	0.7 W	0.3 W
PA efficiency	55%	40%	15%
PAPR of test signals	0 dB	3.2 dB	8 dB

As can be seen from the table, regardless of the required output RF power, PA efficiency is inversely proportional to the peak-to-average power ratio of the transmitted signal. It can also be noted that as spectral efficiency of wireless standards continues to increase with time, power efficiency of commercial amplifiers implemented in regular class AB architecture will continue to fall.

1.1.1 Average Output Power

Efficiency problems posed by signals with high PAPR are exacerbated by the fact that very few power amplifiers are operated at their peak output power. For most mobile systems power control is utilized to ensure equal power level of signals arriving at the basestation from all mobile devices. In many standards the output power of the PA has to be adjusted over the range of well over 50 dB [12]. Since in urban environments the density of basestations is quite high, the majority of cell-phones

spend most of their time transmitting far below their peak power capability. As can be seen from Figure 2, the average transmit power for both urban and suburban environments for the WCDMA standard is around +5 dBm, whereas the peak power is around +27 dBm [68, 71]. Due to lower average output power, average and peak efficiencies of RF power amplifiers operating in real-world environments can be drastically different [64].

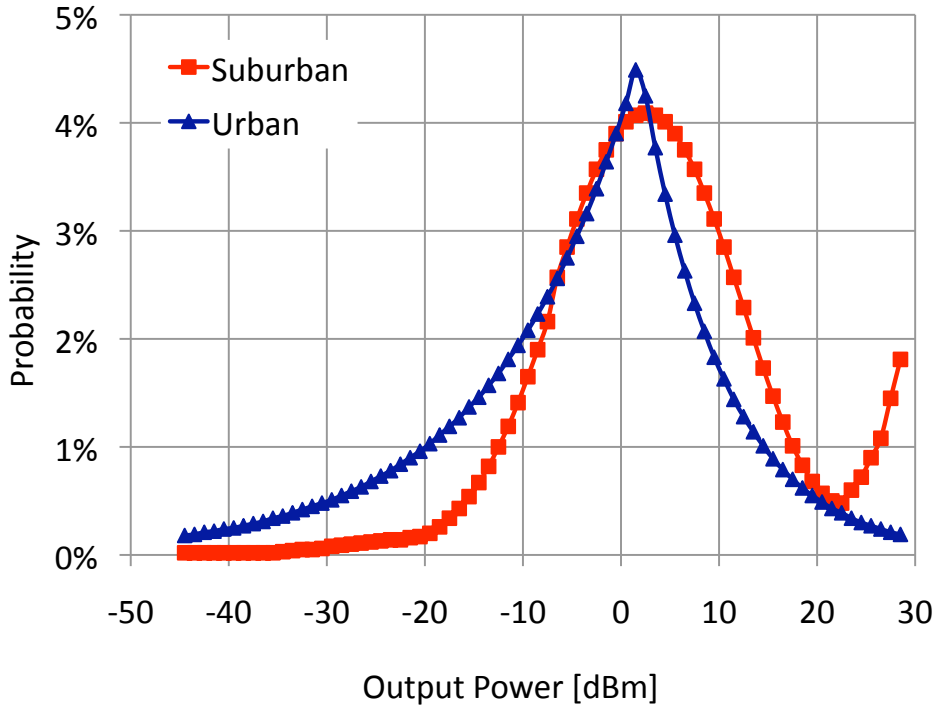

Figure 2: CDMA probability distribution function used in [71].

1.2 Efficiency Enhacement Techniques

To improve average efficiency of RF power amplifiers, a number of efficiency-enhancement techniques have been proposed over the years. Several techniques, such as reduced conduction angle, stage bypassing, Doherty, Chireix outphasing and polar modulation are briefly described in this section [18]. There are numerous variations of these techniques and we are only going to outline the basics here along with their advantages and drawbacks.

1.2.1 Reduced Conduction Angle Amplifiers

High quiescent current significantly contributes to degradation of amplifier efficiency. Therefore it is not surprising that reduction of quiescent current has been explored since the early days of RF engineering. Under class A operation quiescent current is set to half of the amplifier's peak current. This arrangement ensures excellent linearity and gain, even with small input signals. However, high quiescent current makes class A amplifiers very inefficient.

Classes AB, B and C were developed to reduce quiescent current of the amplifier through reduction of the PA's conduction angle. Basic principle of operation of amplifiers with reduced conduction angle can be described by using a typical RF PA schematic, shown in Figure 3, in conjunction with simplified current and voltage waveforms occurring in class B amplifiers (Figure 4).

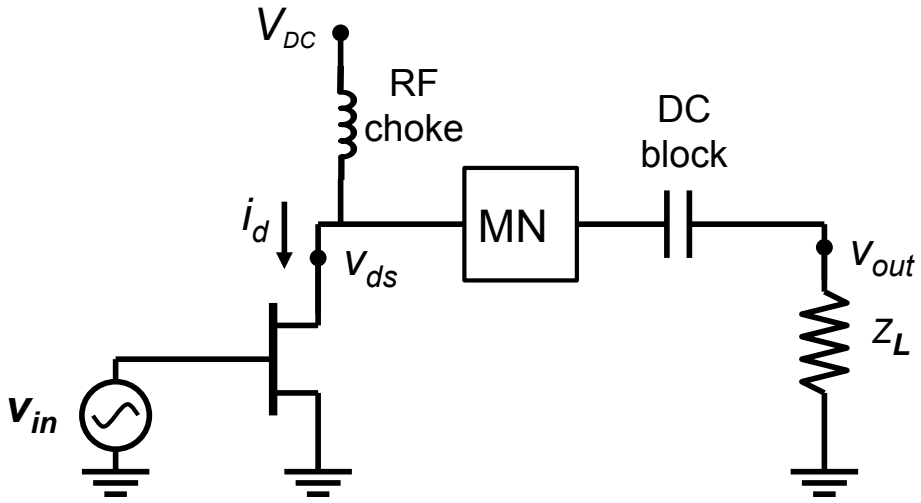

Figure 3: Circuit for PA waveform analysis.

Gate of a class B amplifier is biased at the threshold voltage of the transistor, which for simplicity is set to 0 V in Figure 4. Biasing the gate at v_t sets quiescent bias of the PA (I_q) to zero. When an RF signal (v_{in}) is applied to the gate of the amplifier, current I_d flows in the transistor for every input of $v_{in} > V_t$. Thus, the

drain current in the transistor becomes a half-wave rectified sinusoid for a sinusoidal RF signal applied to the gate, biased at V_t.

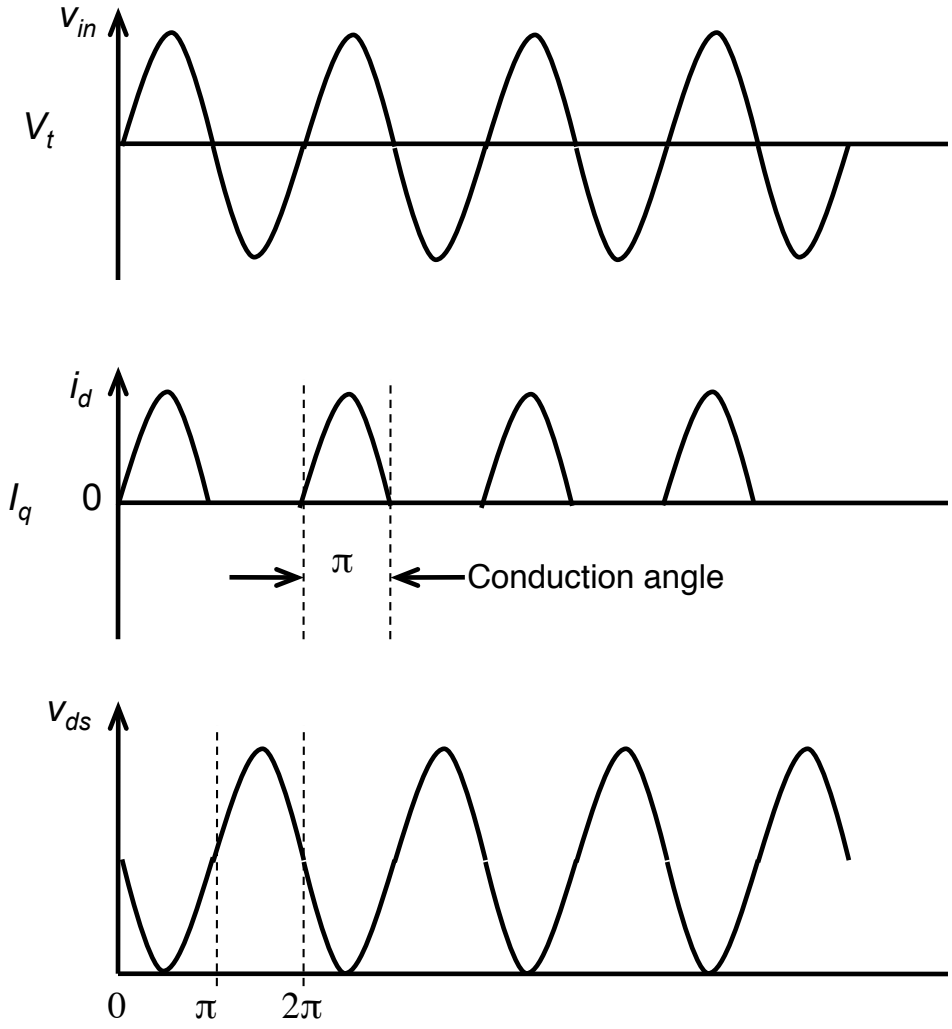

Figure 4: Reduced conduction angle wavforms. Class B operation.

In the absence of a harmonic trap introduced by the matching network, drain current waveform, shown in Figure 4, would induce an output voltage V_{out} across Z_L, rectified in the same manner as i_d. However, if one makes an assumption that the matching network is a high-Q resonator tuned to the frequency of operation, it can be stated that all harmonic currents are eliminated. As a result, only the fundamental component of the rectified drain current waveform is presented to the load. Therefore

the output voltage waveform of the class B amplifier is ideally an unclipped sinusoid.

The magnitude of the conduction angle is determined by the portion of the cycle of the current waveform flowing through the drain of the transistor. Full cycle of current flows in class A amplifiers, thus their angle of conduction is considered to be 2π radians. In the case of the PA operating in class B, drain current flows in the PA only during half of the cycle. Corresponding conduction angle is therefore π radians. Conduction angles for linear amplifier classes are summarized in Table 2.

Table 2: Classes of linear PA operation and their corresponding conduction angles.

Class of operation	Conduction angle range
A	2π
AB	$2\pi > \alpha > \pi$
B	π
C	$\pi > \alpha$

The main advantage of reduced conduction angle amplifiers is in their lower quiescent current and therefore higher efficiency. Class B amplifier, for example, can achieve theoretical efficiency of up to 78.5%, whereas maximum theoretical efficiency of a class A amplifier is only 50%. Class C amplifier theoretically delivers even higher efficiency, however the output power is significantly reduced. There are several other drawbacks as well. Presence of a strong RF input signal is necessary to turn on amplifiers biased in classes B or C. Thus amplification of small signals is primarily relegated to class A amplifiers. The biggest drawback of using amplifiers biased at lower conduction angles lies in the significant degradation of linearity due to growing harmonic content, as the conduction angle is reduced [18]. In addition amplifiers relying on reduced conduction angle for efficiency enhancement can achieve good efficiency only with full swing of output voltage. That efficiency drops quickly as the amplifier enters back-off.

1.2.2 Stage Bypassing and Parallel Amplification

As mentioned in Section 1.1.1 the majority of handset power amplifiers operate well below their peak power most of the time. To reduce power consumption many commercial power amplifiers have high- and low-power modes of operation. These modes are typically digitally controlled and can be achieved by adjustment of current or voltage bias, as in [71].

Complete bypassing of one of the stages can also be used to reduce power consumption when the amplifier is operating in the low power mode [51]. Output stages of power amplifiers tend to be more nonlinear than first or second stages of signal amplification due to attempts to increase their efficiency. Therefore when the output stage is bypassed, the linearity of the amplifier tends to improve, since now the load is driven by a more linear stage. Efficiency is also significantly increased. However, extra matching networks need to be implemented to properly match second stage of the PA to the load, which is normally driven by the final stage with significantly lower output impedance. Also, additional power is lost in RF switches, needed to bypass the output stage.

Another approach to reducing average power consumption involves operating several transistors in parallel and turning some of them off when entering low-power mode. Two transistors are typically used in the parallel architecture [35]. However this number can be increased to provide better power control and eventually construct a PA based on the architecture used in digital-to-analog converters (DACs) [66]. Biggest challenge in realizing parallel architectures lies in combining RF signals at the output of the power amplifiers. Elimination of one of the parallel amplifiers changes load impedance seen by the rest of the PAs and detunes the circuit, resulting in the loss of output power. Power combiner losses also need to be taken into account.

Overall parallel amplification and stage bypassing are quite mature technologies

and are incorporated into some commercial products. Unfortunately, efficiency enhancement provided by these techniques is limited.

1.2.3 Doherty Technique

Doherty technique was originally developed in the 1930s for increasing efficiency of vacuum tubes in multi-kilowatt broadcasting stations [22]. Doherty amplifiers consist of a main and a peaking amplifier, as can be seen in Figure 5. The main amplifier is usually biased in class AB, whereas the peaking amplifier is biased in class C. During normal operation at lower output power only the main amplifier is on. However, as the input power increases, the peaking amplifier biased in class C turns on to provide extra power.

The amplifiers are connected with a network of quarter-wavelength ($\lambda/4$) transmission lines for impedance transformation. The $\lambda/4$ transformer at the output provides seamless modulation of the load impedance seen by the main power amplifier as the peaking amplifier turns on and off.

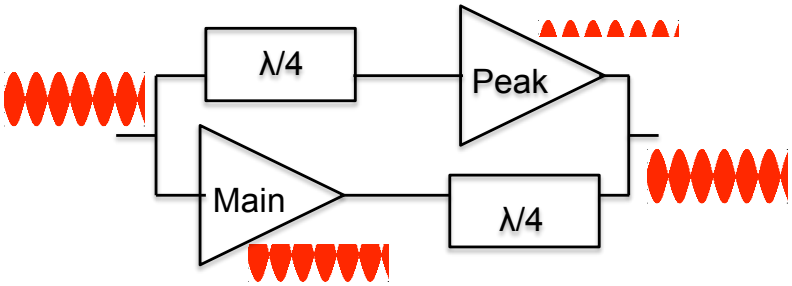

Figure 5: Diagram of a Doherty RF power amplifier.

Currently, Doherty is the most commonly used efficiency-enhancement technique for base station amplifiers due to its relative simplicity. However, quarter-wavelength lines at low gigahertz frequencies employed in cellular transmission are several centimeters long. While not a hurdle for base station amplifiers, these transmission lines

make the design less compact, and therefore are not well-suited for handset PA applications. Recent works have addressed some of these shortcomings by implementing transmission lines in lumped components [50]. Despite recent advancements, Doherty technique provides only a modest increase in power amplifier efficiency, and is usually relegated to basestation applications.

1.2.4 Chireix Outphasing

As described in Section 1.1, greatest efficiency is achieved when constant envelope waveforms are amplified by compressed PAs. This principle is used in Chireix outphasing, where signals with constant envelope and variable phase are efficiently amplified by saturated PAs [17]. Chireix combiner then adds these signals as vectors at the output of the PA, thus producing a waveform of variable amplitude.

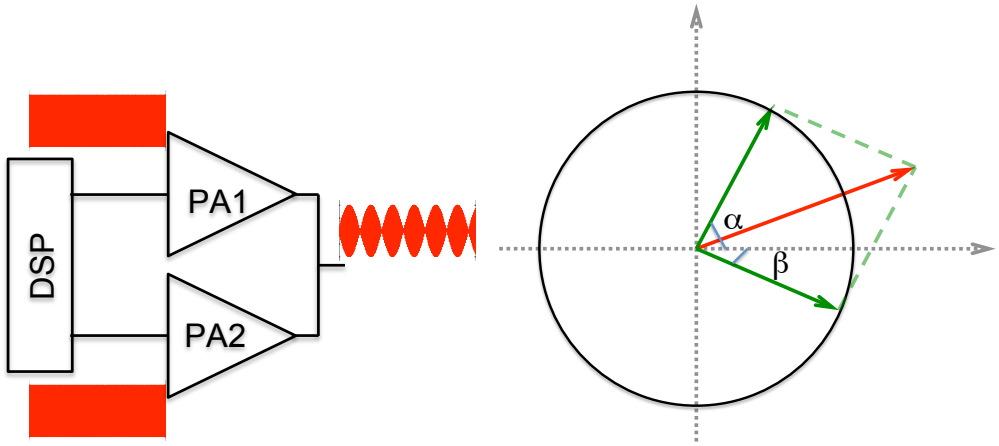

(a) Diagram of a Chireix outphasing RF power amplifier.

(b) Principle of operation.

Figure 6: Chireix outphasing RF power amplifier and basic principle of operation.

The basic principle of operation of Chireix amplifiers can be illustrated with the help of Figure 6. Two green vectors of unit length in Figure 6(b) represent constant-envelope input signals of different phase applied to the power amplifiers, as can be seen in Figure 6(a). The signals are then added to produce the red vector of different

amplitude. By varying phase difference between two constant-envelope input signals, one can obtain an output signal with varying envelope.

Because Chireix combiner does not isolate one amplifier from the other, load impedance seen by each amplifier varies with varying outphasing angle. This property greatly improves low output power efficiency of Chireix amplifiers, since the bias current is significantly lowered as the outphasing angle approaches 180°.

The biggest challenge in implementation of Chireix amplifiers lies in overcoming amplitude and phase mismatch between the two branches. Chireix combiner is also often realized with quarter-wavelength lines, which makes it less viable for implementation in portable devices. It has been demonstrated, however, that despite many problems, it is possible to design a viable high efficiency Chireix amplifier for WLAN applications [31].

1.2.5 Polar Modulation and its Varieties

Polar modulation is a concept, in which power supply of a power amplifier is modulated with the envelope of the amplified signal [36]. Modulation of the power supply eliminates, or significantly reduces, the gaps between the supply and output signals with varying envelope, seen in Figure 1(a), thus significantly increasing efficiency. Theoretically, polar-modulated power amplifiers can achieve efficiency of up to 100%.

Originally introduced by Leonard Kahn in 1950s as a technique for efficient single-sideband amplitude modulation in radio broadcasting, this technique has been experiencing a revival with the development of cellular industry. A number of varieties of polar modulation has been developed over the years: envelope elimination and restoration (EER), also known as Kahn architecture, envelope tracking (ET), power tracking, etc. While we are not trying to give a comprehensive overview of all the flavors of polar modulation, we will briefly describe the main types and outline their advantages and disadvantages.

The original technique introduced by Kahn was dubbed envelope elimination and restoration for its use of an analog envelope detector and a limiter to eliminate the envelope from the input signal, and later restore it at the output by varying the PA's supply voltage. With advancements in digital technology, envelope detector and limiter have been replaced by a digital signal processor (DSP), which generates amplitude and phase waveforms from the in-phase/quadrature (I/Q) input signals. Given a typical baseband input signal of the form $I(t) + jQ(t)$, baseband envelope and phase waveforms can be calculated as follows:

$$Env(t) = \sqrt{I(t)^2 + Q(t)^2} \tag{2}$$

$$\phi(t) = \tan^{-1}\left(\frac{Q(t)}{I(t)}\right). \tag{3}$$

Amplitude signal $Env(t)$ is then fed to the envelope amplifier, whereas constant-amplitude phase signal $\phi(t)$ drives the gate of the RF PA, as can be seen in Figure 7. The RF PA, then needs to amplify only a constant-amplitude phase signal, thus nonlinear and highly-efficient compressed RF PA can be used for this application. The amplitude signal passed through the envelope amplifier modulates the drain of the RF PA, reconstructing the original input signal. As a result, linear amplification is achieved through the use of nonlinear and efficient components.

The advantages of EER lie in its ability to utilize nonlinear components for linear amplification. Efficiencies of up to 100% can theoretically be achieved with this architecture. However a number of drawbacks exist for this architecture. Both the amplitude and phase signals are generated with nonlinear operations. Thus the bandwidth of the original I/Q signal is significantly expanded in phase and envelope signal paths. Efficiency of the EER technique depends greatly on the efficiency of the envelope amplifier (EA). Since the overall system efficiency is now a product of the efficiencies of the envelope amplifier and the RF PA, degradation in the EA efficiency can offset any improvements in the efficiency of the RF PA. In addition to efficiency,

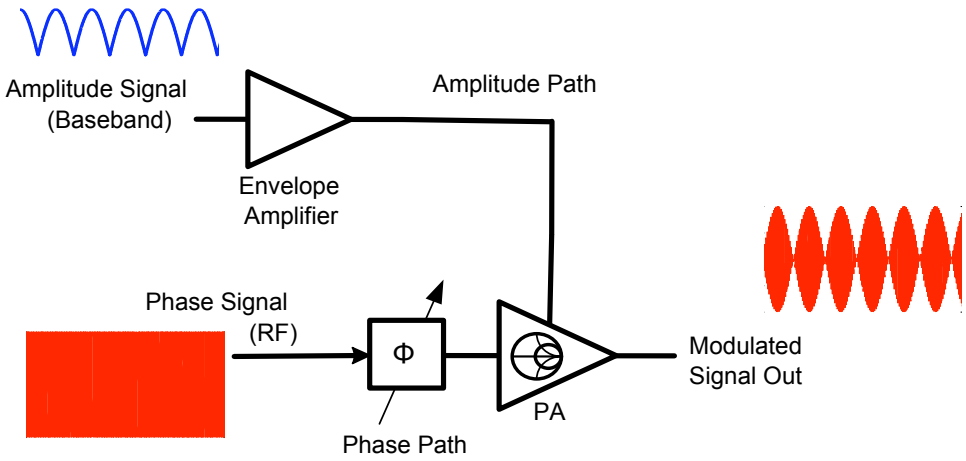

Figure 7: Polar modulator implemented as an EER power amplifier.

realizing a true EER system capable of amplifying signals with zero crossings has been problematic [18].

Implementation of an efficient envelope amplifier capable of fully tracking the entire envelope bandwidth has been quite challenging. To overcome this issue, envelope tracking (ET) technique is used. As in EER amplifiers, ET modulates the drain of the PA, however now the RF signal in the phase path is not hard-limited, but rather has full amplitude modulation [75]. A linear RF PA is then used for amplification, while its supply voltage follows the modulated waveform. Since both amplitude and phase information are already encoded in the RF signal, the bandwidth requirements on the envelope signal are not as stringent as those in the EER systems.Therefore bandwidth constraints of the envelope amplifier can be relaxed, resulting in higher efficiency, as long as the voltage at the drain of the amplifier does not drop below that of the envelope signal. While envelope tracking amplifiers are easier to implement than their EER counterparts, they provide smaller efficiency benefits. In addition, linear RF PAs need to be used with envelope tracking.

When neither EER nor ET can be implemented due to the envelope bandwidth limitations, power tracking can be utilized with relative ease. In power tracking, a

highly efficient direct current-to-direct current (DC-DC) converter or a linear regulator tracks the average power of the envelope at significantly lower speeds than the envelope bandwidth [13]. This approach offers even less efficiency improvement than ET or EER, but can be practically implemented in today's RF solutions.

Unlike Doherty and Chireix outphasing techniques, Kahn polar modulation technique does not have any theoretical limitations on its efficiency. In addition, no quarter-wavelength lines need to be used and a number of processing steps can be relegated to the digital circuitry. Kahn EER amplifiers are also seen as promising candidates for implementation of multi-mode multi-band RF transmitters [45]. Due to these reasons, EER power amplifiers have become the focus of research in the RF community in recent years. They are also viewed as the most practical solution for efficiency enhancement of handset RF power PAs. Even though Kahn polar modulation has no fundamental drawbacks that would limit its efficiency, a number of practical implementation issues must be overcome. These include maintaining high efficiency of the envelope amplifier over large bandwidths and achieving adequate linearity of the system by reducing or cancelling distortion arising from the modulating the supply voltage of RF transistors.

1.3 Linearization of Power Amplifiers

Increase in efficiency of RF power amplifiers often comes at a price of reduced linearity. To maintain acceptable linearity in the PAs designed for efficient mode of operation, several linearization techniques can be used.

When talking about linearity, feedback naturally comes to mind. The concept introduced in the beginning of the twentieth century by Harold Black has been used throughout analog circuitry ever since [8–10]. The frequency of RF signals, however, is too high to use systems with direct signal feedback due to the delay and stability issues. Even envelope feedback is not preferred, since the envelope bandwidth reaches

into megahertz frequencies in modern transmission standards.

The same group of patents and additions to them by Black describes reconstruction of the signal at the output node. This feedforward architecture can be successfully applied to RF power amplifiers [62, 63]. Commercially available feedforward systems provide good third-order intermodulation distortion (IMD3) correction. Another advantage of this approach is that the correction is applied almost instantaneously, and therefore feedforward systems are capable of correcting distortion resulting from memory effects. On the downside, feedforward systems need to use a number of extra components for combining signals at high power. An additional RF power amplifier is also needed, which reduces power efficiency and economic attractiveness of such systems [18]. Gain and phase of two paths require careful matching for precise cancellation. With development and cost reduction of digital signal processing feedforward architecture slowly gives way to pre-distortion solutions.

1.3.1 Pre-distortion of RF Power Amplifiers

Amplitude distortion in conventional power amplifiers usually takes a form of gain compression at high output power levels, as can be seen in Figure 8(b). This distortion can be approximated in its most basic form by a polynomial model:

$$z = a_0 + a_1 y + a_2 y^2 + a_3 y^3 \ldots . \tag{4}$$

Coefficients a_0, a_1, a_2, a_3 and so on can be complex to allow for modeling of both amplitude and phase transfer characteristics. Even order coefficients are not of much concern, since the distortion they produce shows up at even harmonics or baseband frequency, where it can be easily filtered out. Only odd-order terms contribute to distortion components near the fundamental. To eliminate distortion near the fundamental frequency one needs to eliminate lower odd-order terms of expression (4) due to their significant distortion contribution.

To eliminate odd-order distortion terms and achieve linear transfer function shown

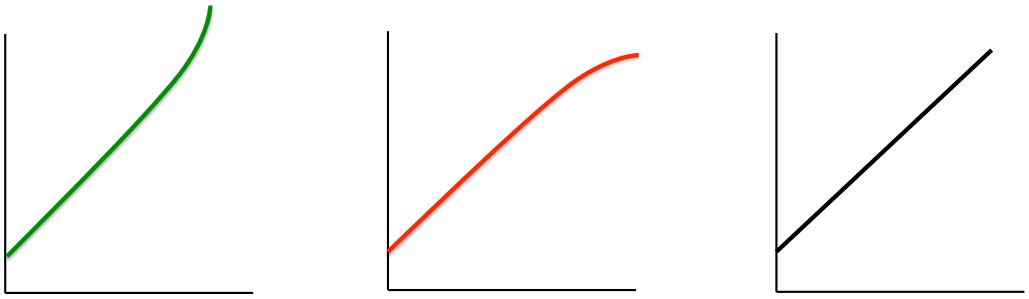

(a) A^{-1} pre-distortion function. (b) A PA transfer function. (c) $A(A^{-1})$ Combined linear transfer function.

Figure 8: Pre-distortion process.

in Figure 8(c), one can apply the inverse of the PA transfer characteristic, A, modeled by a polynomial in (4), to the input signal. Such transfer function A^{-1}, shown in Figure 8(a), is a direct inverse of A and can also be modeled as a complex polynomial:

$$y = b_0 + b_1 x + b_2 x^2 + b_3 x^3 \ldots . \tag{5}$$

Following the signal chain in Figure 9 from left to right, one can calculate the output of the system, z by plugging in (5) into (4). The output signal z is defined as follows:

$$\begin{aligned} z = c &+ (2a_2b_0b_1 + 3a_3b_0^2b_1 + a_1b_1)x + \\ &(a_1b_2 + a_2b_1^2 + 3a_3b_0b_1^2 + 2a_2b_0b_2 + 3a_3b_0^2b_2)x^2 + \\ &(6a_3b_0b_1b_2 + a_1b_3 + a_3b_1^3 + 2a_2b_1b_2 + 3a_3b_0^2b_3 + 2a_2b_0b_3)x^3 + \ldots \\ &\ldots + (a_3b_3^3)x^9, \end{aligned} \tag{6}$$

where c is a constant, and x^3 is the term to be eliminated to reduce third-order distortion at the fundamental frequency. Third-order coefficient of A^{-1}, b_3 can be chosen to eliminate x^3 term from Equation (6). One can see, that setting b_3 to

$$\frac{-b_1(6a_3b_0b_2 + a_3b_1^2 + 2a_2b_2)}{a_1 + 3a_3b_0^2 + 2a_2b_0}$$

will set the entire coefficient in front of x_3 to zero, thus eliminating third-order distortion components of the linearized system. It should also be noted from (6) that pre-distortion process necessarily introduces extra higher order polynomial terms, thus contributing to higher order distortion. This sometimes reduces PAs' ability to meet second adjacent channel power ratio specifications [18].

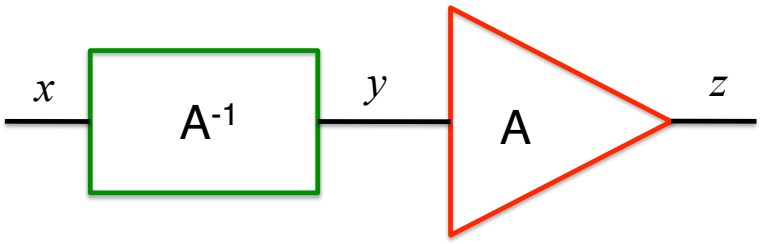

Figure 9: Concept of a pre-distortion system.

Pre-distortion linearization can be practically implemented using either analog [78], or digital [24] approach. Analog solutions tend to be cheaper and exhibit much lower power consumption, however their linearization capability is significantly lower than that of digital systems. Currently digital pre-distortion dominates basestation PA linearization market.

Inverse of PA transfer function, A^{-1}, is usually stored in the look-up table (LUT) in digital pre-distortion systems. This look-up table is updated over time as the PA transfer function changes with changing operating conditions. However if the PA transfer function, A, changes faster than the pre-distortion algorithm updates the look-up table, containing A^{-1}, linearity of the entire transmission system deteriorates. To linearize systems exhibiting memory effects, more complex memory pre-distortion is utilized by using several time-delayed look-up tables. The size of the look-up table depends on the nonlinearities exhibited by the PA, whereas the amount of memory taps (number of time-delayed look-up tables) and unit delay between them can be best optimized by knowing the nature of memory effects of a particular amplifier.

1.3.2 Memory Effects

Fast changes of power amplifier transfer function over time have been dubbed "memory effects", since the output of the amplifier no longer depends on the current input, but also on the previous inputs. Memory effects can be observed in measurements as amplitude-to-amplitude (AM-AM) and amplitude-to-phase (AM-PM) curves exhibiting hysteresis. In frequency domain, asymmetric amplitudes and phases of third-order intermodulation components are also indicative of memory effects [21]. Memory effects do not directly impact power amplifier linearity, instead they impact the linearity and complexity of transmission systems, employing pre-distortion linearization.

While memory effects in RF power amplifiers are still a topic of ongoing research, their origins have been identified to stem from three main sources: semiconductor trap effects, dynamic heating effects and baseband frequency response of bias networks. Semiconductor trap effects exhibit the largest time constants, often comparable to adaptation time of modern digital pre-distortion systems. Thermal memory effects, on the other hand, have lower time constants with significant variability. Generally only high power PAs are susceptible to thermal memory effects, with handset devices being largely immune. Thermal memory effects present considerable challenge to RF designers, since they cannot be eliminated through circuit techniques, and change PAs' transfer characteristic faster than standard memoryless pre-distortion algorithms can adapt the look-up table. Electrical memory effects occur due to imperfect termination of baseband currents in the PA bias networks. These memory effects have the shortest time constant and tend to be associated with narrowband resonances. These effects can be mitigated, or even completely eliminated, by careful design of bias networks.

Memory effects in RF power amplifiers are analyzed in detail in Chapter 3 of this dissertation as a way to build knowledge for analysis of phase distortion in EER RF power amplifiers in Chapters 4 and 5.

1.4 Thesis Organization

The thesis is organized as follows. Chapter 2 outlines motivation for development of envelope elimination and restoration amplifiers, challenges to their practical implementation, and reasons for in-depth understanding of phase distortion, occurring in EER RF PAs.

In Chapter 3 memory effects in conventional two-port power amplifiers are analyzed in detail. Specifically, asymmetric phase response of third-order intermodulation distortion components is studied. System for measurement of phase deviation of intermodulation components is developed. A physically-based behavioral model of RF PAs is proposed to identify origins of memory effects based on the measurements of relative IMD3 phase. Subsequently, the benefits of knowing the origins of memory effects for design of pre-distortion systems are demonstrated.

Chapter 4 first introduces the system used for measurement of phase distortion in EER RF power amplifiers. The distortion, occurring in the EER amplifier, based on a depletion-mode heterojunction field-effect transistor (HFET) is analyzed. Several hypotheses for sources of distortion are tried and eliminated by subsequent experiments. In addition, a simple circuit-level technique is proposed to reduce phase distortion in EER RF PAs. While this technique reduces phase distortion, amplitude distortion is modestly increased in the process, which limits the attractiveness of the proposed solution.

Chapter 5 builds on the research outlined in Chapter 4 to further investigate phase distortion in EER PAs. This time devices based on heterojunction bipolar transistor (HBT) technology are used for analysis. Nonlinear base-collector capacitance is identified as the primary source of phase distortion in HBT EER RF power amplifiers. Following this finding, a new push-pull EER architecture is proposed to reduce the impact of nonlinear C_{bc} on the overall system linearity. This architecture successfully mitigates both phase and amplitude distortion in the EER PA under test, and is

superior to the mitigation technique outlined in Chapter 4.

Lastly, the thesis is concluded in Chapter 6 with a summary of work performed and the key contributions of the work. Suggestions for future research, as it relates to further development of linear EER RF power amplifiers, are outlined in Section 6.4.

CHAPTER II

CHALLENGES IN PRACTICAL REALIZATION OF ENVELOPE ELIMINATION AND RESTORATION RF POWER AMPLIFIERS

2.1 Motivation

Undoubtedly efficiency enhancement, described in Section 1.2.5, is the primary driver for development of envelope elimination and restoration power amplifiers. EER architecture, however, offers a number of other practical advantages over standard class-AB PAs. EER amplifiers have been proposed for the use in software-defined radio systems (SDR) due to their potential of cost-effectively realizing multiband, multimode RF transmitters [45].

The need for multiband, multimode RF PAs increases as more and more mobile device users travel frequently around the world. Most of the people need cellular phone connectivity wherever they go; therefore the RF front end should be capable of operating in multiple cellular standards deployed worldwide. As the convergence of data and voice services continues, new RF front ends will have to support high data rate standards, such as WCDMA and WiMAX. At the same time new standards support legacy modes, such as code division multiple access (CDMA) and GSM, where high data rate coverage is not available [7]. The challenge outlined above can be potentially solved by an EER system, shown in Figure 10. In this system, a single wideband envelope amplifier can be controlled by a digital signal processor to apply the envelope of the digitally-selected modulation waveform to the drain of the RF transistor. If the envelope amplifier is implemented as a fast switching DC-DC converter, its bandwidth, and respectively efficiency, can be digitally controlled by

changing its switching speed. While digitally-controlled envelope amplifier can be used to achieve multimode operation with relative ease, multiple RF amplifiers are necessary to provide operation across several RF bands.

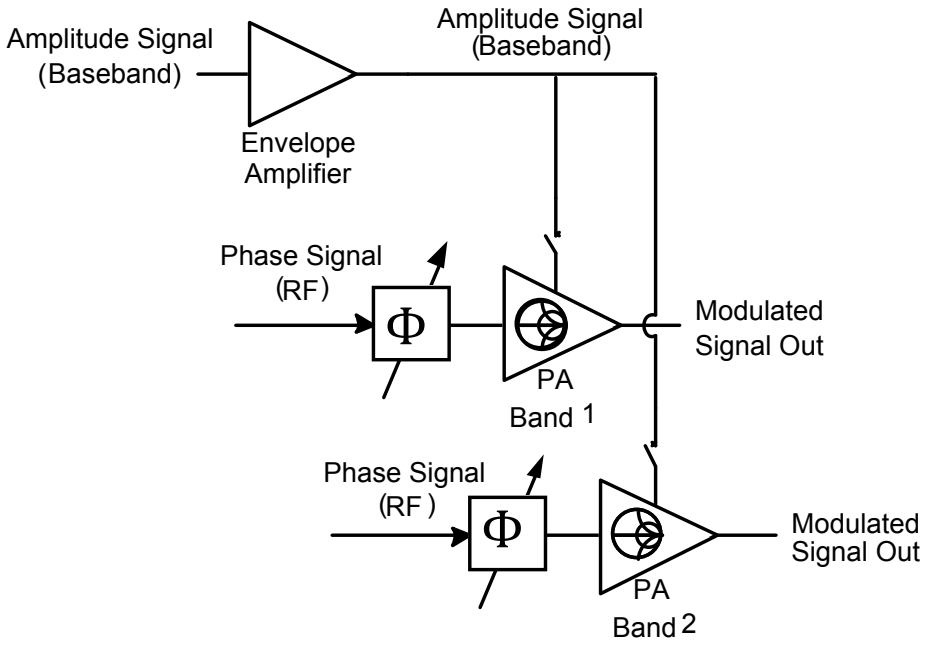

Figure 10: Multiband PA based on the EER architecture.

It has been noted in the literature that RF PAs, implemented as intentional ON/OFF switches, similar to the complementary metal-oxide semiconductors (CMOS), used in digital systems, can have minimal impact on the overall circuit performance [45]. This notion is very different from the operation of fully analog PAs that control output voltage, where the active device is responsible for determining the majority of RF performance. This shift is likely to enable multiband operation of RF transmitters with a single RF path, where a switching RF amplifier is used across multiple RF frequencies. While this approach sounds ideal, a number of fundamental drawbacks exist that will inhibit the development of multiband EER systems, based on a single RF transistor.

The biggest challenge to implementation of fully digital RF PAs comes from the

inability of true EER systems to accurately amplify wireless modulation signals that cross through zero, due to RF feedthrough. Another related challenge is the need for large power control range. Drain control cannot provide output power control well in excess of 50 dB required by some standards. While traditional EER architecture, where input RF signal power stays constant and drain level varies, are unable to meet these challenges with current technology, hybrid EER architecture can be used.

Hybrid EER operates as traditional EER architecture when the signal output power is large, and then switches to power-tracking when the required output power drops below the knee voltage of the RF device. When in the power-tracking mode, the input RF drive of the amplifier can be backed-off to control the output power, or present minimal distortion to signals with zero crossings. In addition to lower distortion, hybrid EER can achieve higher power-added efficiency than conventional EER at low output powers, due to the fact that strong RF drive will not be applied to the input of the device when only weak output is required.

2.2 Challenges in Realizing EER RF Power Amplifiers

To make multimode and multiband polar transmitters, shown in Figure 10, a reality, regardless of whether they are implemented as true EER, or hybrid EER architectures, a number of design challenges need to be overcome. An efficient envelope amplifier with sufficiently wide bandwidth and good linearity needs to be designed. Distortion arising from the delay mismatch between amplitude and phase paths needs to be minimized. Also, since most RF PAs, currently used in EER systems, were designed for operation under constant power supply, they tend to exhibit new types of distortion, previously not seen in conventional power amplifiers [27, 46]. Distortion, arising from modulating the drain of an RF PA, needs to be studied and mitigated to ensure low error-vector magnitude (EVM) and adjacent-channel power ratio (ACPR) required for complex transmission standards, such as WiMAX. All the major challenges for

practical realization of EER RF power amplifiers are outlined in Figure 11 along with the published papers, describing each particular area in detail.

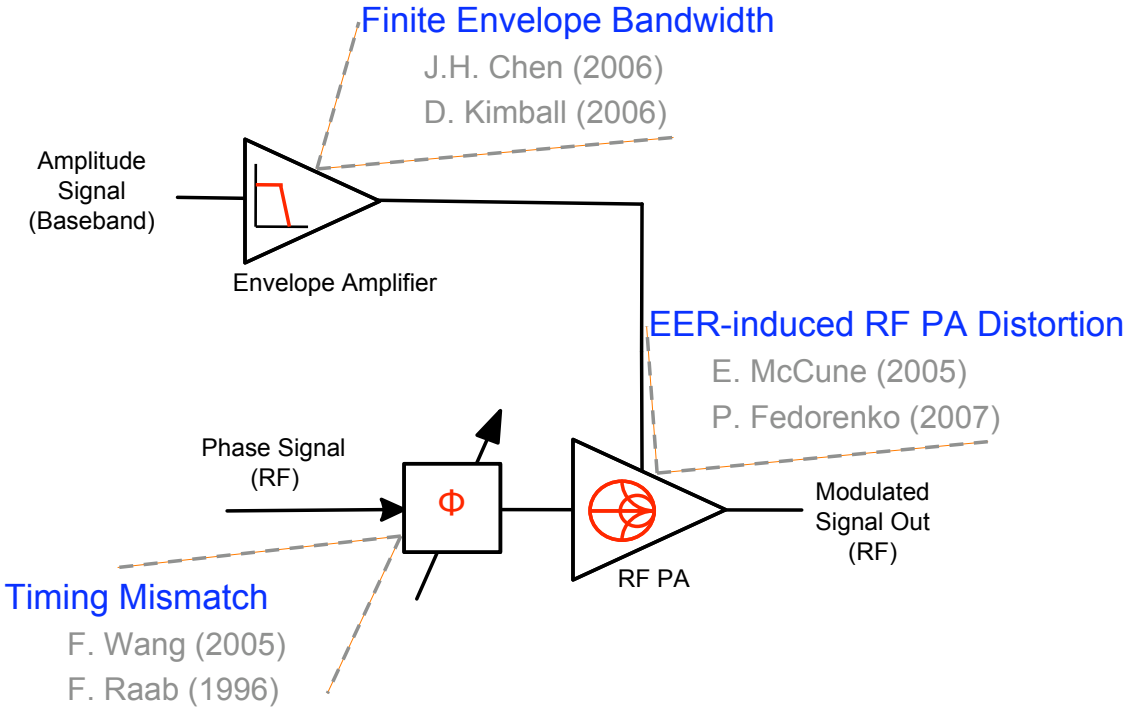

Figure 11: Challenges in practical implementation of EER systems [14, 27, 38, 46, 55, 76].

2.2.1 Efficiency and Bandwidth of the Envelope Amplifier

The design of an efficient wideband envelope amplifier has been the main practical obstacle to the widespread adoption of EER techniques [18]. In recent years several university research groups successfully developed practical wideband envelope amplifiers. It is likely that similar systems were developed in the industry as well, however due to the general corporate secrecy, these designs were never revealed to the public. One of the envelope amplifier designs recently developed in academia by Chen et. al relies on a high-speed power converter employing an efficient switcher. The switcher is driven by a pulse-width-modulated (PWM) signal and is followed by a band-pass filter [14]. This approach achieves power-added efficiency just shy of 50%, which is

a substantial improvement for handheld WCDMA amplifiers. In addition, the use of polyphase PWM switcher allows for better potential integration into software-defined radio systems, since the switcher's clock speed, and therefore, bandwidth can be digitally controlled.

Another approach for envelope amplifier implementation, developed by Kimball et. al, relies on a more complex hybrid architecture, where an efficient narrowband switcher supplies low frequency current component, whereas less efficient linear amplifier supplies the high-frequency current to the PA [38]. Since 85% of the power of the envelope waveform lies below 200 kHz, and can be amplified with an efficient switching modulator, the overall efficiency of this system with a WCDMA signal is reported to be at about 50%.

The bandwidth of the envelope amplifier is of the utmost importance, since the spectrum of the amplitude signal is several times that of the original I/Q signal. It has been mathematically proven that finite bandwidth of the envelope amplifier gives rise to significant intermodulation distortion products (IMDs) at the output of the system [55]. To date, pre-distortion has been used to mitigate distortion arising in the EER system from the finite bandwidth of the envelope amplifier [14].

Both approaches for envelope amplifier implementation show significant promise, however, more work remains to be done to realize a practical efficient wideband envelope amplifier for both handset and basestation systems.

2.2.2 Delay Mismatch of Amplitude and Phase Signals

Another source of fundamental distortion that arises in EER systems, and is agnostic to the implementation techniques, is the delay mismatch between amplitude and phase signals. The magnitude of the distortion signal, generated by the system due to delay mismatch, can be determined analytically [54, 55]. Delay mismatch presented significant challenge to classic EER systems, implemented fully in analog

domain with hard limiters and envelope detectors, since adaptive analog delays are quite challenging to realize. As analog limiters and detectors, used in classic EER systems, gave way to digital generation of envelope and phase signals, implementation of time delay became rather trivial. Simple digital delays are used in current EER implementations.

Delay estimation, however, remains a challenge for practical EER systems. In current university implementations, delay is adjusted off-line to the level, producing minimum distortion at the output of the system. While this type of calibration is adequate for research purposes, commercialization of products, relying on careful initial calibration can be quite challenging, especially as the delay mismatch varies over temperature and hours of operation. To solve this challenge, some form of signal feedback needs to be used to iteratively adjust the time delay. Stringent delay match criteria can also be somewhat relaxed by switching from EER to more forgiving envelope tracking or power tracking applications [76].

2.2.3 RF Transistor Distortion Induced by EER Operation

In addition to the technology-agnostic sources of distortion, such as finite bandwidth of the envelope amplifier and delay mismatch, distortion, occurring in the RF transistor itself, needs to be taken into account. Traditional two-port power amplifiers in the absence of memory effects are adequately characterized by AM-AM and AM-PM transfer functions. Because amplitude and phase signals are split into separate paths in EER (three-port) RF PAs, an additional metric of envelope-to-phase distortion needs to be introduced. Since these broad three metrics only describe the behavior of distortion, but not its origins, more work needs to be done to analyze the distortion arising in the RF transistor itself when used in the EER configuration. Several issues, unique to EER systems and not posing a problem for regular two-port amplifiers, such as RF carrier feedthrough, were raised in the literature [46]. However,

not many distortion mechanisms originating in RF transistors used for EER systems have been investigated in detail or widely published [47]. In fact, currently most of the RF transistors used in EER systems are off-the-shelf devices, originally designed and manufactured for use in conventional two-port power amplifiers.

To overcome transistor-specific distortion and deliver viable EER systems to the market, industry engineers utilize techniques such as pre-distortion and feedback. The open-loop polar system utilized in RF Micro Devices' (RFMD) Polaris® transceiver employs pre-distortion in the phase signal path to achieve acceptable performance for GSM signals [33, 34]. Skyworks Solutions' engineers employed a closed-loop architecture to mitigate phase and amplitude distortion of the system [67]. While these systems perform well with low-bandwidth and low-PAPR signals, they will necessarily run into problems with more complex standards, such as WiMAX. Non-discriminate distortion correction schemes are likely to have higher cost and power consumption overhead than those capable of distinguishing sources of distortion and treating them in the most efficient manner for a given distortion origin. The cost and power consumption of systems capable of indiscriminately treating distortion of demanding WiMAX signals might prove to be unrealistically high for a ubiquitous multimode mobile solution.

To advance the development of multiband mobile EER transmitters, we concentrated our research efforts on determining the root causes of distortion arising in the RF transistors when operated in the EER mode. Specifically, envelope-dependent phase rotation of out-of-band distortion products, resulting from operating RF PA with a rapidly varying drain voltage is examined [27]. This knowledge can be leveraged by others to develop more efficient pre-distortion algorithms for mobile EER PAs. Also, this research can serve as a starting point for the design of RF transistors, specifically geared for the use in three-port amplifiers.

Simple circuit techniques aimed at mitigating phase distortion in EER PAs are

also studied. The distortion-mitigating circuit techniques investigated during this study significantly reduce phase distortion in EER RF PAs. For some applications use of these techniques provides adequate linearity performance and therefore reduces the need for correcting the phase signal altogether. For other applications these techniques may reduce complexity of linearization systems employed.

2.3 In-band and Out-of-band Distortion Components

Distortion in all power amplifiers is commonly separated into in-band and out-of-band components, regardless of its physical origins. In-band distortion is often measured as error-vector magnitude. EVM is measured in either percent or decibels as the ratio between the error signal and the reference RF signal, as can be seen in Figure 12 and Equation (7). This distortion directly impacts quality of transmission and can be correlated to the bit-error rate (BER) for each wireless communication standard.

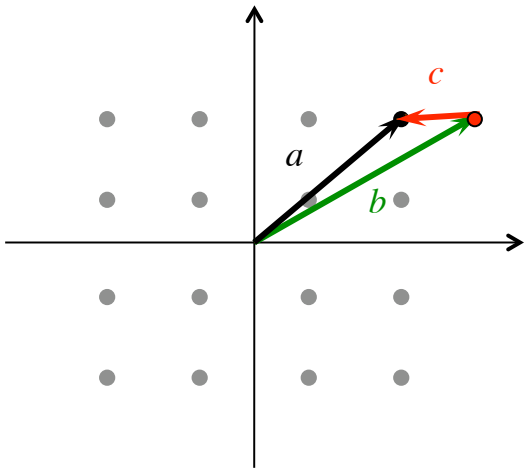

Figure 12: EVM for a specific point in a 16-QAM constellation.

$$EVM = \frac{|b-a|}{|a|} \times 100\% \tag{7}$$

Out-of-band distortion does not directly impact the quality of the transmitted signal. However, it significantly affects the quality of the signals, transmitted in the

neighboring channels. Federal Communications Commission (FCC) in the United States and respective regulatory bodies in other countries impose strict restrictions on out-of-band emissions of all transmitters. These emissions are usually measured in the amount of energy in the adjacent channel and the second adjacent channel, ACPR1 and ACPR2 respectively. A symbolic rendering of the signal spectrum with significant ACPR1 and ACPR2 is shown in Figure 13. The majority of RF energy in the first adjacent channel is caused by the third-order nonlinearity in the transmit chain. Fifth-order nonlinearity, in turn, is responsible for the majority of RF energy spilled into the second adjacent channel.

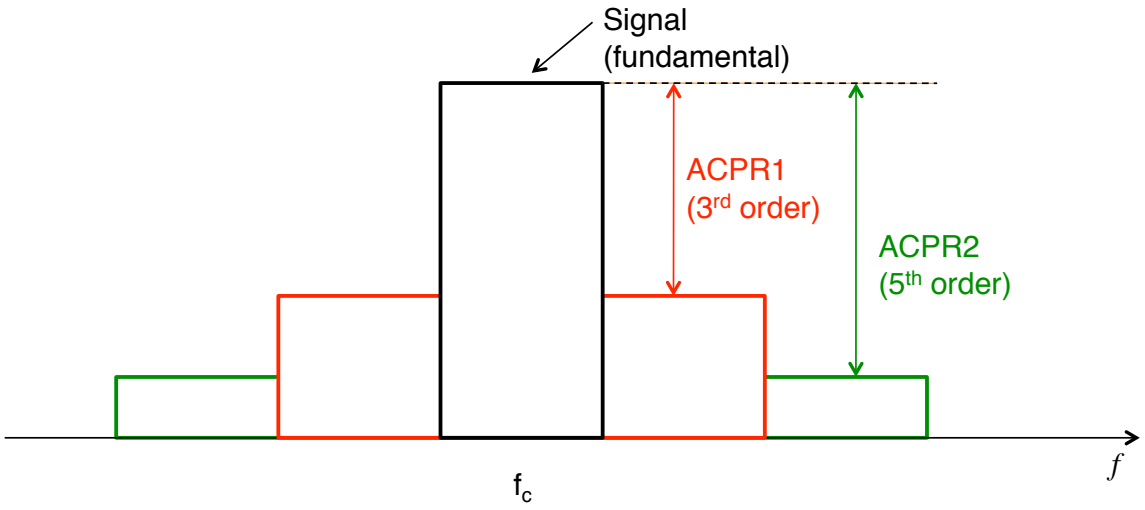

Figure 13: Magnitude of out-of-band distortion components.

To effectively measure out-of-band emissions of RF PAs without the use of complicated modulation schemes, two-tone sinusoidal signal is generally used. If a two-tone sinusoidal signal is used for testing linearity of RF PAs, intermodulation products are generated in the nonlinear transfer function of the PA. Third-order nonlinearities are primarily responsible for generation of third-order intermodulation products (IMD3), even though at high compression, higher odd-order nonlinearities significantly contribute to the size of IMD3. Similarly, fifth-order nonlinearities contribute

the majority of power to the fifth-order intermodulation products (IMD5). IMD3 for a two-tone signal is synonymous with ACPR1 in a system, employing complex modulation. IMD5 is related to ACPR2 in the same manner. The spectrum of fundamental tones, IMD3 and IMD5 can be seen in Figure 14. Conventionally, intermodulation components, just like adjacent channel power ratios (ACPR), are measured in decibels of power with respect to the carrier (dBc).

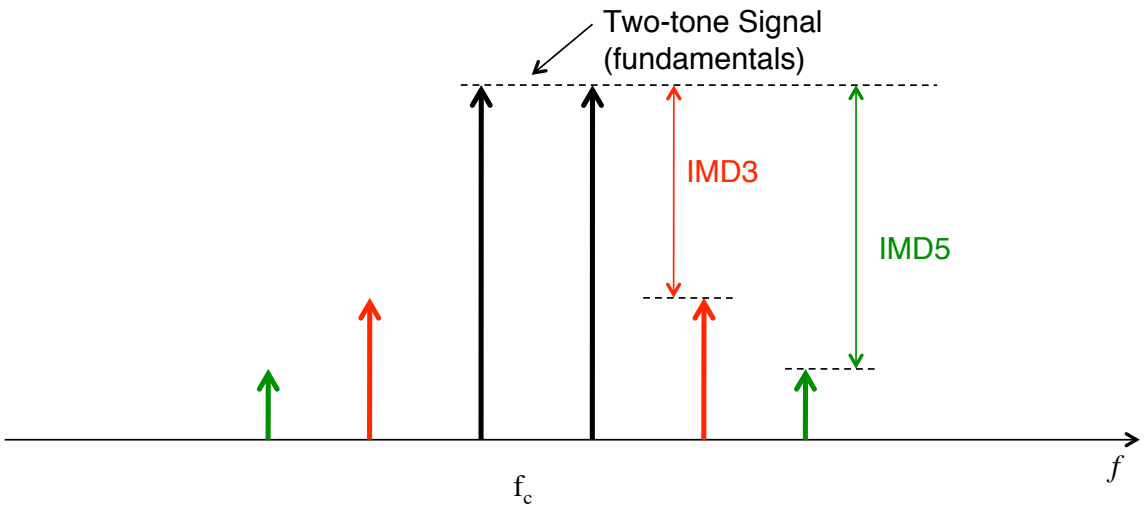

Figure 14: Spectrum of a two-tone test signal with out-of-band distortion components.

2.3.1 Intermodulation Vectors

Intermodulation components IMD3 and IMD5 appear as scalars in Figure 14. In fact, this is exactly how they are measured in the laboratory with the help of a spectrum analyzer. In reality, however, IMD components, just like fundamentals, are vectors with both phase and magnitude. Generally, in memoryless systems phase and magnitude of left and right intermodulation products are identical, and asymmetry is often caused by memory effects [21]. Even smaller distortion vectors, generated in various nonlinearities of the PA, are added together to form IMD3 or IMD5.

A number of studies was performed on analyzing relative contribution of each

distortion-generating mechanism. Maas reports 180° phase difference between the distortion components generated in the nonlinear current source of a heterojunction bipolar transistor (HBT), and those due to the nonlinear base-emitter capacitance [43]. Aikio and Rahkonen show that linear portions of device capacitances introduce a 90° to the already generated nonlinear distortion components [1, 2]. It is also well-known that signals at second harmonic frequency can mix down and add to the IMD3 vectors, generated purely by odd-order nonlinearities. Similar effect can happen when baseband components are up-converted in frequency. The phase of distortion components, appearing at the IMD3 frequency due to up- or down-conversion, greatly depends on their phase at their original frequency, which in turn, depends on the phase presented to the PA at that frequency by the matching networks. Thus it can be stated that the phase of distortion signals, generated in even-order nonlinearities and appearing at IMD3 frequency, is greatly dependent on the PA matching at even-order frequencies.

A lot more work needs to be done to analyze distortion-generating mechanisms in transistors, but the findings above enable us to construct a rudimentary picture of the main vector components affecting phase and magnitude of out-of-band distortion in RF transistors. Generalized structure of distortion vectors is shown in Figure 15.

Figure 15 should not be used as an absolute truth, but rather as a rough guide to the types of distortion contributing to the change of phase of intermodulation vectors. Real axis is arranged to point in the direction of fundamental signals. As can be seen from the distortion diagram, often individual distortion vectors are out of phase and can actually reduce the overall magnitude of the entire IMD vector when added. Maas, for example, attributes good linearity of HBTs to the distortion cancellation, occurring between signals generated in nonlinear g_m and nonlinear C_{be} [43]. Aikio and Rahkonen manipulate second harmonic termination to achieve better cancellation of intermodulation distortion [1].

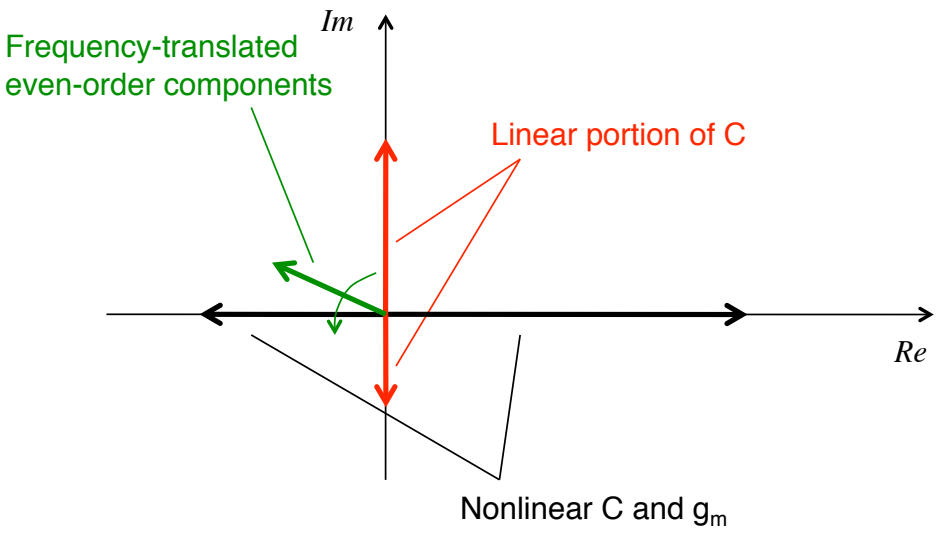

Figure 15: Breakdown of distortion components contributing to IMD vectors.

In this section we introduced nonlinear distortion, occurring in RF PAs. Intermodulation components were assumed to be symmetric for our rudimentary analysis, which is an acceptable assumption for memoryless systems. We later will return to the concept of distortion vector addition in memoryless systems in Chapters 4 and 5, when talking about phase distortion in EER RF PAs. Analysis of memory effects and their impact on the phase of intermodulation components in conventional RF power amplifiers is described in Chapter 3.

CHAPTER III

PHASE DISTORTION AND MEMORY EFFECTS IN CONVENTIONAL POWER AMPLIFIERS

Phase distortion of conventional RF power amplifiers is analyzed to determine the origins of memory effects occurring in these amplifiers. During this phase of the research, a system for the direct measurement of the phase of intermodulation products is developed [26]. In addition, a model for the attribution of phase distortion to thermal and bias-related memory effects is proposed [37]. The benefits of potentially incorporating knowledge about distortion-generating mechanisms into a linearizer design are also outlined [25].

3.1 System for Measurement of Memory Effects

Identification of memory effects in RF PAs is important in determining the potential improvement in their distortion performance, using pre-distortion linearization [39]. Such memory effects often manifest themselves as asymmetries in the magnitude and phase of third-order intermodulation distortion products [21, 73].

Vuolevi et al. attributed asymmetry of intermodulation components to thermal memory effects, namely the opposite phases of the thermal transfer function of the amplifier at negative and positive envelope frequencies. As the envelope signals due to the amplifier's thermal response are upconverted to the carrier frequency, they are added to one sideband and subtracted from the other, thus causing IMD asymmetry [73]. IMD asymmetries were also observed by Sevic, who linked them to opposite phase introduced by the second-order nonlinear transfer function, caused by envelope electrical termination [65]. More detailed discussion on IMD imbalance and its

connection to the memory effects can be found in [40], [39] and [21].

While measuring the amplitude of IMD3s is easily done with an ordinary spectrum analyzer, making accurate phase measurements at multiple frequencies has proved to be quite challenging. Vuolevi and Rahkonen discuss a method for measuring the IMD3 phase through canceling third-order intermodulation components at the input [73, 74]. Suematsu et al. proposes a method for canceling IMD3 components using the signal generated in a reference nonlinearity at the output of the power amplifier [70]. These techniques give phase information of IMD3s relative to each other and the fundamentals. However, these methods require either phase calibration at every data point (i.e., each frequency spacing and power level), or require an accurate and well-characterized analog reference nonlinearity, which is difficult to obtain. We have developed an IMD3 measurement testbed that allows accurate relative phase and amplitude measurement of IMD3 that only needs one calibration step at the beginning of a measurement run. The testbed is fully automated using the Instrument Control Toolbox of MATLAB. Moreover, the testbed can be assembled with standard RF test equipment. Since the setup is fully digital, significant measurement accuracy can be achieved. Also, the system allows for the easy sweep of tone spacings.

Another advantage of this technique is in the fact that it utilizes only simple RF test equipment, available in most laboratories. There is no need for the expensive vector signal analyzer, employed by Hammi et al. [32]. Unfortunately the main down-side of the technique is in the amount of time it takes to sweep each power level and envelope tone-spacing point. Typical plots, shown in Figures 17 and 18 consist of 100-120 test points and take about 6 hours to obtain with the fully automated setup.

The IMD3 test setup that measures relative phase and magnitude of IMD3 components is shown in Figure 16. A two-tone input signal, along with an IMD3 canceling signal, is digitally generated in MATLAB. Both data waveforms are then loaded into separate arbitrary waveform generators (Agilent E443x). To ensure phase coherency,

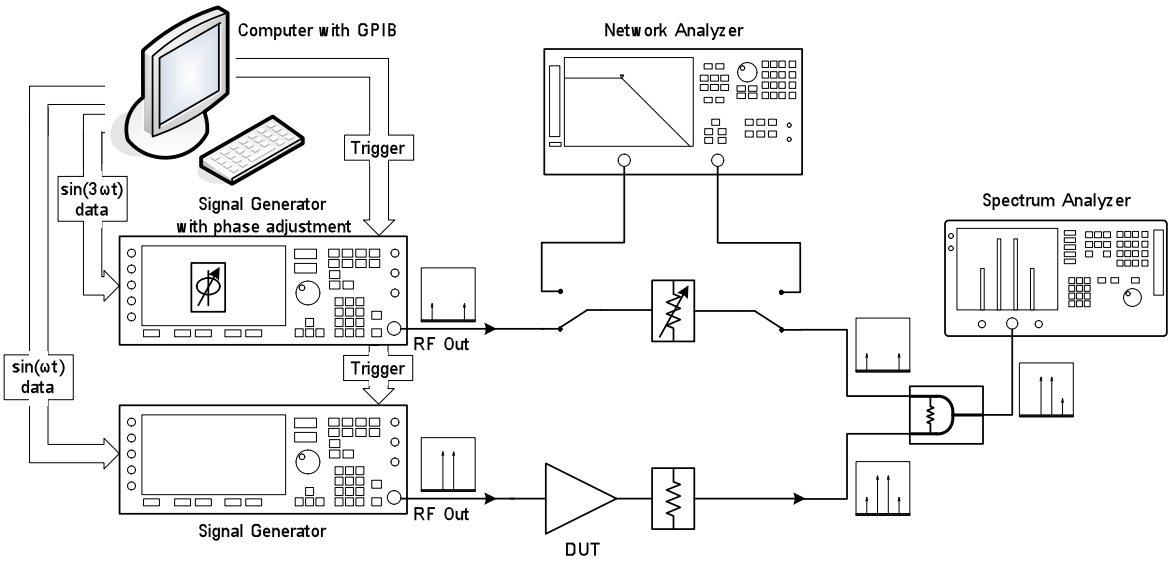

Figure 16: Relative IMD3 phase and magnitude measurement setup.

the generators are set up to trigger one another. The phase and amplitude of the up-converted IMD3 canceling signal are then adjusted to cancel the lower IMD3 component ($IMD3L$), which is monitored by an Agilent E4404 spectrum analyzer. Phase and magnitude adjustment is performed by a common bisection optimization algorithm, which can be found in Appendix A. The phase is adjusted by adding a phase offset in the IMD3 canceling generator. An external voltage variable attenuator (Hittite HMC346), controlled by a programmable power supply (Keithley 2304A), is used to adjust the signal amplitude. Both the attenuation and any phase error that it introduces are then measured using a vector network analyzer (Agilent HP8753E). If significant memory effects are present, the amplitude and phase of the lower and upper IMD3 components are asymmetric [21]. Hence, in power amplifiers exhibiting memory effects, the upper IMD3 component ($IMD3U$) will not be completely cancelled at the phase and amplitude settings used to cancel the $IMD3L$. To measure the relative phase and amplitude between $IMD3L$ and $IMD3U$, the same bisection algorithm is used to determine the amplitude and phase settings to cancel the $IMD3U$. The difference between the two settings used for canceling $IMD3L$ and

$IMD3U$ is then calculated to obtain the relative phase and magnitude of IMD3 components generated by the PA. It is also possible to measure IMD phase relative to the fundamental tones; however, this capability was not considered to be necessary for this study.

Prior to moving further, the concept of phase difference between signals at different frequencies needs to be explained. It is often pointed out that one cannot compare phase of $IMD3U$ and $IMD3L$ simply because the signals have different frequencies and the whole idea of calculating phase asymmetry of signals at difference frequencies seems absurd. This argument has some merit, however the phase difference can be explained in two ways. For envelope frequencies in the kilohertz range $2f_1 - f_2 \approx 2f_2 - f_1$, and thus phase difference can be practically approximated without accounting for any frequency difference. This assumption, however, is no longer true when the envelope signal is in the megahertz range.

For envelope frequencies in the megahertz range phases of $IMD3L$ of $IMD3U$, as well as those of fundamental signals at frequencies f_1 and f_2, are converted to group delays. Any phase shift, resulting from the signals' frequency difference in a system with constant group delay will be linear and can be calibrated out by careful measurement of delays in the cables. In the setup described earlier, this delay is estimated by measuring linear phase difference between the fundamental signals, since even in amplifiers with significant memory effects, the linear phase between the fundamentals is not perturbed. Once constant group delay indicated by linear phase between frequency components is calibrated out, remaining non-constant delays seen at frequencies $2f_1 - f_2$ and $2f_2 - f_1$, when memory effects are present, are converted to phase, referenced at the carrier frequency $(f_1 + f_2)/2$. The phase difference between signals $IMD3L$ and $IMD3U$, referenced to the carrier frequency is shown in Figures 17(a) and 18(a).

The system's performance was validated by testing a 1 W gallium arsenide (GaAs)

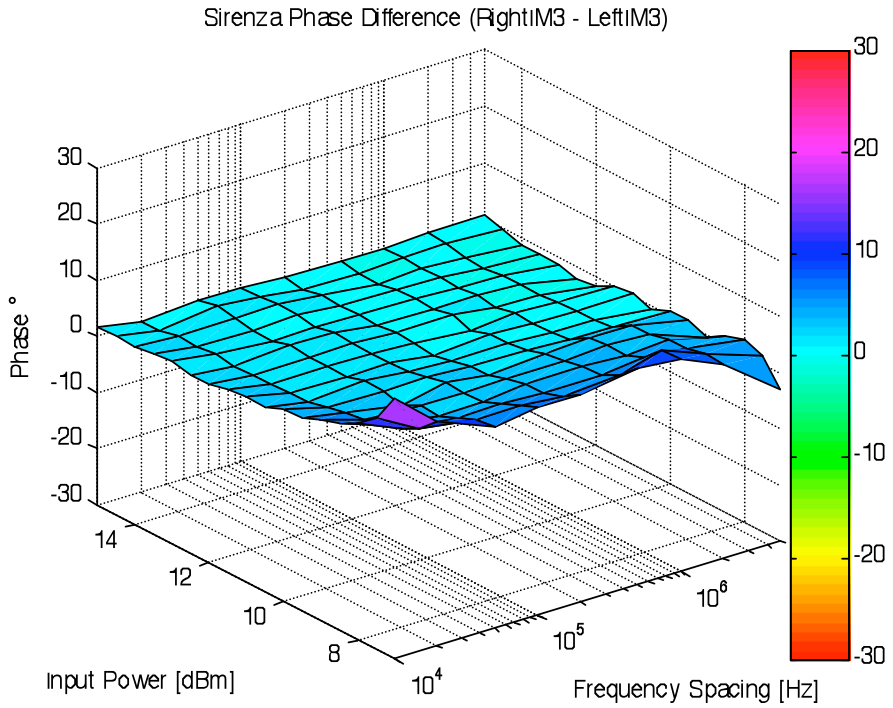

(a) Phase

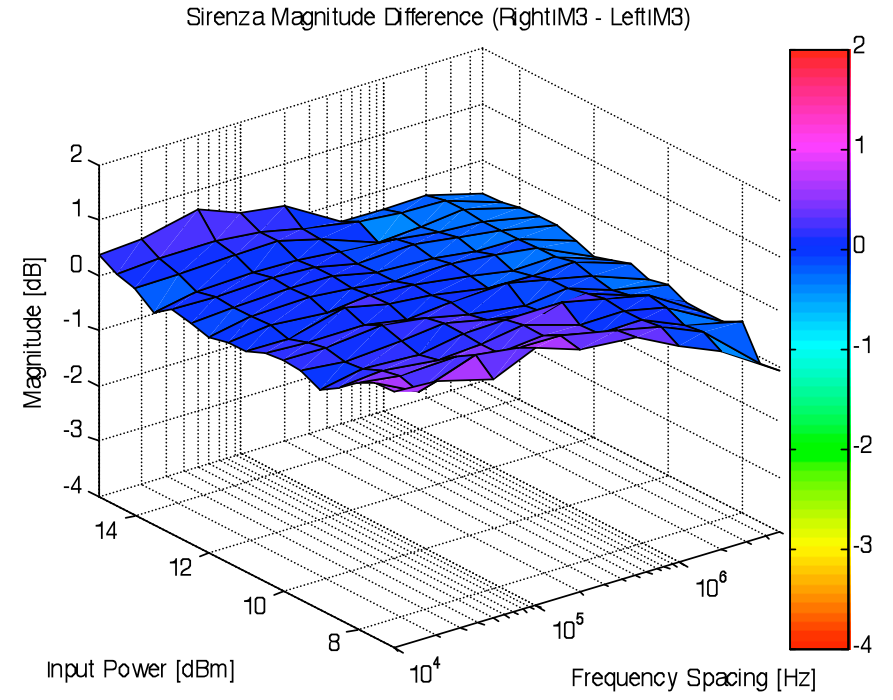

(b) Magnitude

Figure 17: Relative IMD3 (a) phase and (b) magnitude of a memoryless 1 W GaAs HFET PA at 1.96 GHz.

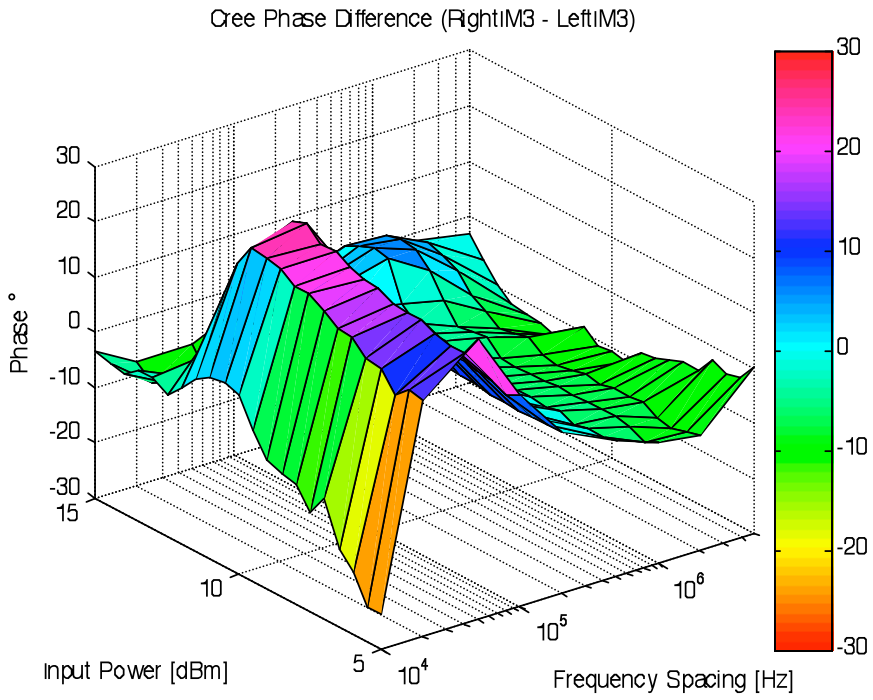

(a) Phase

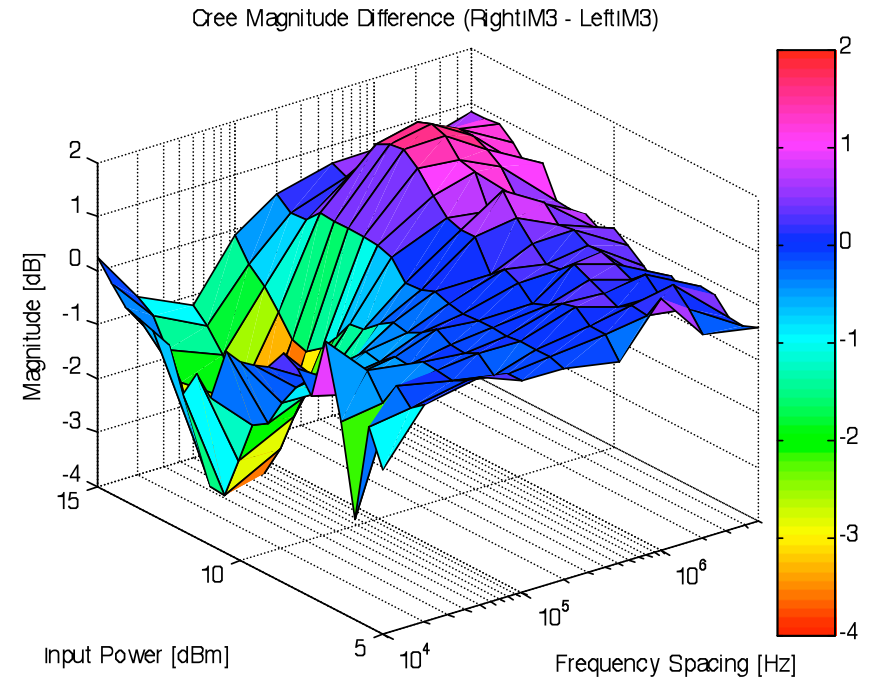

(b) Magnitude

Figure 18: Relative IMD3 (a) phase and (b) magnitude of a 20 W LDMOS Doherty PA showing significant memory effects at at 1.96 GHz.

hetero-structure field-effect transistor (HFET). Figure 17 shows the response of a 1 W GaAs HFET PA (Sirenza SHF-0289), which is known from pre-distortion measurements to be quite memoryless [39]. One can observe that the phase and magnitude responses vary within less than $\pm 5^\circ$ and ± 0.5 dB, respectively, with input power or tone frequency spacing. A second measurement was performed on a 20 W laterally diffused metal-oxide-semiconductor (LDMOS) Doherty PA module (Cree PFM21020). A phase and amplitude asymmetry of more than $\pm 20^\circ$ and ± 3 dB, respectively, suggests the presence of significant memory effects. This effect can be observed in Figure 18.

3.2 Identification of Memory Effect Origins

The system shown in Figure 16 was used to measure the IMD amplitude and phase asymmetry of two different PAs over a range of tone spacings and output power. Figure 19 shows the response of an 880 MHz CDMA base station PA, manufactured by Danam Communication, which uses a 170 W peak envelope power (PEP) silicon LDMOS device (Freescale MRF9180R6). Figure 20 shows the response for a PA based on a 90 W gallium nitride (GaN) pseudomorphic high-electron mobility transistor (pHEMT) device (Eudyna EGN21A090IV). The GaN PA is measured at 2.14 GHz. In each case, the responses indicate the presence of significant memory effects. The IMD phase and amplitude asymmetries of the LDMOS PA range from -20° to $+30^\circ$ and from -2 dB to $+3$ dB, respectively. The GaN PA shows a similar range of asymmetry: -20° to $+30^\circ$ and -2 dB to $+4$ dB.

Noticeable differences between the two PA responses are visible. The IMD asymmetry for the GaN device is confined to a small tone spacing range (Δf) centered at 100 kHz. In contrast, the asymmetry is spread rather uniformly over the entire 10 kHz to 1 MHz span of Δf for the LDMOS PA. Likewise, the range of power levels over which the asymmetry occurs is more confined for the GaN PA compared to the

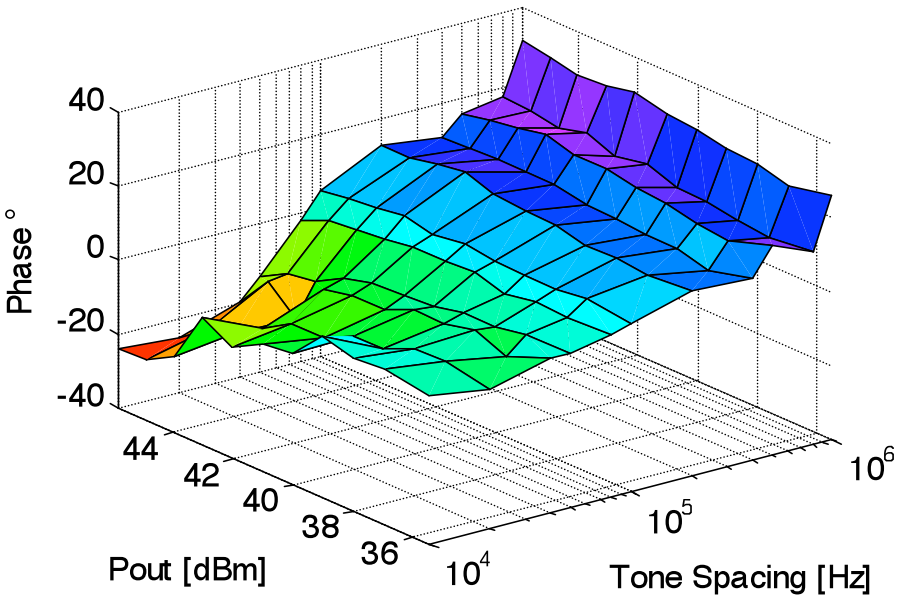

(a) Phase

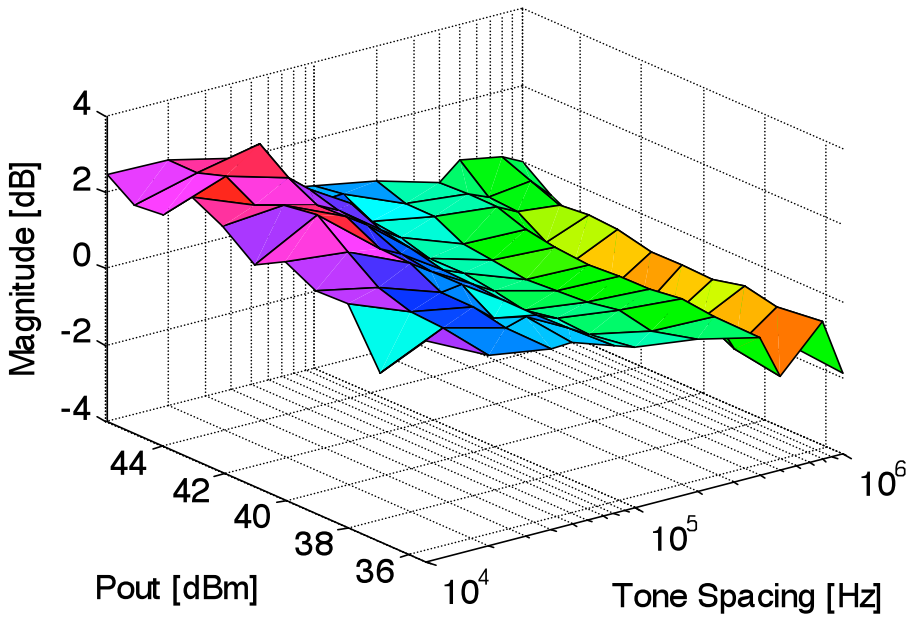

(b) Magnitude

Figure 19: Relative IMD3 (a) phase and (b) magnitude of a 170 W LDMOS PA.

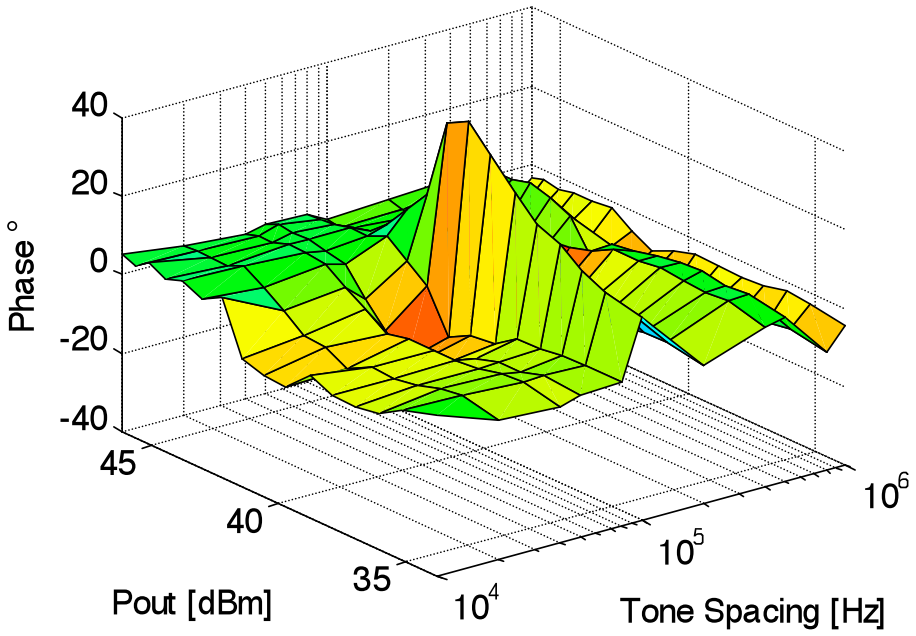

(a) Phase

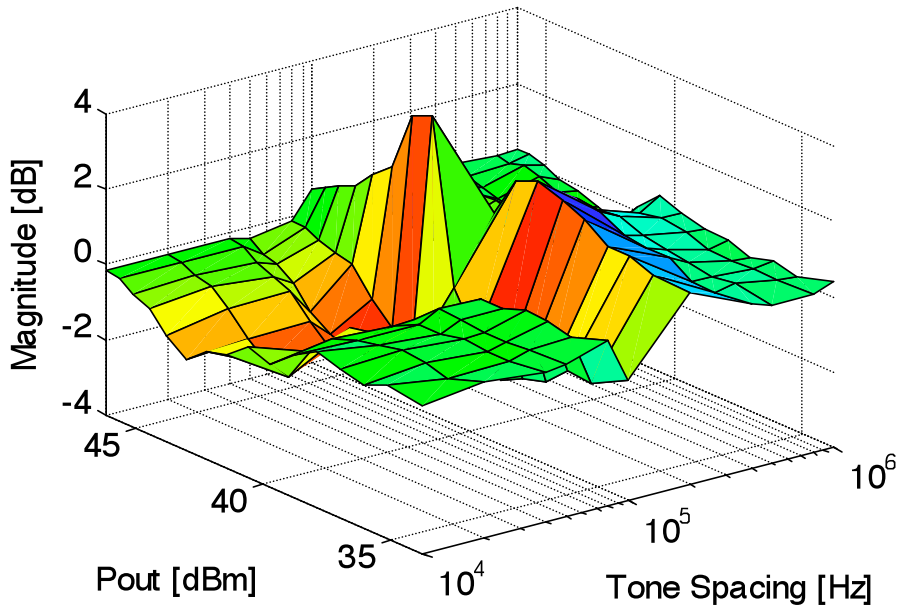

(b) Magnitude

Figure 20: Relative IMD3 (a) phase and (b) magnitude of a 90 W GaN PA.

LDMOS PA. Our experiences have shown that high-Q resonances, like the one occurring in the GaN PA response, are often the result of baseband currents interacting with nonzero bias circuit impedances. While harmonic currents can also contribute to IMD asymmetry, we have not found their contribution to long time constant memory effects to be significant. In contrast to bias effects, thermal effects change more slowly with Δf and P_{out}, as seen in the LDMOS PA. Due to the silicon-carbide (SiC) substrate's high thermal conductivity in the GaN device, one would expect smaller thermal responses in the GaN PA compared to the LDMOS PA, the self-heating effects of which are well known [20].

Because the pre-distortion linearization architectures must account for the responses of different memory effects, we seek a method to differentiate between bias-related and thermal effects, based on statistically quantifiable signatures in PA IMD asymmetry responses. Using the notion that intermodulation components can be treated as phasors, one can decompose them into real and imaginary parts along the axes shown in Figure 21.

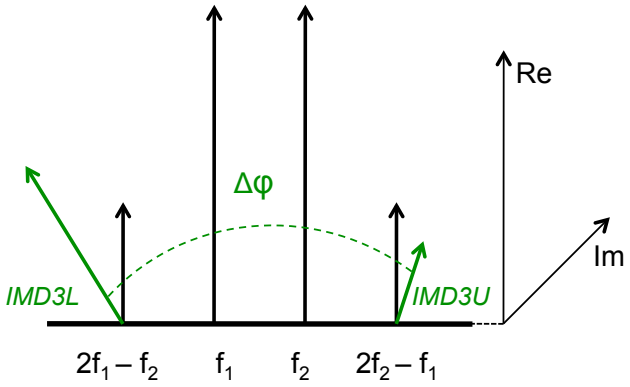

Figure 21: Two-tone signal with intermodulation components shown as phasors.

These phasors, and their real and imaginary components, may then be analyzed in detail, as shown in Figure 22. As in [77] it is assumed that each sideband is the sum of two phasors.

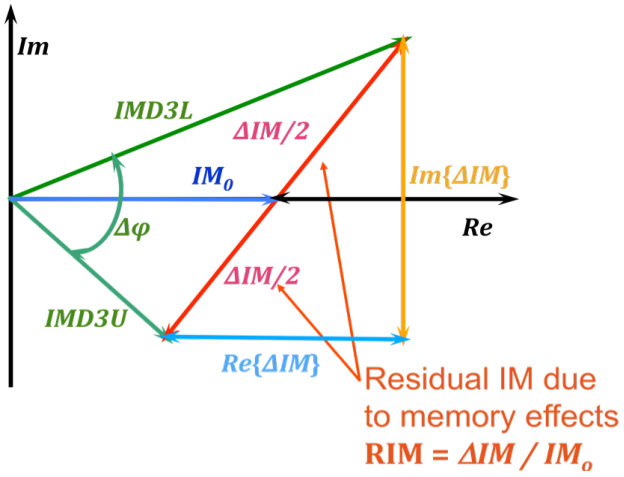

Figure 22: Phasor diagram illustrating memoryless components of IMD3 (IM_0) and those due to memory effects ($\Delta IM/2$).

A memoryless component IM_0 is equal in magnitude and is in phase for both sidebands. Residual IM components, $\pm\Delta IM/2$, represent the memory effects. Using the previously described setup, we are able to make accurate measurements of $|IMD3L|$, $|IMD3U|$ and $\Delta\varphi$. Using this information, it may be determined from the geometry of the phasors that

$$\varphi_L = \cot^{-1}\left[\frac{\frac{|IMD3L|}{|IMD3U|} + \cos\Delta\varphi}{\sin\Delta\varphi}\right] \tag{8}$$

and

$$\varphi_U = \Delta\varphi - \varphi_L. \tag{9}$$

Combining the angle information outlined in Equations (8) and (9), with magnitudes of $IMD3L$ and $IMD3U$ measured with a spectrum analyzer, we can construct complex phasors that represent lower and upper IMD3 components. From these, it is clear that one can determine the residual component as

$$\Delta IM = IMD3U - IMD3L. \tag{10}$$

Moreover, the memoryless portion of IMD may be determined as the vector average of $IMD3U$ and $IMD3L$:

$$IM_0 = \frac{IMD3U + IMD3L}{2}. \tag{11}$$

The memoryless portion of intermodulation components must always be real. It is the behavior of ΔIM that is used to determine the origin of the dominant memory effects in each of the aforementioned PAs. Using Equations (8-11) one can define expressions for $Re\{\Delta IM\}$ and $Im\{\Delta IM\}$ as follows:

$$Re\{\Delta IM\} = \frac{\frac{|\Delta IM|^2}{2} + |IM_0|^2 - |IM3U|^2}{|IM_0|} \tag{12}$$

$$Im\{\Delta IM\} = 2\sin\left[\cos^{-1}\left[\frac{\frac{Re\{\Delta IM\}}{2} + |IM_0|}{|IM3L|}\right]\right]|IM3L|. \tag{13}$$

3.2.1 Behavioral Model for Determining Origins of Memory Effects

The behavioral model shown in Figure 23 is proposed to represent the action of self-heating and bias feedback. This model is based on knowledge of the physics of device operation, and on equivalent circuit models that represent their operation [21, 53].

The model shows three branches, each with distinct nonlinear transfer characteristics and frequency response functions. The top branch of the model, consisting of the cascade of $G(A)$ and $H_{RF}(\omega)$, represents the memoryless complex gain function and the RF frequency response, respectively. Assuming that $H_{RF}(\omega) \approx 1$ over the desired bandwidth of operation, the top branch may be considered entirely memoryless and thus the origin of IM_0. The second branch represents the contribution by device self-heating, or thermal feedback. To a first-order approximation, the junction temperature T_j is a function of power dissipation and thus related to the square of the amplitude of the output power. For convenience, we chose to represent this as a

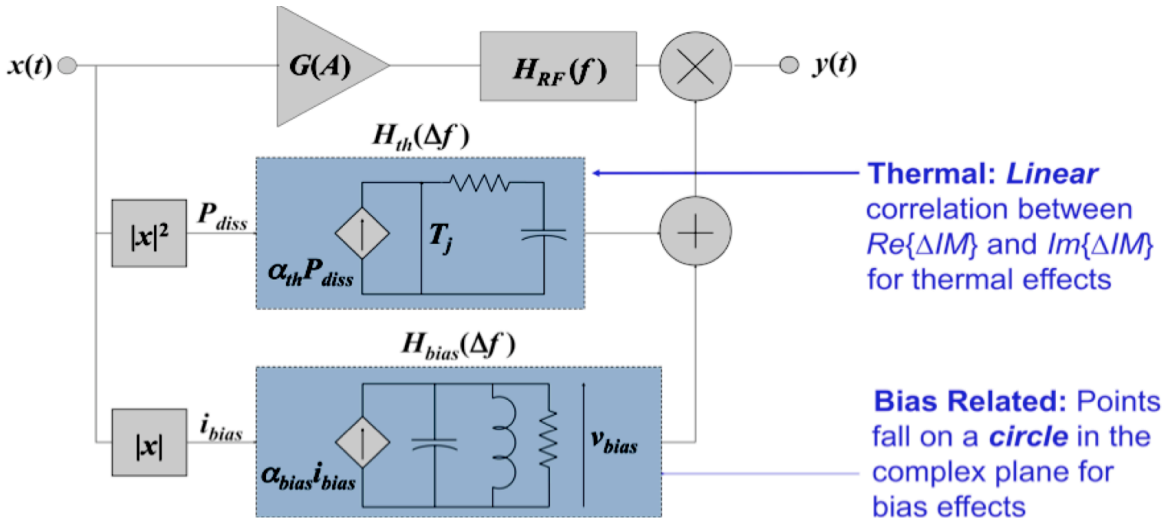

Figure 23: Behavioral model for RF PA including physically-based memory effects

dependence on a scaled version of the input power. This second-order nonlinearity produces a baseband (or difference frequency) response that is filtered by the thermal response of the device. The simplest model for such an effect is an RC network having the transfer function

$$H_{th}(\Delta\omega) = \frac{\alpha_{th}}{1 + j\Delta\omega\tau_{th}}, \tag{14}$$

where α_{th} is related to the thermal resistance of the junction to base plate, and τ_{th} is the thermal time constant, which depends on the mass and thermal capacity of the material. Thus, the dissipated power is low-pass filtered and converted to a thermal signal $T_j(t)$, which modulates the transconductance and hence the gain. It is clear from Equation (14) that there is a relationship between the real and imaginary part of the IMD due to the phase lag at higher frequencies:

$$\frac{Im\{H_{th}(\Delta\omega)\}}{Re\{H_{th}(\Delta\omega)\}} = -\Delta\omega\tau_{th}. \tag{15}$$

Therefore, it is expected that the linear dependence of the real and imaginary parts of the residual IMD should be seen in regions dominated by thermal effects.

Unlike thermal effects, bias-related effects are purely electrical [21]. Though bias

circuits vary considerably, it is assumed that the simplest model of a parallel RLC circuit would be sufficient to capture the nature of the memory effects occurring in the bias network. We also assume that the baseband currents in a class-AB amplifier are directly proportional to the amplitude of the input voltage via a parameter α_{bias}, related to the channel length modulation effect (λ-parameter) in the device. Thus, the contribution of these currents to the residual IMD may be determined from the impedance of the parallel RLC circuit:

$$H_{bias}(\Delta\omega) = \frac{j\Delta\omega L\alpha_{bias}}{1 + j\Delta\omega L/R - \Delta\omega^2 LC}. \tag{16}$$

It is well known that the impedance of an RLC maps out a circle on the complex plane. Therefore, it is expected to see such behavior of the residual IMD at a frequency spacing where the bias-related effects are dominant.

The model, shown in Figure 23, is different from those widely published in the literature [39] in the sense that each branch is describing a memory effect stemming from a particular physical origin. Whereas, normally parallel-branch models use delayed transfer functions for describing memory effects, while ignoring their physical origins.

3.2.2 Experimental Results

Scatter plots of ΔIM can be formed from the IMD amplitude and phase asymmetry responses for the LDMOS and GaN PAs. Plots of portions of IMDs due to memory effects can be seen with corresponding phase responses of the power amplifiers in Figures 24-26. It is clear that the LDMOS PA shows a linear trajectory in Figure 24(b) in plotting ΔIM as a collection of points independent of power and tone spacing. The standard error of $R^2 = 0.38$ indicates strong correlation to this linear dependence. The memory ratio (MR) was calculated to be -16.8 dB [39] .

This linear dependence of the residual IMD plot indicates significant presence

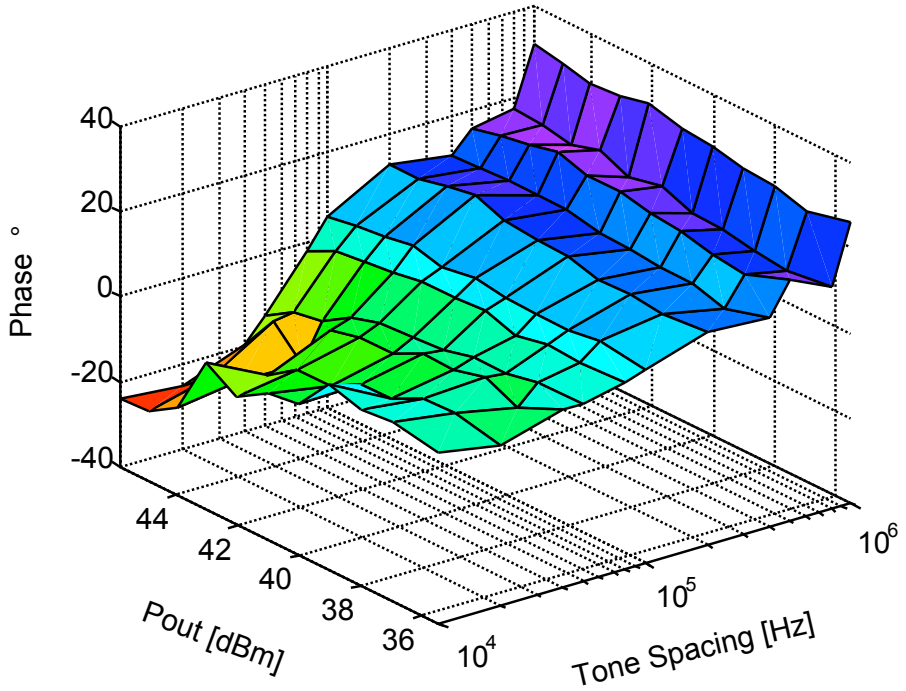

(a) Phase asymmetry indicating presence of broadband thermal memory effects.

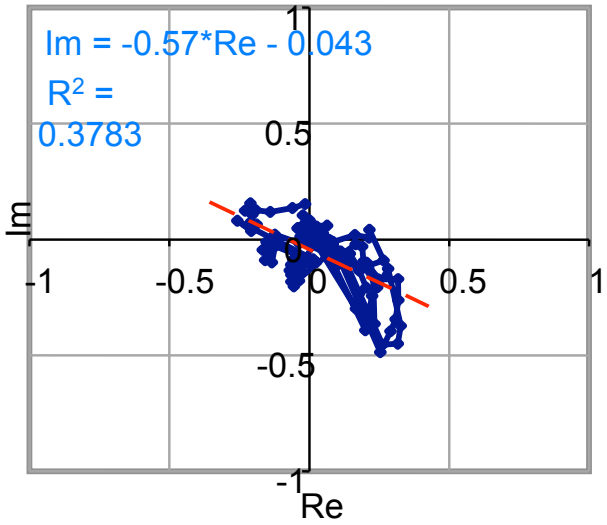

(b) Residual IMD (ΔIM) confirming strong presence of thermal memory effects.

Figure 24: Plots of (a) phase asymmetry and (b) resulting residual IMD (ΔIM) for a 180 W LDMOS PA.

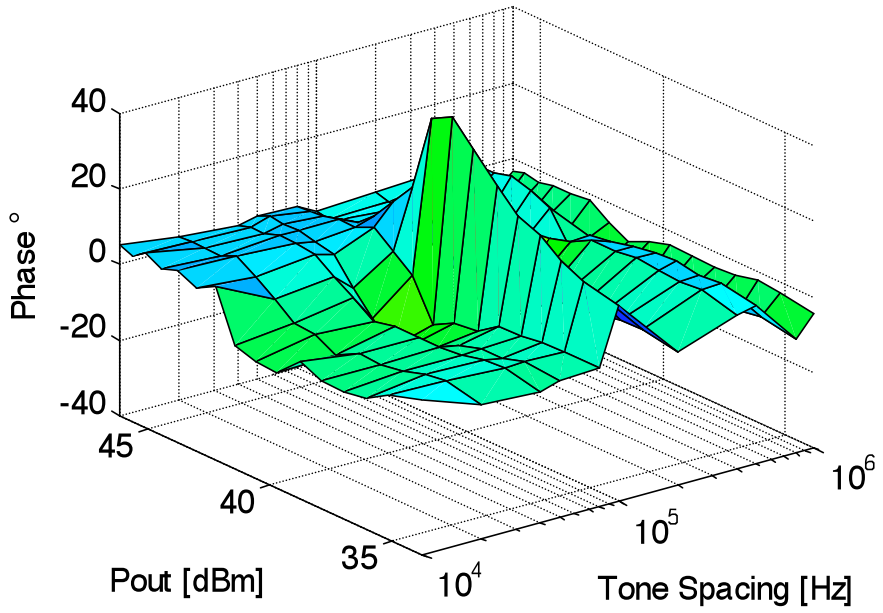

(a) Phase asymmetry indicating presence of bias memory effects at 100 kHz tone spacing.

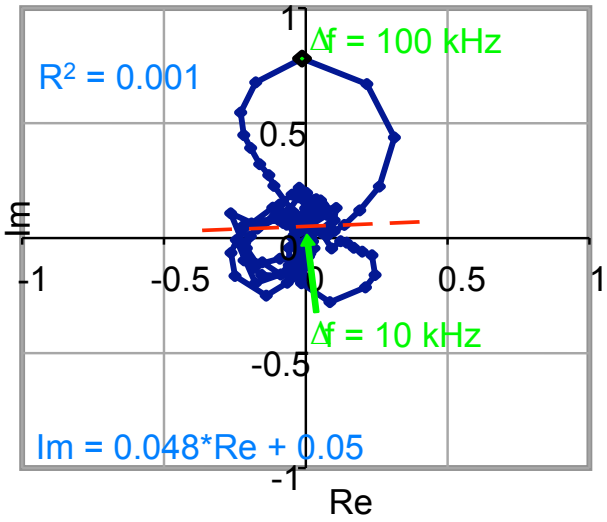

(b) Residual IMD (ΔIM) confirming strong presence of bias memory effects at 100 kHz tone spacing.

Figure 25: Plots of (a) phase asymmetry and (b) resulting residual IMD (ΔIM) for a 90 W GaN PA with poorly decoupled bias feed.

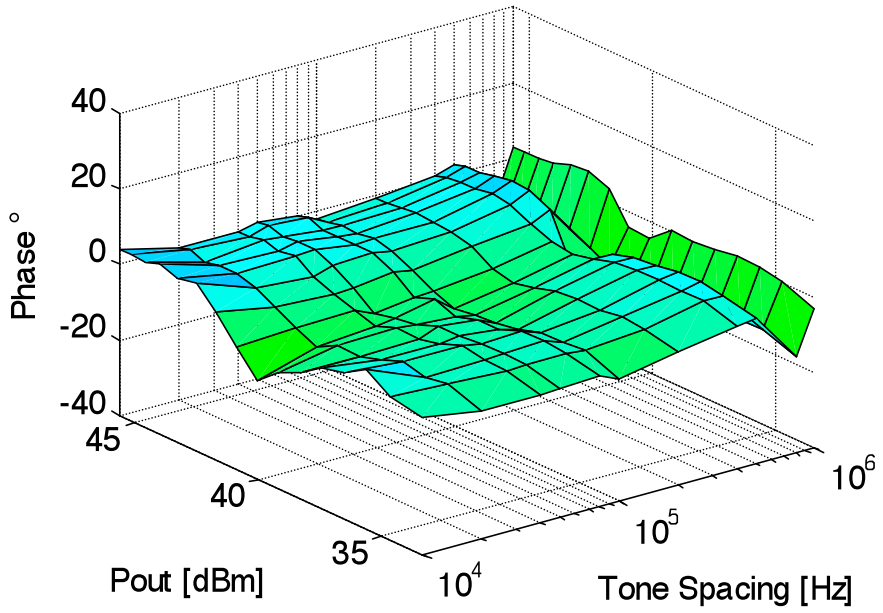

(a) Phase asymmetry indicating little presence of memory effects.

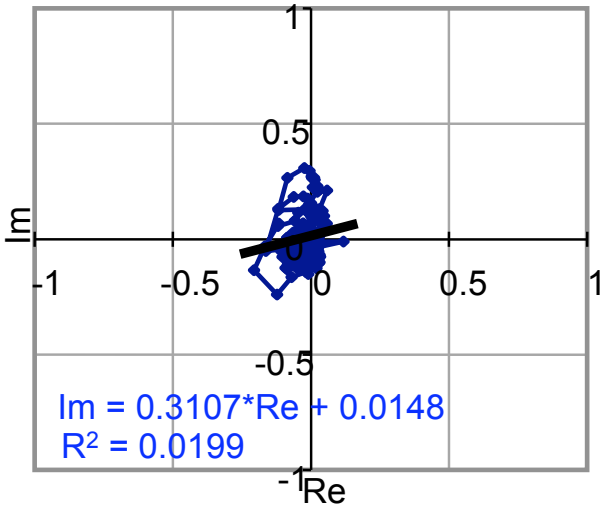

(b) Residual IMD (ΔIM) indicating little presence of memory effects.

Figure 26: Plots of (a) phase asymmetry and (b) resulting residual IMD (ΔIM) for a 90 W GaN PA with well decoupled bias feed.

of thermal memory effects, which is qualitatively confirmed by the plot of phase asymmetry of the LDMOS PA seen in Figure 24(a). The LDMOS PA shows the largest phase asymmetry at high output power across a broad range of tone spacings, which is indicative of thermal memory effects [26].

In contrast, the GaN PA shows no clear linear correlation of ΔIM in Figure 25(b), but does exhibit circular trajectories indicative of a bias-related memory effect. The biggest loop is seen at the tone spacing of 100 kHz. This information corresponds to Figure 25(a), where the most significant phase asymmetry can be seen along the ridge at the tone spacing of 100 kHz. The calculated MR was -16.4 dB.

Additional bypass capacitors were added to the drain bias line of the GaN PA, resulting in an improved MR of -24.0 dB. As can be seen in Figure 26(a), the ridge at 100 kHz due to bias memory effects vanished. Also, no significant loops can be seen in Figure 26(b). While the linear dependence is not as highly correlated in the decoupled GaN PA as in the LDMOS PA, it did increase by a factor of 20 over the unmodified GaN PA. Larger R^2 indicates that thermal effects started to contribute a larger portion of the residual IMD due to the lower contribution of bias-related effects.

3.3 Simplifying Linearization through Knowledge of Physical Origins of Distortion

The insight obtained from identifying sources of memory effects in RF PAs can be used to simplify pre-distortion algorithms for power amplifiers operating under specific conditions. We developed a hypothesis that bias memory effects, due to their narrowband nature, are likely to introduce minimal distortion into systems amplifying wideband signals. If the stated hypothesis is true, pre-distortion linearization might not provide any additional benefits for RF PAs with narrowband bias-related memory effects when wideband signals are amplified. The elimination of unnecessary linearization components is likely to decrease both cost and power consumption of

the entire system.

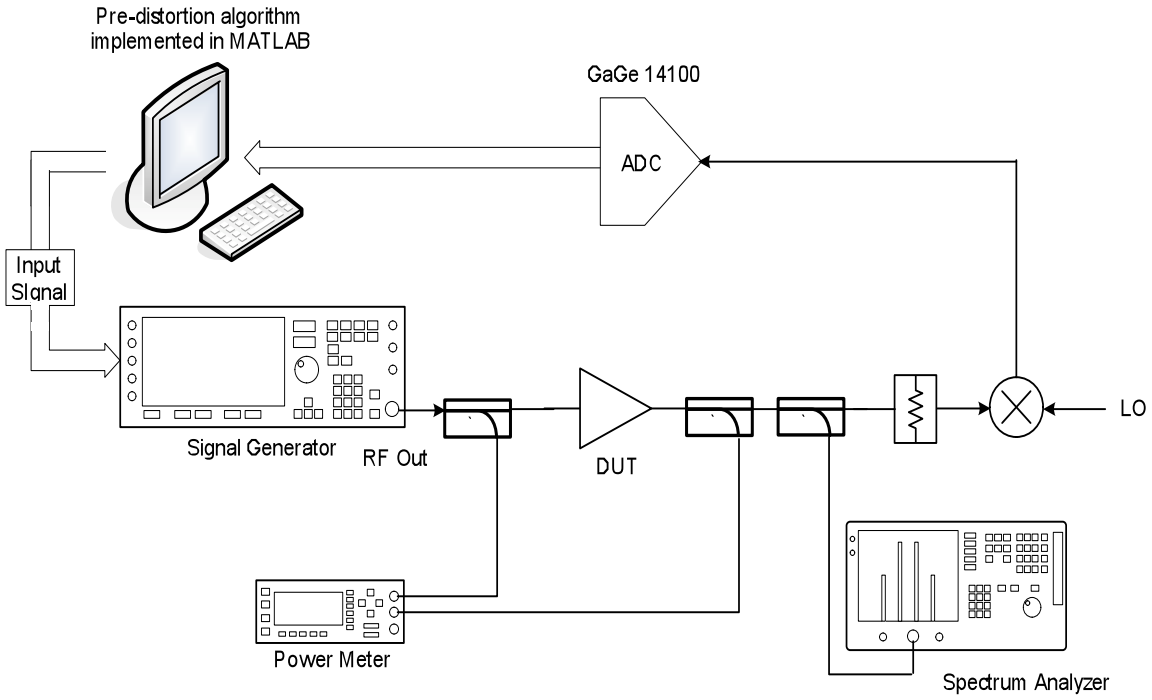

Figure 27: Pre-distortion testbed.

Normally, memory ratio, or related metrics developed by university groups are used to measure pre-distortability of power amplifiers [39, 40, 44]. While these metrics might somewhat differ, their general goal is to compare ratios of components due to memoryless distortion and those due to memory effects. For example, we can define a typical memory ratio by looking back at Figure 22 as the following:

$$MR = \frac{\sum_{i=1}^{n}\sum_{j=1}^{m}|\Delta IM|}{\sum_{i=1}^{n}\sum_{j=1}^{m}|2IM_0|}, \tag{17}$$

where i represents envelope tone spacings and j represents power levels, at which single point memory ratios, defined as $|\Delta IM|/|IM_0|$ are calculated. The downside about memory ratio, as defined in Equation 17, lies in the fact that it does not account for the bandwidth and power probability distribution function of the signal

being used.

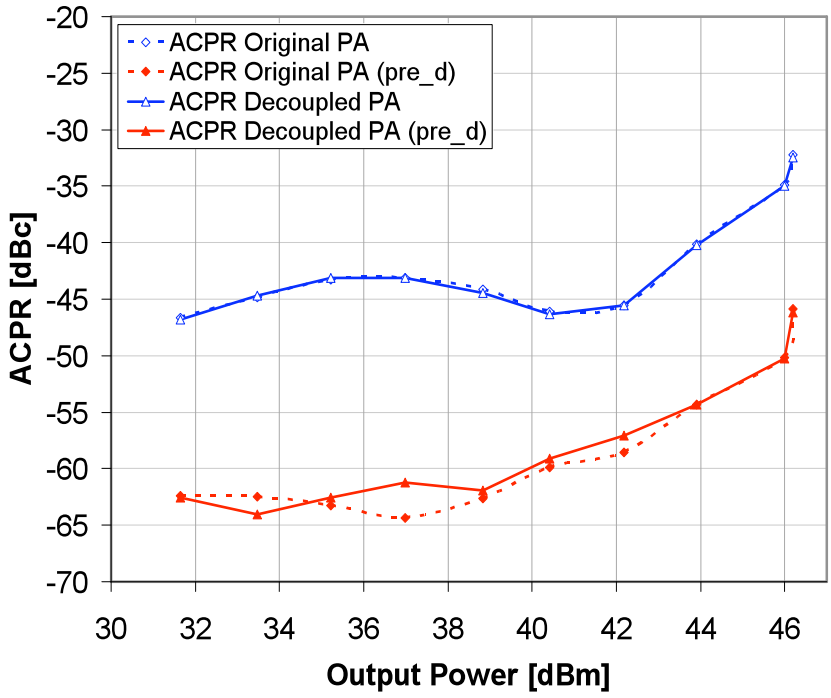

Figure 28: ACPR before and after pre-distortion for original and decoupled GaN PA using WCDMA signal at 2.16 GHz.

To quantify the information about the nature of memory effects and bandwidth of the signal, bandwidth-specific memory ratio was introduced. The metric comprises a normalized integral of conventional memory ratio values weighted over the bandwidth of the transmitted signal. The correlation between bandwidth-specific memory ratio and relative pre-distortability of the amplifier is explored. Figure 27 shows an adaptive memoryless pre-distortion testbed assembled for this task. The testbed is based on an iterative LMS algorithm for phase and magnitude lookup table (LUT) update. The algorithm is implemented in MATLAB, and it adapts the LUT based on the ideal input and output signals of the PA, which is down-converted and sampled by an analog-to-digital converter (ADC) implemented with a GaGe CS14100 board. An arbitrary waveform generator with an in-phase/quadrature modulator (Agilent E4438C) is used as the source for the power amplifier. Because the pre-distortion

algorithm compares the PA output signal to the ideal signal generated in MATLAB, the entire system, including the digital-to-analog converter (DAC) of the waveform generator as well as the down-conversion mixer, is linearized. Full system linearization enables ACPR measurements that are not significantly affected by equipment imperfections.

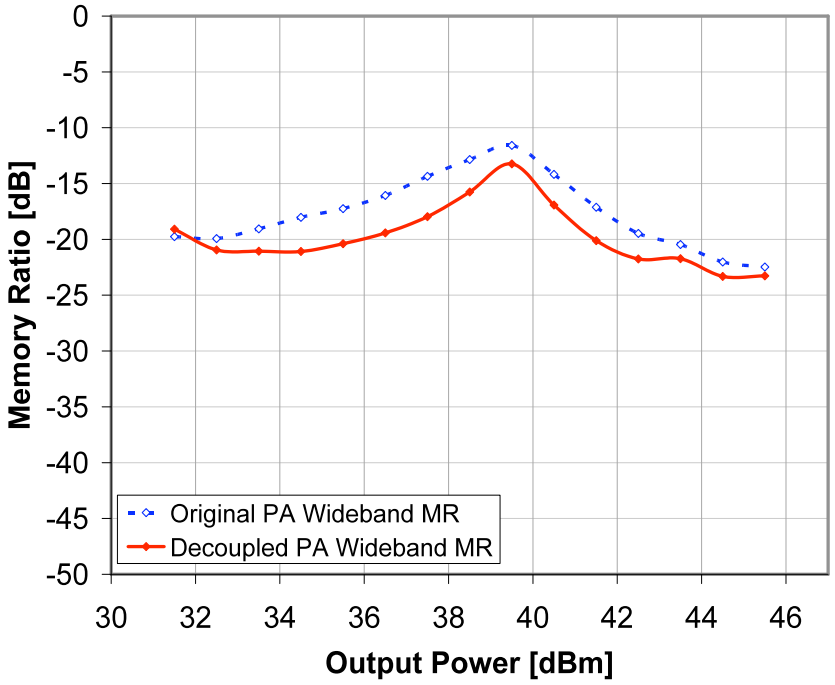

Figure 29: Memory ratio of original and decoupled GaN PA averaged over a 5 MHz bandwidth WCDMA modulation signal.

A 90 W GaN high electron mobility transistor (HEMT) amplifier manufactured by Eudyna was used in the experiment. It has been noted earlier that this amplifier presented a strong bias memory effect at 100 kHz, which was alleviated by adding extra decoupling on the drain bias line. A single PA with different bias line configurations was chosen to illustrate the difference in performance for narrowband and wideband signals, while keeping variability of PA parameters to a minimum. It can be seen in Figure 28 that little difference in correction is observed between the two amplifier configurations when a WCDMA signal is used. Such a result contradicts the generally

accepted notion that memory effects significantly degrade PA pre-distortability.

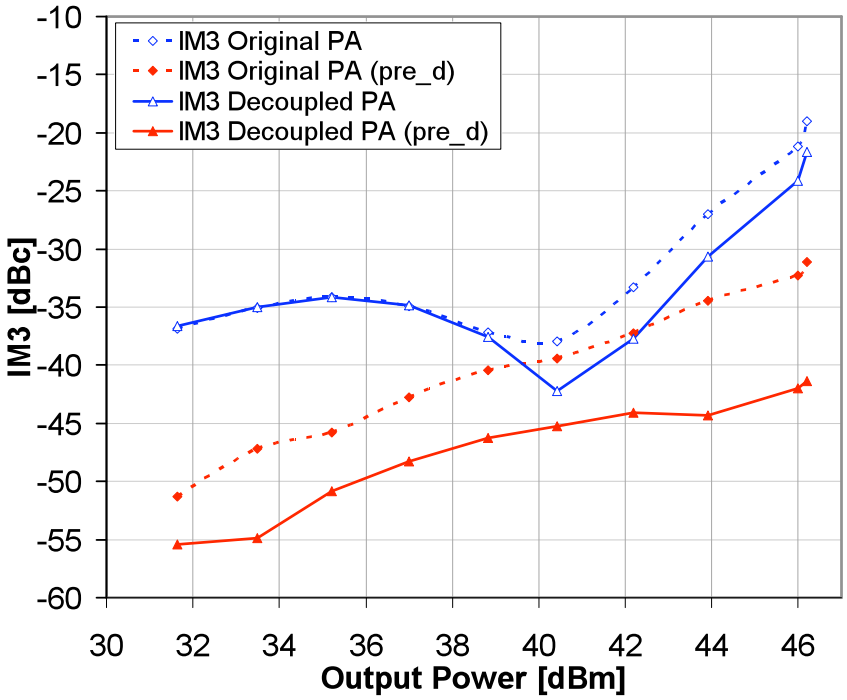

Figure 30: IMD3 levels before and after pre-distortion for original and decoupled GaN PA using a two-tone 100 kHz signal at 2.16 GHz.

However, if one integrates MR over the bandwidth used by the signal, it becomes clear why both PA configurations show similar pre-distortion results. The MR integrated over the 5 MHz WCDMA bandwidth is shown in Figure 29. The average MR taken over the range of output power weighted accordingly to the WCDMA instantaneous power probability distribution function amounts to -15.5 dB for the original PA and -17.9 dB for the decoupled PA [61]. As can be seen, the ~ 2 dB difference in the bandwidth-specific memory ratio does not have a significant impact on the pre-distortability of the PA.

At the same time, it can be observed in Figure 30 that pre-distortion results differ significantly between the two PA configurations when a two-tone signal with tone spacing of 100 kHz is used. The decoupled amplifier exhibits 8-10 dB lower IMD3 than the original version after pre-distortion is applied. Figure 31 shows a consistent

10 dB difference in narrowband MR between the original and decoupled PA.

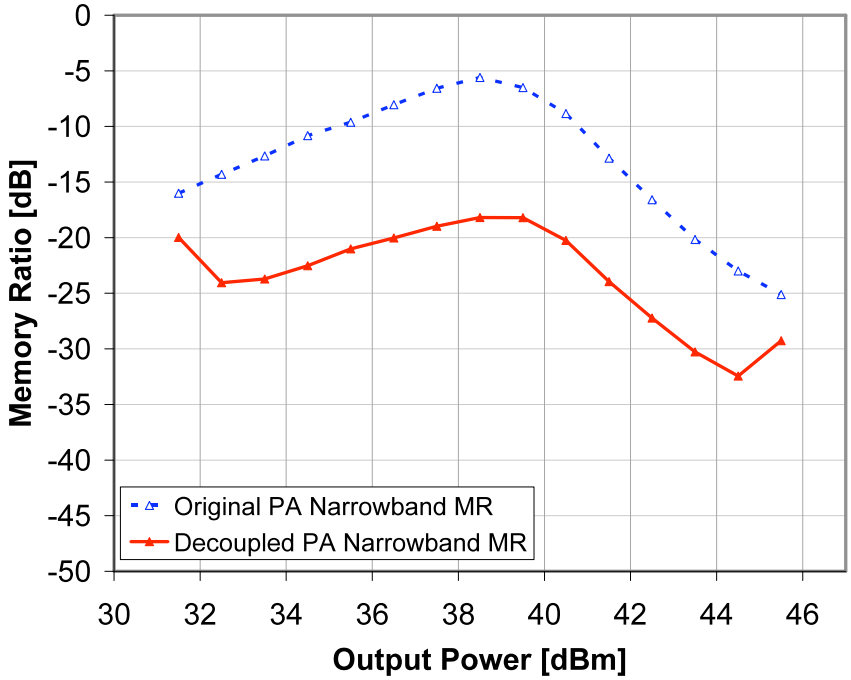

Figure 31: Memory ratio of original and decoupled GaN PA at 100 kHz tone spacing.

From the entire measurement set one can observe a direct correlation between the improvement in memoryless pre-distortion correction, achieved for a specific signal, and the difference in the PA MR integrated over the desired signal bandwidth. This finding is in line with the original hypothesis. It suggests that by knowing the origins of distortion, as well as the target application for the power amplifier, one can design a much leaner system capable of performance similar to that of more expensive and power-hungry solutions, which treat all distortion the same by applying a black-box pre-distortion approach.

CHAPTER IV

PHASE DISTORTION IN HFET ENVELOPE ELIMINATION AND RESTORATION RF POWER AMPLIFIERS

The growing popularity of envelope elimination and restoration radio frequency power amplifiers has increased the demand for understanding distortion generated by such systems. Our group's expertise and previous work in identifying sources of distortion and designing linearization solutions for two-port power amplifiers provide a unique opportunity to extend this research to the analysis of distortion occurring in Kahn power amplifiers. The goal of the research is to investigate phase distortion in the RF transistor, resulting from operating the RF PA with rapidly varying drain voltage, and propose simple distortion-mitigating circuit techniques. To achieve this goal, three main tasks are accomplished. A system capable of directly measuring phase distortion in EER PAs is built based on a similar system used for conventional power amplifiers [27]. Phase distortion occurring in the RF transistor is isolated from other types of distortion and analyzed in order to uncover its origins [28]. Concurrently with identification of distortion sources, simple circuit and device-level distortion-mitigating techniques are investigated [27, 29].

4.1 System for Measurement of Phase Distortion in EER RF Power Amplifiers

The measurement system previously developed for conventional power amplifiers was modified into the one capable of measuring phase distortion of handset EER RF PAs. The new system is shown in Figure 32 and uses a baseband signal to modulate the

drain of a PA. Both signal generators in the setup are phase-locked to enable stable signal cancellation by adjusting magnitude and phase of the canceling signal. The signal generator supplying the input signal to the PA under test generates both the RF carrier signal, driving the phase path of the EER PA, and the modulated envelope signal driving the drain of the EER PA. Both signals are synchronized with each other and with the cancellation signal, generated in the signal generator with phase and amplitude adjustment. The phase and amplitude input signals to the PA are then combined directly at the drain of the transistor to form a modulated signal around the RF carrier. The output signal is taken after the output matching network of the PA. Photograph of the laboratory implementation of the EER phase-measurement setup can be found in Appendix B. Standard GPIB-controlled RF equipment can be used for the setup, envelope amplifier, being the only exception.

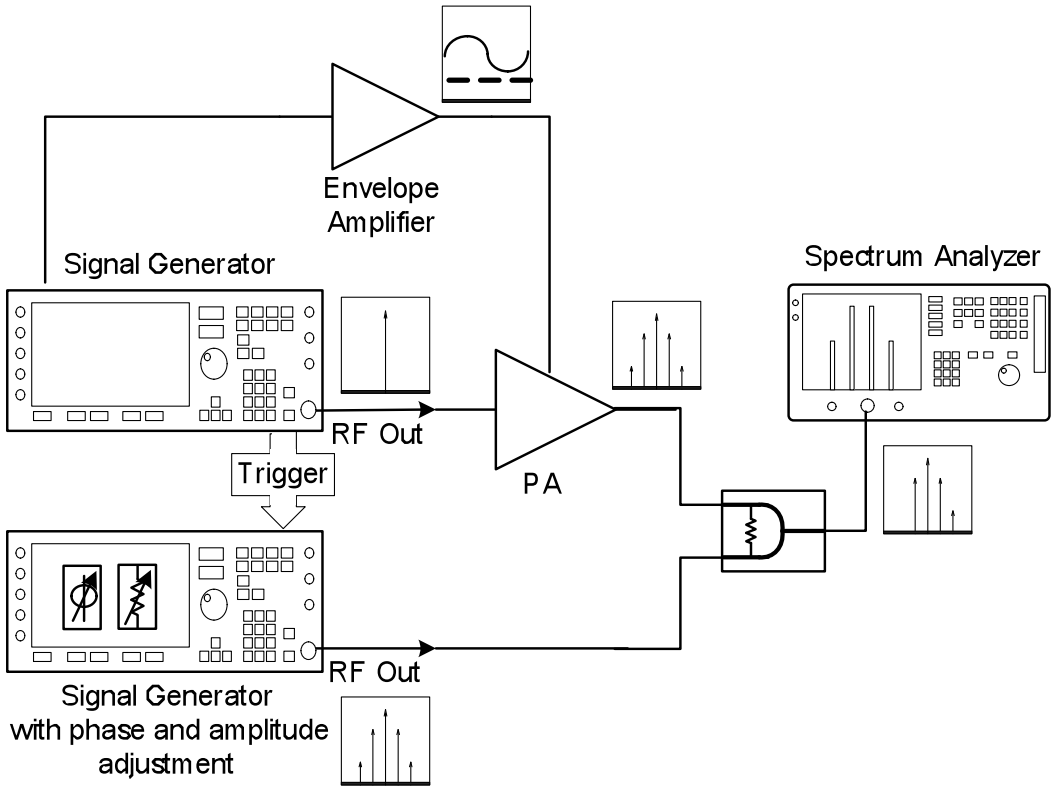

Figure 32: Measurement setup used to characterize the modulation transfer characteristic of an EER PA.

For simplicity, single-stage RF power amplifiers are used for the tests. In the majority of power amplifiers the final stage of the PA is responsible for 75% of power consumption. Hence it makes sense to apply the EER technique only to the final stage of the PA. Therefore our simplification does not impact applicability of our findings to practice.

4.1.1 Envelope Amplifier

Because the original goal was to examine only the distortion within the RF PA and not the envelope amplifier (EA), the EA was designed as a high bandwidth linear regulator, shown in Figure 33, as opposed to a high-speed DC-DC converter, used in the majority of EER PA papers to achieve high efficiency [14]. The envelope amplifier is implemented with a rail-to-rail high output current operational amplifier from Analog Devices (AD8397) and a 20-V n-channel enhancement mode MOSFET, manufactured by Zetex.

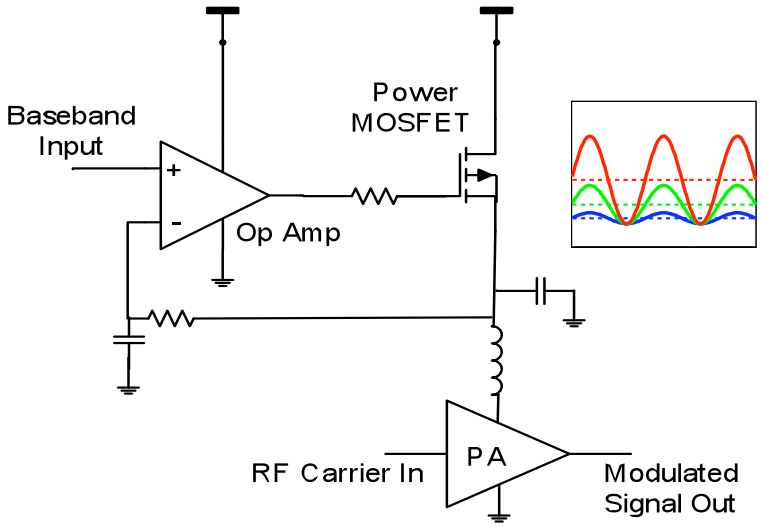

Figure 33: Envelope amplifier.

The operational amplifier is intended for use as a twisted-pair line driver. It exhibits large signal bandwidth of 14 MHz, slew rate of 53 V/μs and can source up to 250 mA of peak current [6]. These characteristics make this amplifier ideal for

driving capacitive load presented by the gate of the Zetex power MOSFET, while maintaining reasonably high output voltage swing, necessary to power most handset RF PAs. The Zetex MOSFET is intended for use in DC-DC converter applications. It can handle up to 1.3 A of continuous current and 7.4 A of pulsed current while presenting only 160 pF of capacitance at the gate [79]. The envelope amplifier circuit comprised of the operational amplifier and the MOSFET is shown in Figure 33. The EA is capable of sourcing up to 500 mA of average current to the RF power amplifier while maintaining a slew rate of 37 V/μs. The amplifier has wide bandwidth, however due to the slew-rate limitations imposed by operating in the large-signal realm, the effective bandwidth is limited to 2.5MHz. At the same time the amplifier is capable of delivering 6.5-V_{pk-pk} waveforms with frequencies of up to 2.5 MHz to the drain of the PA while handling 500 mA of average current.

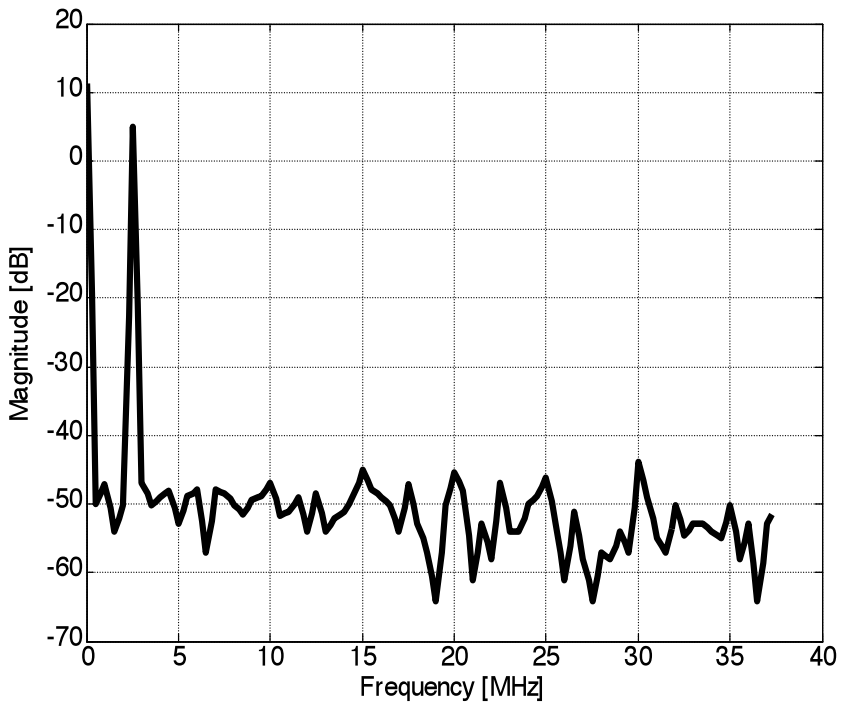

Figure 34: Harmonic content of modulating waveform at the drain of the PA.

Care was taken to avoid nonlinearities and frequency response in the EA circuit,

including interactions with the nonlinear PA load, by using unity feedback around the EA as it was driving the PA. The frequency response of the modulator is negligible up to 2.5 MHz, permitting memoryless modulation up to that frequency at baseband. Such bandwidth of the envelope amplifier allows us to cover 5 MHz of signal bandwidth at the carrier frequency of the PA. As seen in Figure 34, spectral purity of the modulating waveform is excellent, with envelope harmonics being 50 dB below AM sidebands.

4.1.2 Test Signal Selection

Various test signals were considered for use with the test setup. Traditional two-tone signals used in PA characterization were avoided due to the large bandwidth requirement in the envelope path, where they are presented as full-wave rectified sine waves with infinite amount of harmonics. Instead, DC offset sinusoids, shown in Figure 35(a), were used so as to observe the harmonic distortion of the AM signal as it is emerging from the PA. These signals are bandlimited in the amplitude path as they are presented by a DC component and a sinusoid. It is important to note that the DC component of the envelope is always larger than the amplitude of the sinusoid to avoid abrupt clipping during rectification.

The offset sinusoidal envelope signal forms a three-tone signal at the output when combined with an RF carrier at the gate. The three-tone output signal shown along with distortion components in Figure 35(b) can be easily compared to the two-tone signal used in conventional RF PAs. First harmonic sidebands are primarily generated by third-order nonlinearity applied to the sum of the carrier and one of the first sidebands. First harmonic sidebands therefore closely resemble $2f_2 - f_1$ and $2f_1 - f_2$ intermodulation components of the traditional two-tone signal, shown in Figure 21. Drawing a parallel between second harmonic sidebands and IMD components of the two-tone signal is less straightforward. Second harmonic sidebands can be caused by

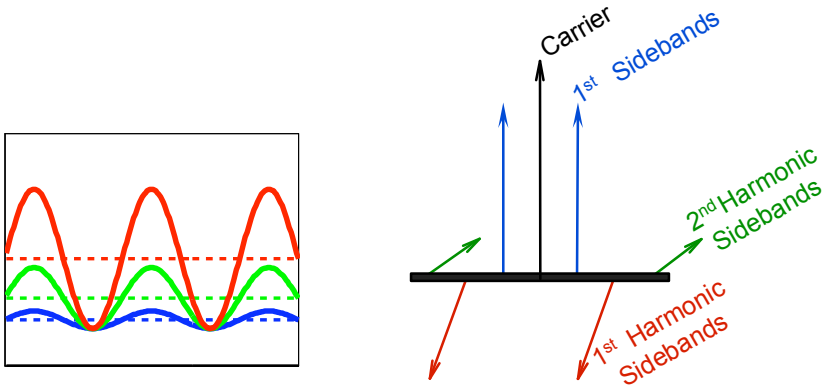

(a) Offset sinusoids with fixed minima and varying maxima and means applied to the drain of the EER PA.

(b) Output spectrum components.

Figure 35: Signals applied to the drain and the resulting output spectrum components shown as phasors.

third-order nonlinearity acting on the sum on the first sidebands. However, they can also be caused by the fifth-order nonlinearity acting on the sum of the carrier and one of the first sidebands. Thus, no clear equivalency to a particular intermodulation distortion component of the two-tone test signal can be established. In addition second harmonic sidebands tend to be too small in the EER RF PAs to reliably measure their phase. In light of these facts we focus our efforts on analyzing behavior of first harmonic sidebands.

In the three-tone signals used in the tests an appropriate DC level was selected for the offset sinusoids to consistently keep the signal minimum at the knee voltage (i.e., the threshold of the triode region) of the PA and minimize the effect of RF feedthrough. Sufficient RF drive level (+16 dBm) was used to ensure PA saturation over the range of characterization drain voltages.

4.2 Investigation of Phase Distortion

Sirenza SHF-0289 GaAs HFET was chosen for distortion analysis because previous studies have shown that this PA has negligible memory effects when operated in

conventional two-port mode [26, 39]. The drain bias feed (modulation input) was designed to achieve wideband frequency response by eliminating low frequency bypassing. The class-AB bias current was set to about 30% of the drain saturation current (I_{DSS}), and the gate bias feed had low frequency bypass to terminate any baseband gate current that might flow. The input and output matching circuits were centered at 2.14 GHz to achieve maximum output power and efficiency in saturated operation. In the initial circuit no particular attention was paid to harmonic terminations.

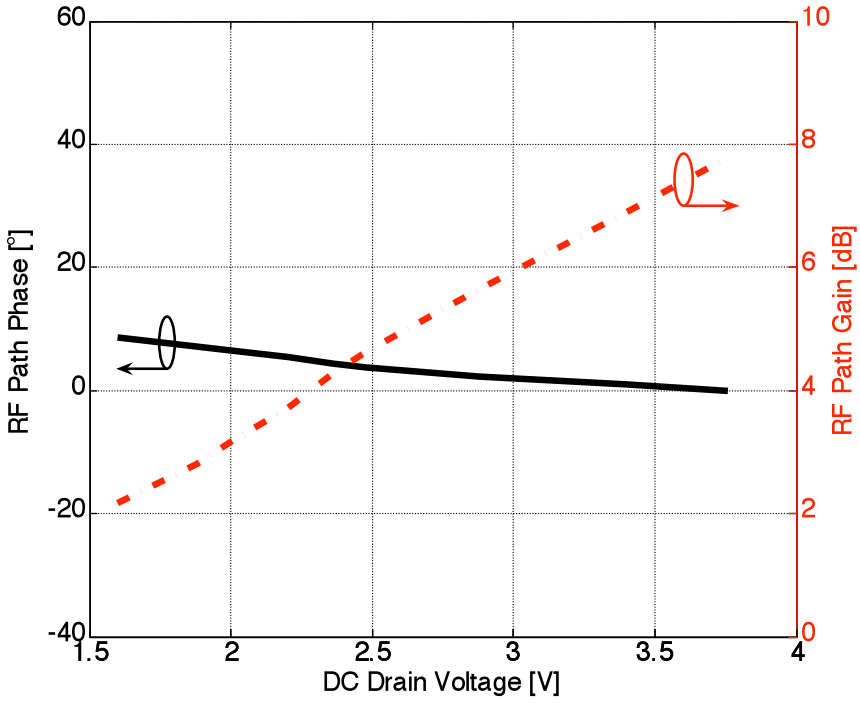

Figure 36: Static modulation transfer characteristics of the EER PA.

The saturated efficiency of the PA vs. drain voltage was found to vary between 40% and 60% over the range of drain voltage from 1.3 V to 6.1 V. The static modulation characteristic over this range was measured using a network analyzer and is shown in Figure 36. The input RF power was kept at a constant +16 dBm, which ensured compression throughout the entire V_{dd} range. Therefore if the input to the

gate of the amplifier does not change, the only way to change the gain and output power is by adjusting the drain voltage. The PA is seen to have a fairly linear static AM characteristic and a small residual static PM characteristic. It should also be noted that in this test the PA did not operate in the back-off region, but rather was always compressed.

Using the previously developed cancellation technique, the relative phase of the first sidebands was measured. The phase of the sidebands is found to deviate less than 5° from the phase of the carrier or from the phase of each other over modulation frequencies ranging from 50 kHz to 5 MHz, and over the range of modulating sinusoid amplitudes of 0.6 V_{pk-pk} to 4.8 V_{pk-pk} above the knee voltage of 1.3 V.

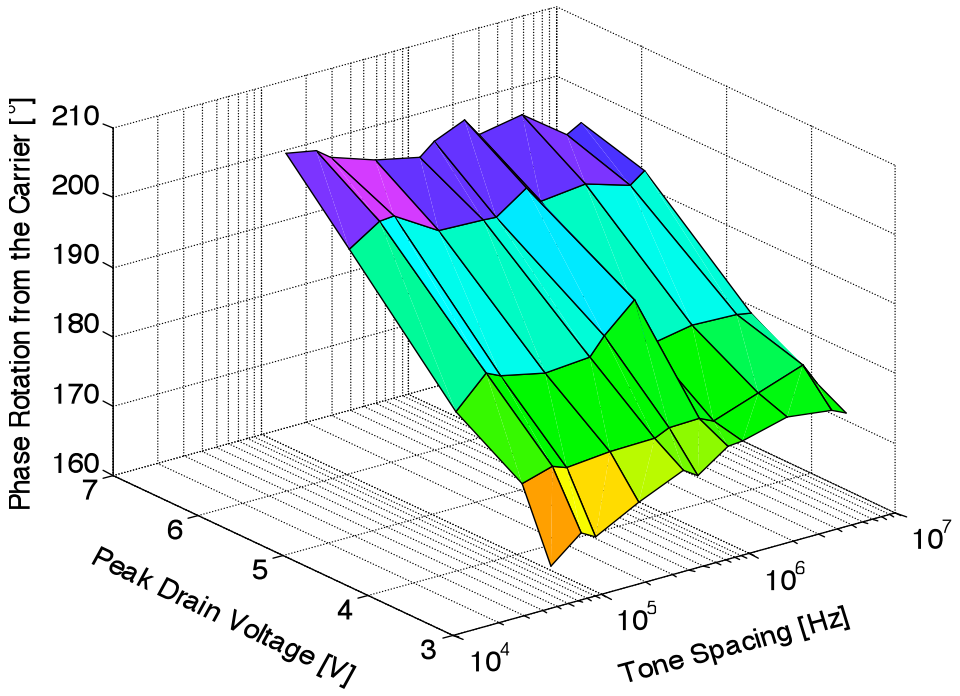

Figure 37: Phase deviation from the carrier of the first harmonic sidebands vs. peak drain voltage and tone spacing.

Next, the phase deviation of the first harmonic sidebands, as seen in Figure 35(b), is measured. The phase of these components is found to deviate significantly from

that of the first sidebands (envelope fundamentals). As seen in Figure 37, the phase deviation of first harmonic sidebands (envelope harmonics) from the carrier varies from 175° to more than 205° over the range of modulation amplitudes, with 0° referenced as in-phase with the carrier. Phase asymmetry of the first harmonic sidebands with respect to each other was found to be less than 3°. This implies that the envelope distortion is dominated by the static AM and PM characteristics and the HFET-based handset EER RF PA does not exhibit significant memory effects. It was also noted that there was little variation of the phase deviation with respect to modulation frequency, which suggests a source of distortion with no significant modulation frequency dependence.

4.2.1 Analysis of the Types of Signals Causing Significant Phase Distortion in EER RF PAs

Further investigation into the origins of EER phase distortion is conducted to reveal the basic types of signals capable of causing the phase distortion described in the previous section [28]. For this analysis the RF PA is arranged in the EER configuration seen in Figure 38. Constant RF signal is supplied to the gate of the device. The level of the input RF signal is chosen such that the device is slightly compressed at the highest V_{dd} level of 6.5 V. This ensures compression under any signal applied to the drain. The fact that the device is always compressed means that gain and output power can be regulated solely by the signals applied to the drain. This arrangement constitutes true EER operation.

Three distinct groups of sinusoidal signals are applied to the drain of the RF PA in EER configuration to test its response. All groups consist of offset sinusoids at frequencies from 50 kHz to 2.5 MHz. The first group of sinusoidal signals applied to the drain of the PA has constant DC level of 3.35 V. The amplitudes of the sinusoids vary from 1 V_{pk-pk} to 5.5 V_{pk-pk}. Qualitative description of these signals can be seen in Figure 39(a). Despite significant variation of the signal amplitude at the drain,

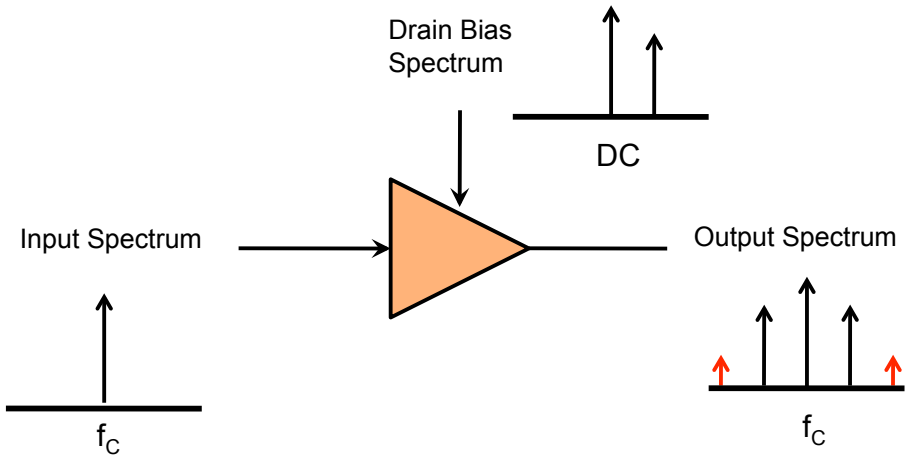

Figure 38: PA operated as a mixer in a true EER mode.

the HFET EER PA under test did not show notable distortion in the form of first harmonic sideband rotation from the carrier. This can be seen in Figure 40 where x-axis is the peak-to-peak amplitude of the sinusoids applied to the drain.

The second group of sinusoids applied to the drain port has constant sine amplitude of 1.35 V_{pk-pk} with a varying DC level, as can be observed in Figure 39(b). The phase distortion measured at the output of the PA can be seen in Figure 41(b). It can be noted that most of the distortion occurs at lower DC level (1.5 - 4 V). The third group of signals applied to the drain has constant minima with proportionately varying amplitudes and DC levels. This signal is similar to the one used in [27] and can be seen in Figure 39(c). Figure 41(a) shows that this group of signals induces significant distortion similar to that induced by the second group. Based on the conducted experiments, it can be concluded that when operated as a polar modulator, the power amplifier exhibits phase distortion determined by the variation of the DC voltage at the drain terminal. At the same time, the amplitude and frequencies of non-DC signals applied to the drain have minimal effect on the distortion exhibited by the EER PA. It should be noted that phase distortion was independent of the frequency of modulating sinusoids for all experiments. Also the phase deviation of

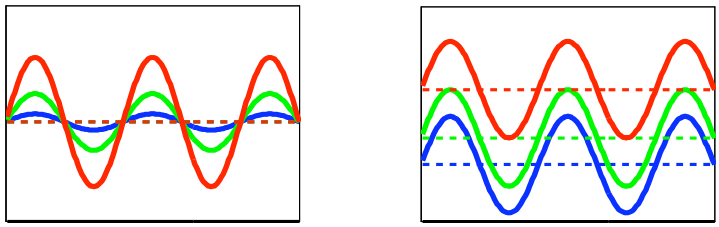

(a) Varying amplitude, fixed DC (b) Fixed amplitude, varying DC

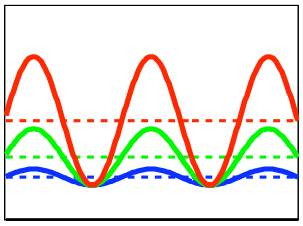

(c) Varying amplitude and DC

Figure 39: Types of signals applied to the drain of the EER PA.

the first sidebands is negligible, as can be seen in Figure 42.

Industry experts expressed a hypothesis that the distortion seen in the RF PA is induced by the nonlinear output capacitance (C_{out}) due to its dependence on the drain voltage [19]. To explore this possibility a PA setup, shown in Figure 43, is put together. Three-tone signal is applied at the gate at a constant power level. High power level of the input signal ensures PA compression throughout the entire V_{dd} range. The compression level is similar to that obtained in the experiments described earlier in this section. Only DC voltage is applied to the drain. Gain and output power of the RF PA is controlled solely by the drain voltage. DC voltage at the drain is varied during the measurement, while phase of the first harmonic sidebands is recorded at the output.

It can be argued that this experiment is significantly different from those performed earlier. While such an argument is correct, this test is effectively used as a tool to determine the effect of nonlinear C_{out} on the phase distortion. The change of V_{dd} ensures the change in C_{out} of the two-port PA similar to that of the EER PA used

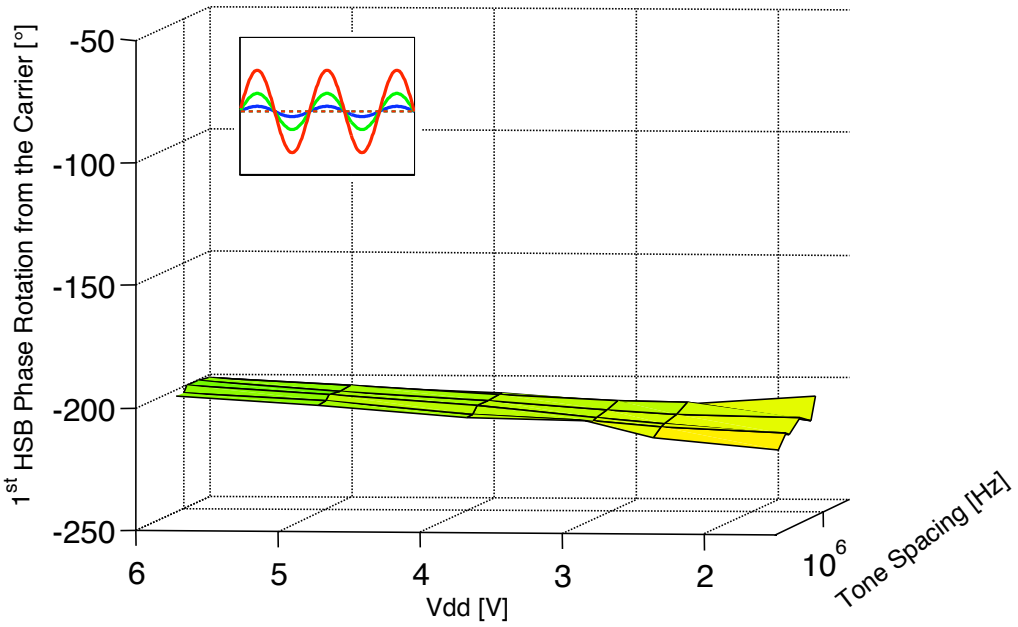

Figure 40: Phase deviation of first harmonic sidebands from the carrier when sinusoids with varying amplitudes and constant DC bias level are applied to the drain of the EER PA.

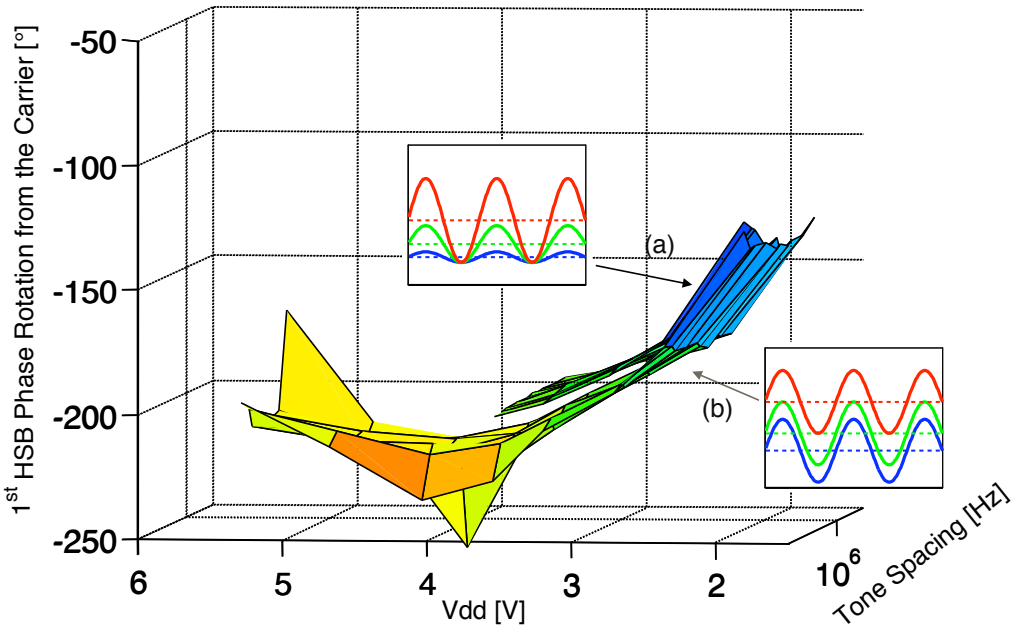

Figure 41: Phase deviation of first harmonic sidebands from the carrier when sinusoids with (a) varying amplitudes DC bias levels, and (b) fixed amplitudes and varying DC bias levels are applied to the drain of the EER PA.

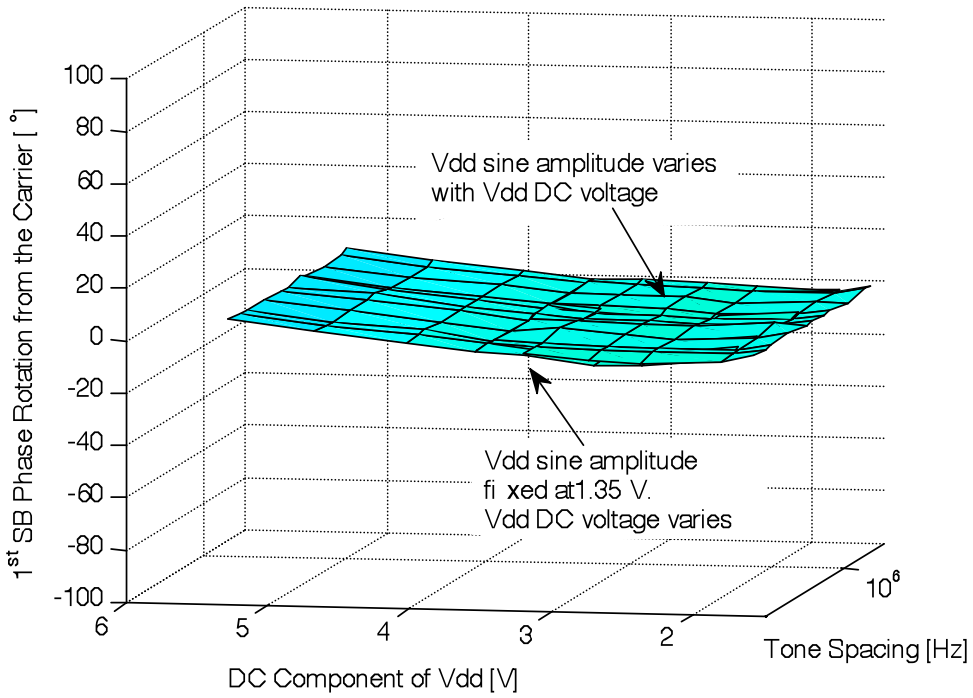

Figure 42: Phase deviation of first sidebands from the carrier for all experiments.

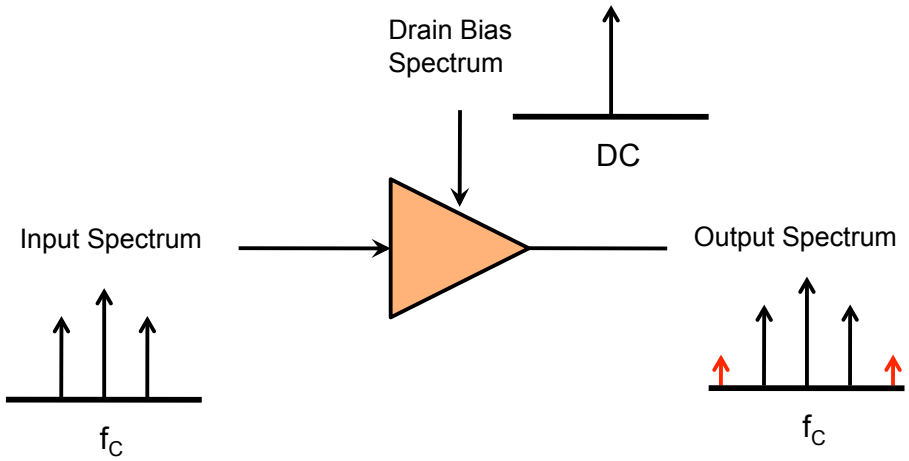

Figure 43: Compressed two-port PA. Resemblance of envelope tracking.

in earlier experiments. As can be seen in Figure 44, minimal V_{dd}-dependent phase distortion is observed at the output. Experimental results from this configuration

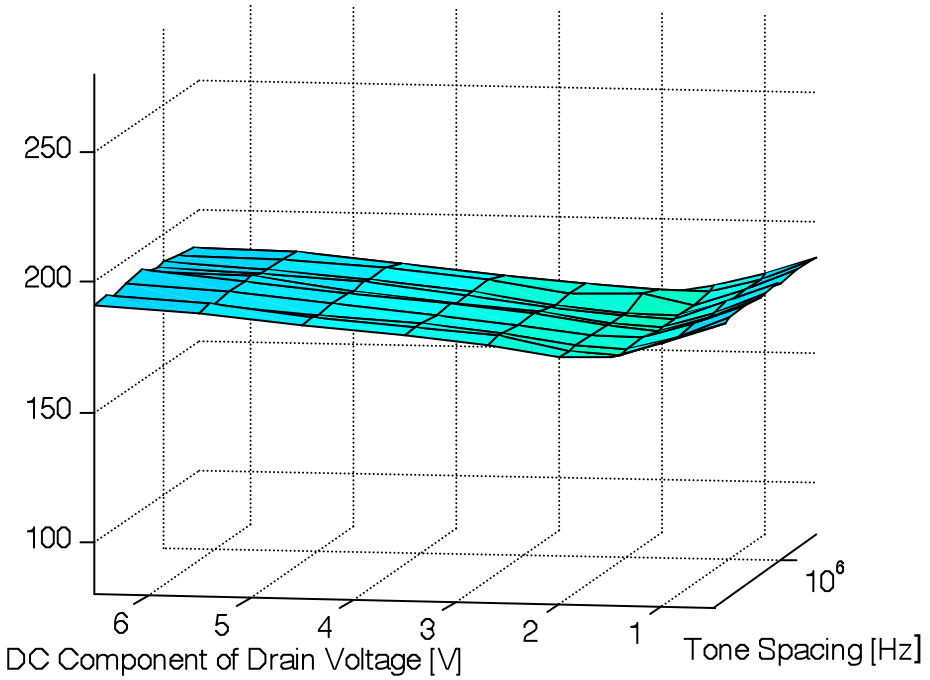

Figure 44: Phase distortion of first harmonic sideband from the carrier for a compressed two-port PA with varying DC V_{dd}. Resemblance of envelope tracking.

suggest that nonlinear C_{out} is likely not the primary cause of the phase distortion. It can be noted that while operating in the EER mode, RF power amplifiers exhibit phase distortion dependent on the average value of the envelope modulation signal applied to the drain of the device. This finding can also be extended to state that amplifiers with modulated signals applied to the gate and DC variation at the drain exhibit significantly smaller phase distortion than those, in which both modulated signal and DC biasing are applied to the drain.

4.3 Mitigation of Phase Distortion through Shorting of Second Harmonic

The identification of the physical origins of phase distortion in EER RF power amplifiers is likely to trigger improvements in linearization systems designed specifically

for polar PAs. At the same time, while primarily working on identifying the physical sources of distortion, we investigate simple circuit techniques aimed at mitigating this phase distortion.

One can leverage the process of identification of distortion sources to develop simple techniques and guidelines for designing low-distortion EER RF PAs. For instance, based on the measurement results reported in the previous section and shown in Figure 37, we theorized that the rotation of the harmonic sidebands is due to the interaction of third-order distortion components with the signals appearing at the drain of the HFET at the second RF harmonic [23]. Figure 45 shows that the second RF harmonic levels, relative to the carrier, are not insignificant. The sidebands of the second RF harmonic signal can mix with the carrier sidebands, and generate a product at the first harmonic sideband frequency within the fundamental band. It is suspected that spurious signals resulting from the mixing of second RF harmonic with the RF carrier, and the third-order distortion products occurring in the nonlinear elements of the RF PA have different phase, and therefore can be added as vectors when they fall in the same frequency band. Thus it is hypothesized that shorting second RF harmonic at the drain would modify the modulated RF waveform in such a way that residual PM is reduced. The contribution of the envelope amplifier to the overall distortion can be ignored. The envelope amplifier, specifically designed as a wideband linear regulator to avoid distortion generation, exhibits spectral purity in excess of -50 dBc, which can be seen in Figure 34.

To validate the theory outlined above, a 1/8-wavelength open circuit coaxial stub is attached to the drain of the PA to suppress the second RF harmonic voltage at the PA output. Figure 45 shows the level of the second RF harmonic before and after the addition of the stub. The phase rotation of the first harmonic sidebands is then measured. A comparison of Figure 46 and Figure 37 shows that harmonic sideband phase deviation of the modified PA is significantly improved over the PA without

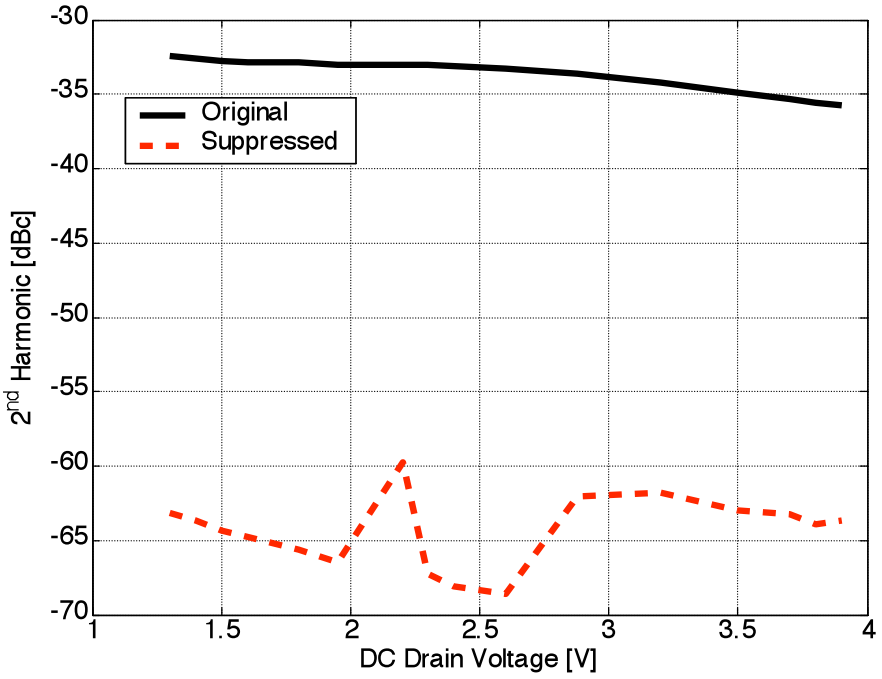

Figure 45: Level of second RF harmonic relative to the carrier before and after suppression.

such modification. The phase deviation of the first harmonic sidebands is reduced from over 30°, as seen in Figure 37, to less than 15° in Figure 46. One can therefore conclude that the addition of the second harmonic terminations to the drain of the PA does indeed impact residual phase modulation distortion (PM) related to amplitude modulation via drain voltage. Suppression of such PM thus reduces the need for phase pre-distortion and allows for simpler amplitude-only pre-distortion techniques to be applied to EER PAs to correct nonlinear modulation transfer characteristics.

It was shown in the literature that intermodulation distortion can be reduced by presenting short circuit to the second harmonic at the output [11]. Thus it was naturally expected to obtain not only lower phase distortion in the EER PA with suppressed second harmonic, but also lower magnitude of the first harmonic sidebands. Unfortunately this turned out not to be the case. As can be seen in Figure 47, EER

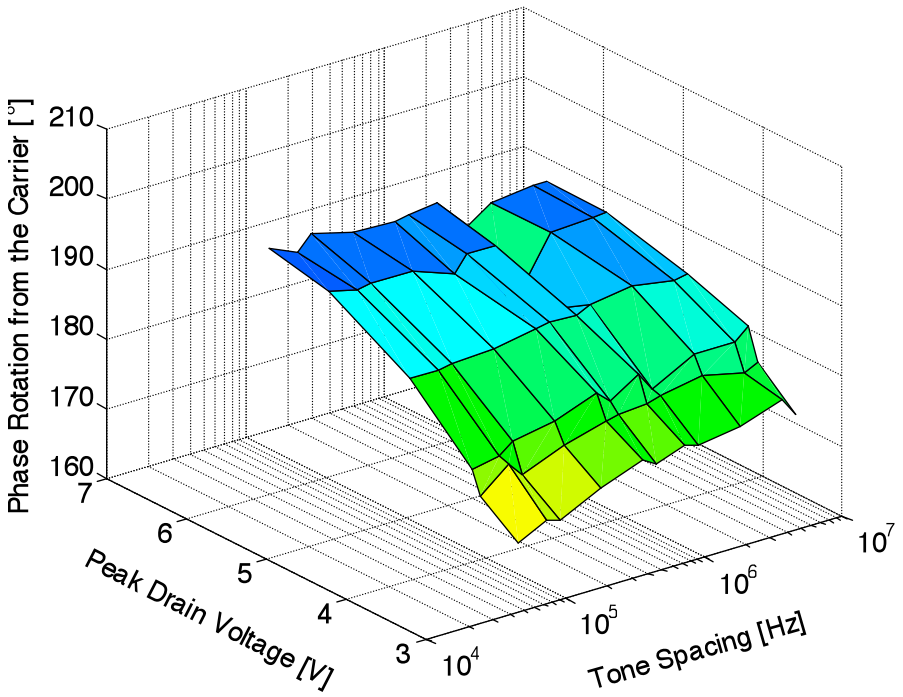

Figure 46: Phase deviation of the first harmonic sidebands from the carrier for the HFET EER PA with suppressed second RF harmonic.

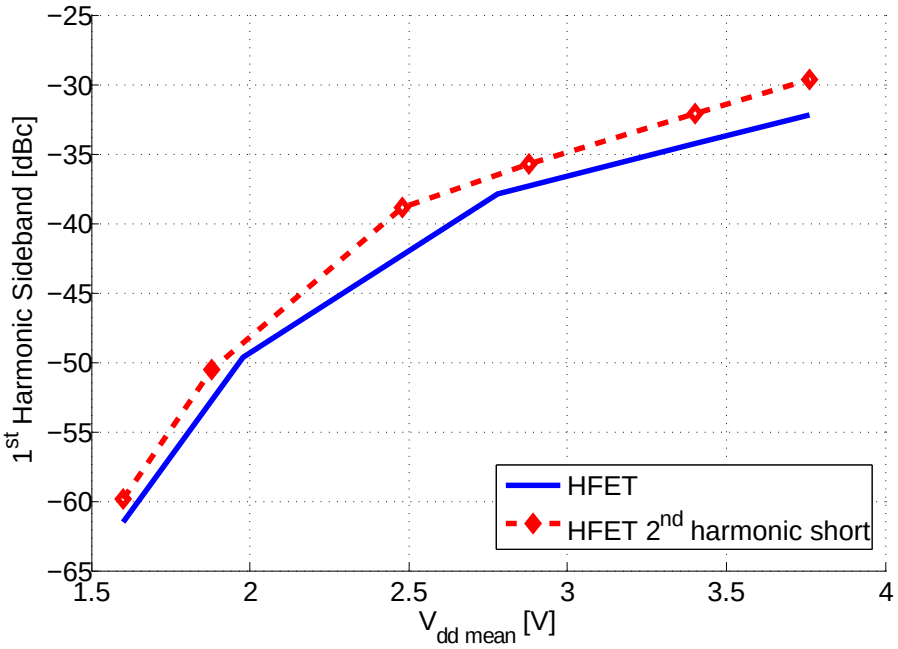

Figure 47: Level of the first harmonic sidebands vs. V_{dd} in the HFET EER PA and the same HFET EER PA with suppressed second harmonic.

PA with the suppressed second harmonic consistently shows 1-2 dB higher first harmonic sidebands than the EER PA without any specific terminations for the second harmonic. This phenomenon can be explained by the fact that the first harmonic sideband components due to the second harmonic are 90° to 270° out of phase with the first harmonic sideband components generated by the odd-order nonlinearities in the device. It can be concluded that in the unaltered EER RF PA a portion of the odd-order nonlinearities at the first harmonic sideband frequency is partially cancelled by the components mixed down from the second harmonic that fall into the same frequency band [1]. In this case, despite the magnitude cancellation, significant phase distortion is produced. When the second harmonic is suppressed, however, the phase distortion is reduced, but so is the magnitude cancellation. As a result, higher levels of the first harmonic sidebands are observed.

Since it is easier to correct amplitude distortion than phase distortion, the technique employing second harmonic shorting can be useful for some EER applications. However a technique capable of reducing both phase and amplitude distortion in the first harmonic sideband frequency band is more desirable. Instead of presenting the short to the second harmonic, one can carefully manipulate second harmonic termination to ensure 180° phase offset between the distortion components due to second harmonic and the IMD3 signals. This arrangement can then reduce both phase and amplitude distortion at the output of the PA.

CHAPTER V

PHASE DISTORTION IN HBT ENVELOPE ELIMINATION AND RESTORATION RF POWER AMPLIFIERS

Most microwave transistors currently used in EER systems were designed for operation in conventional RF PAs with constant bias supplies, and therefore are susceptible to distortion induced by varying supply voltage. In Chapter 4 we talked about dynamic supply-dependent phase distortion in HFET EER power amplifiers. The distortion manifests itself as phase rotation of first harmonic sidebands with respect to the carrier, where first harmonic sidebands in the EER three-tone signal, as seen in Figure 35(b), are equivalent to third order intermodulation distortion products in conventional PAs under two-tone excitation.

Supply-induced phase distortion can complicate linearization of EER PAs. While both amplitude and phase distortion can be linearized in a conventional PA with a single I/Q pre-distorter, an EER RF PA would require different pre-distorter for each signal path. Therefore it is advisable to mitigate one of the distortion effects in order to reduce complexity of pre-distortion system. It is best to alleviate distortion effects in the phase path of EER RF PA since the amplitude path can be corrected by analog feedback.

This chapter investigates phase distortion in EER GaAs HBT power amplifiers and experimentally identifies its origins. In addition, a simple circuit technique is presented to mitigate phase distortion occurring in EER RF PAs [29].

5.1 Hypothesis and Simulation

First harmonic sidebands in EER power amplifiers closely resemble IMD3 components seen in conventional RF PAs under two-tone excitation. Due to this fact analysis of distortion of EER PAs is based on a vast pool of knowledge generated for analysis of third-order intermodulation distortion. It is well known that typical IMD3 components are sums of vectors present at the intermodulation frequencies. These vectors are generated due to contributions from the transistor's nonlinear current source and capacitances, as well as signals mixed down from second harmonic and up from base-band frequency [2]. All these components have different phase. If two dominant components are out of phase and one of them grows faster than the other with varying collector voltage, phase rotation of the resultant vector will be observed.

It has been shown that IMD3 components generated in an HBT nonlinear current source and base-emitter capacitance are either parallel or antiparallel, and thus are not capable of producing phase rotation of the resultant vector [43]. However, it has also been reported that IMD3 distortion voltage at the base of the transistor applied to the linear portion of transistor's parasitic capacitances creates current vectors perpendicular to those generated by nonlinear portion of the current source [1].

Even though the contribution of C_{bc} to the overall IMD3 vector was found to be negligible in [1], its impact is suspected to be significant in EER PAs due to a notable increase in base-collector capacitance with decreasing V_{cb}. A hypothesis is made that dependence of C_{bc} on changing base-collector voltage is primarily responsible for phase rotation of first harmonic sidebands.

5.1.1 Device Parameters

To validate the assumption that C_{bc} is primarily responsible for phase distortion in EER RF PAs, two nearly identical amplifiers were designed and fabricated using similar GaAs HBT processes. Device layout and process selection are performed to

ensure the same gain and 1dB compression point. The input and output impedance for both devices are also similar. Similar input and output impedances enable the use identical matching networks for both amplifiers. Each device is comprised of 24 $160\mu m^2$ cells. Both HBT A and HBT B devices are mounted on identical circuit boards with low-pass input and high-pass output matching networks. Identical design and implementation of the matching networks ensures nearly identical fundamental and harmonic terminations. This design approach made it possible to achieve similar performance metrics for both PAs shown in Table 3. The measurements are performed at a constant $V_{cc} = 3.6$ V for both devices. Collector currents are recorded at 100 mA and 90 mA for HBT A and B, respectively.

Table 3: Performance of class-AB power amplifiers based on HBT A and HBT B devices.

	HBT A	HBT B
S_{21} at 2.5 GHz	11.04 dB	11.06 dB
P_{out} $1dB$ at 2.5 GHz	26.74 dBm	26.49 dBm

Despite similar RF performance, HBT A and HBT B devices have significant differences in their nonlinear depletion base-collector capacitance. C_{bc} of both devices is nearly equal at V_{cb}=3 V, which explains similarities in their RF performance under class-AB bias conditions. However depletion C_{bc} in HBT A changes significantly faster than the capacitance in HBT B with decreasing collector-base voltage. As a result, by the time collector-base voltage drop reaches -0.5 V, depletion C_{bc} of HBT A is 50% higher than the equivalent capacitance of HBT B, as can be seen in Table 4. The increase in depletion capacitance over decreasing V_{cb} voltage is nonlinear: the majority of the change is happening at lower collector-base voltages. The rate of change of depletion C_{bc} vs. V_{cb} of HBT A is roughly twice that of the same capacitance in HBT B.

HBT device designers often use collector doping to control depletion base-collector

Table 4: Depletion capacitance and its dependence on V_{cb} for HBT A and HBT B devices.

	HBT A	HBT B
C_{bc} at $V_{cb} = 3V$	*same*	
C_{bc} at $V_{cb} = -0.5V$	$1.5x$	x
$-\partial C_{bc}/\partial V_{cb}$	$2y$	y

capacitance [48]. It therefore comes as no surprise that HBT A and HBT B have different levels of collector doping, while maintaining similar levels of doping at the base, as can be observed in Table 5. Lighter collector doping of HBT B is likely responsible for lower depletion C_{bc} compared to HBT A.

Table 5: HBT A and HBT B parameters

	HBT A	HBT B
Collector doping	*heavy*	*light*
Base doping	*same*	

In the absence of other significant differences between the devices it is hypothesized that HBT A, with its larger and more nonlinear C_{bc}, would exhibit higher phase distortion than HBT B. To test this assumption large signal simulation is performed in Agilent ADS with two-tone harmonic balance. A +16.5 dBm CW RF signal at 2.5 GHz is applied to the base, biased at 1.25 V. Groups of offset 1 MHz sinusoids with fixed minima and increasing means and amplitudes, as seen in Figure 39(c), were applied to the collector. The minima of sinusoids were set to $0.67V$ and the maxima varied from 1.4 V to 3.6 V. Under these input signals PA acts as a mixer, effectively producing a three-tone output with harmonic sideband distortion components qualitatively described in Figure 35.

Preliminary circuit simulation using standard compact HBT models confirmed that first harmonic sideband phase rotation with respect to the carrier was dependent

on base-collector capacitance. As can be seen in Figure 48, the largest difference in phase rotation between HBT A and HBT B occurred at lower V_{cc} level. Maximum phase rotation corresponds to the maximum difference in C_{bc} and $-\partial C_{bc}/\partial V_{cb}$, both of which occur at lower V_{cc} as well.

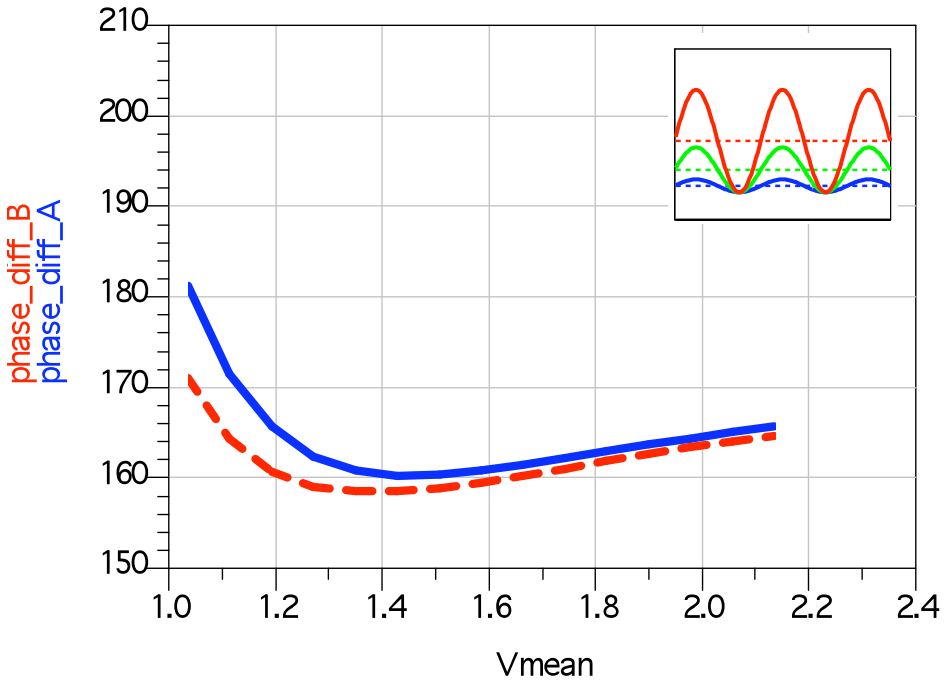

Figure 48: Simulated phase rotation of first harmonic sidebands vs. V_{cc} at tone spacing of 1 MHz in HBT A (solid) and HBT B (dashed).

5.2 Measurement Results

A setup similar to that described in Section 4.1 is used to measure phase distortion in both amplifiers. Same input signals and biasing are used as in the simulation described in the previous section. However, offset sinusoids applied to the collector have frequencies ranging from 50 kHz to 2.5 MHz to test dependence of phase distortion on the frequency of modulating signals. The same signals were used to map out the phase response of HFET GaAs PAs in Chapter 4. The RF input signal level is held at +16.5 dBm to ensure compression throughout the entire V_{cc} swing. This ensures that gain and P_{out} are solely dependent on V_{cc}. One can trace the trajectory of output

signal by following the line of EER operation across AM-AM curves taken at various static V_{cc} levels in Figure 49.

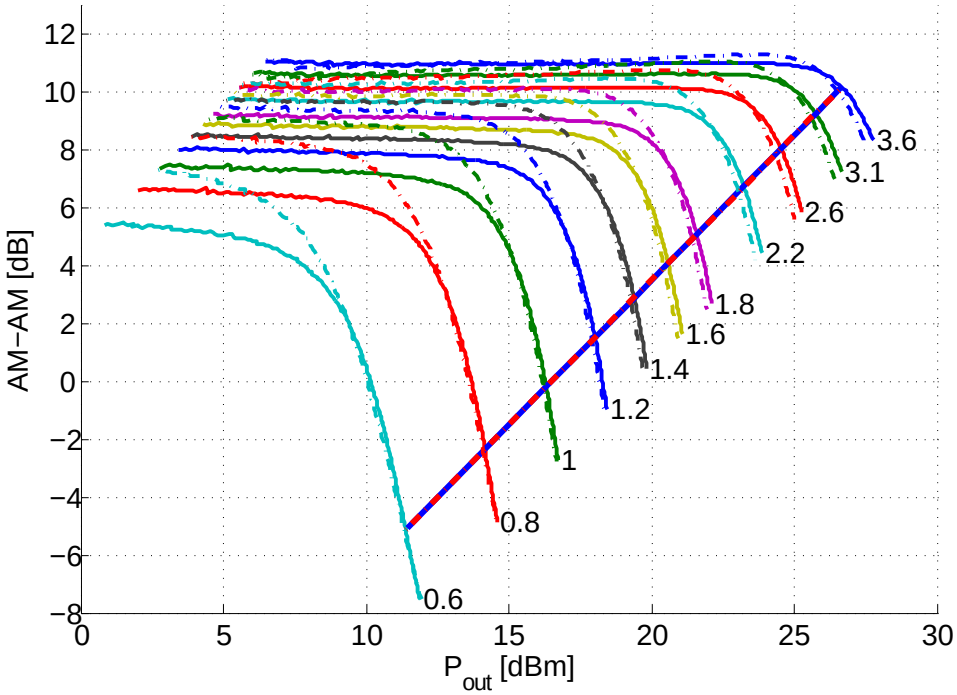

Figure 49: Measured AM-AM response vs. P_{in} and V_{cc} of HBT A (solid) and HBT B (dashed). Overlapping lines of EER operation are also shown for HBT A (blue solid) and HBT B (red dashed). Numbers alongside curves represent static V_{cc} in volts at which AM-AM measurements were taken.

The measurement performed revealed phase distortion similar to that found in GaAs HFETs [27]. Similarly, first harmonic sideband rotation is found to be independent of tone spacing of V_{cc} signal, as can be seen in Figure 50. At the same time HBT A surprisingly shows much lower distortion than HBT B, which is contrary to the hypothesis and simulation described earlier.

5.2.1 Model Imperfections

Deeper analysis of the models commonly used for simulation revealed that standard HBT compact models are quite good at predicting deviations in RF performance stemming from nonlinear depletion capacitance, which is larger in HBT A. However, these models often fail to accurately predict performance of RF devices resulting

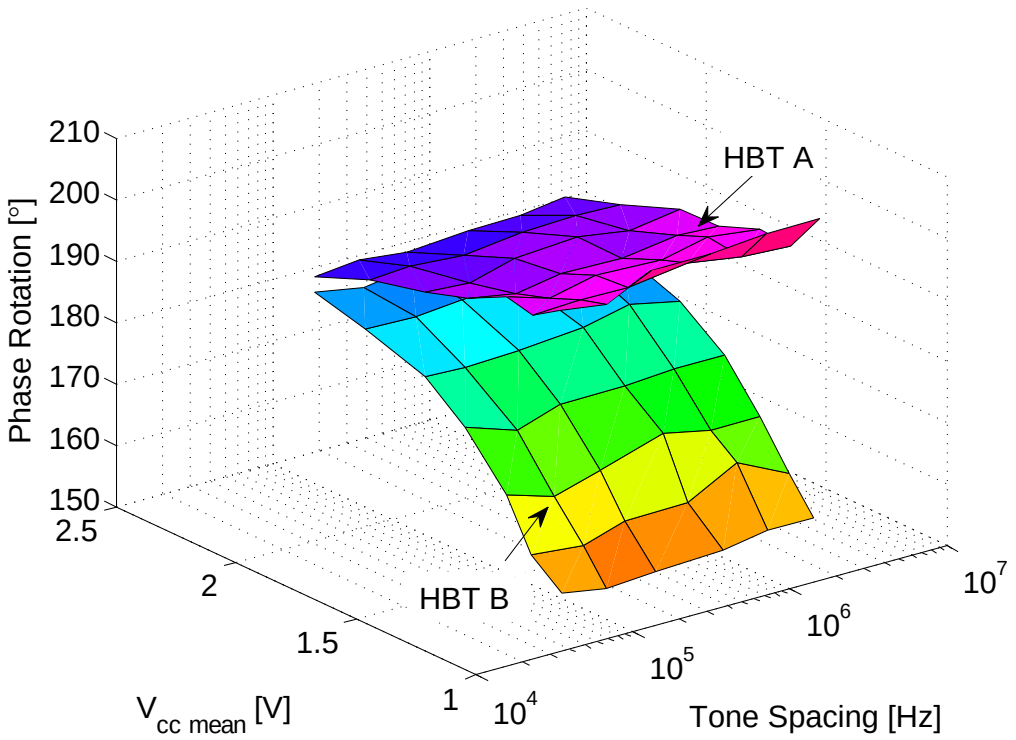

Figure 50: Measured phase rotation of first harmonic sidebands vs. V_{cc} and tone spacing in HBT A and HBT B.

from minority carrier injection, commonly occurring in EER RF power amplifiers at negative V_{cb} [52]. Minority carrier injection effectively increases C_{bc} once the base-collector junction becomes forward-biased. The larger the buildup of minority carrier charges in the collector, the slower can the junction voltage change, since the charges stored in the collector need to be dissipated or recombined first. This effectively increases recovery time, which can be modeled as an increase of C_{bc} [16].

It should be noted that minority carrier injection is dependent on collector doping. Lightly doped collectors in GaAs HBTs help device designers achieve lower C_{bc} under typical RF PA operation, where the base-collector junction remains reverse-biased most of the time. However, lightly doped collectors are more prone to minority carrier injection, which triggers an increase in collector transit time. This phenomenon effectively increases C_{bc} once the junction becomes forward-biased [48].

In the case of HBT A and HBT B, as the base-collector junction becomes forward-biased, the much lighter collector doping in HBT B produces a larger C_{bc}, due to minority carrier injection. This effect is believed to be significantly smaller in HBT A due to its heavier collector doping. As a result, the effective C_{bc} comprising of components due to depletion and injection is higher in HBT B at low collector voltages and large base input signal. A larger effective C_{bc} in HBT B is in turn responsible for more severe phase distortion generated in the device. While the dominant origins of C_{bc} in EER PAs are revised from the original hypothesis, the finding that large nonlinear C_{bc} is responsible for the phase distortion in HBT EER RF power amplifiers is still valid and supports the original hypothesis and simulation.

5.3 Mitigation of Phase Distortion by Push-Pull Cancellation

In the previous section voltage-dependent base-collector capacitance was determined to be the dominant cause of first harmonic sideband rotation with respect to the carrier. In light of this explanation a common-emitter push-pull structure with identical HBT devices is chosen to reduce the portion of C_{bc} linearly-dependent on V_{bc}. The collectors of these devices are driven in phase by the same signals applied earlier to single-ended parts.

To qualitatively analyze cancellation of phase distortion signals in push-pull EER PA, a simple mathematical analysis is performed. This analysis is neither meant to fully describe circuit behavior, nor is it intended for rigorous modeling. It is rather used as a quick and simple way to identify major signal components cancelled in the push-pull EER RF PA.

Using Figure 51 as a guide, one can see that current i_L can be written as a difference between $-g_m v_1$ and i_{Cbc}. Using Miller approximation, i_{Cbc} can be written as

$$i_{Cbc} = (v_1 - v_2) \cdot jwC_{bc} = v_1(1 + g_m R_L) \cdot jwC_{bc}. \tag{18}$$

Applying KCL at the load, one can determine that

$$i_L = -g_m v_1 - j v_1 (1 + g_m R_L) w C_{bc}. \tag{19}$$

As described in [42] voltage-dependent capacitance can be modeled as a polynomial:

$$C_{bc} = a_0 + a_1 v_1 + a_2 v_1^2 + \ldots. \tag{20}$$

By substituting (20) into (19) and multiplying v_1 throughout, one obtains i_L with distinct in-phase and quadrature components:

$$i_L = -g_m v_1 - j(1 + g_m R_L) w (a_0 v_1 + \underline{a_1 v_1^2} + a_2 v_1^3 + \ldots). \tag{21}$$

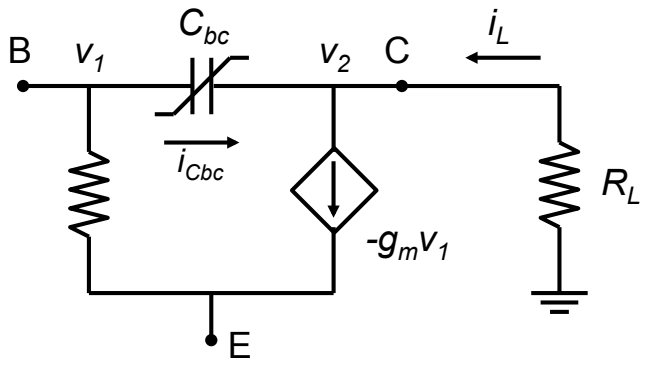

Figure 51: Simplified HBT model.

It can be fairly noted that while representing C_{bc} as a polynomial in (21), g_m should be expanded as a nonlinear component as well. However, Lee et. al found nonlinear C_{bc} to be the strongest contributor to third order intercept point (IP3) when collector voltage was varied [41]. While nonlinear g_m certainly contributes to distortion generation, part of this distortion is reduced by antiparallel distortion generated in base-emitted capacitance [43]. Exact comparison of distortion resulting from nonlinear g_m and nonlinear C_{bc} under low V_{cc} requires more accurate device models and proprietary simulation software. Since this level of device analysis is out of the scope of this work, g_m is treated as a constant in the quick analysis of push-pull cancellation.

Cancellation of odd-order voltage-dependent terms of C_{bc} can be achieved by arranging two identical transistors in push-pull configuration, as shown in Figure 52. The current at the output transistor $X+$ can be denoted as i_L^+, v_1 being the voltage at its base. Current i_L^- can be denoted as the current at the output of transistor $X-$, $-v_1$ being the voltage at its base. The current at the output of the balun will then be equal to the difference between i_L^+ and i_L^-

$$i_L^+ - i_L^- = -2g_m v_1 - j2(1 + g_m R_L)w(a_0 v_1 + a_2 v_1^3 + \ldots) \tag{22}$$

It can be seen from (22) that the term $\underline{a_1 v_1^2}$, representing distortion introduced by the portion of C_{bc}, linearly varying with voltage across it, is cancelled. Cancellation of this signal significantly reduces dependence of the imaginary term on base-collector voltage. Thus the phase rotation of first harmonic sidebands is also reduced. It is also worth mentioning that all odd-order terms of C_{bc} are cancelled when the EER PA is operated in push-pull configuration.

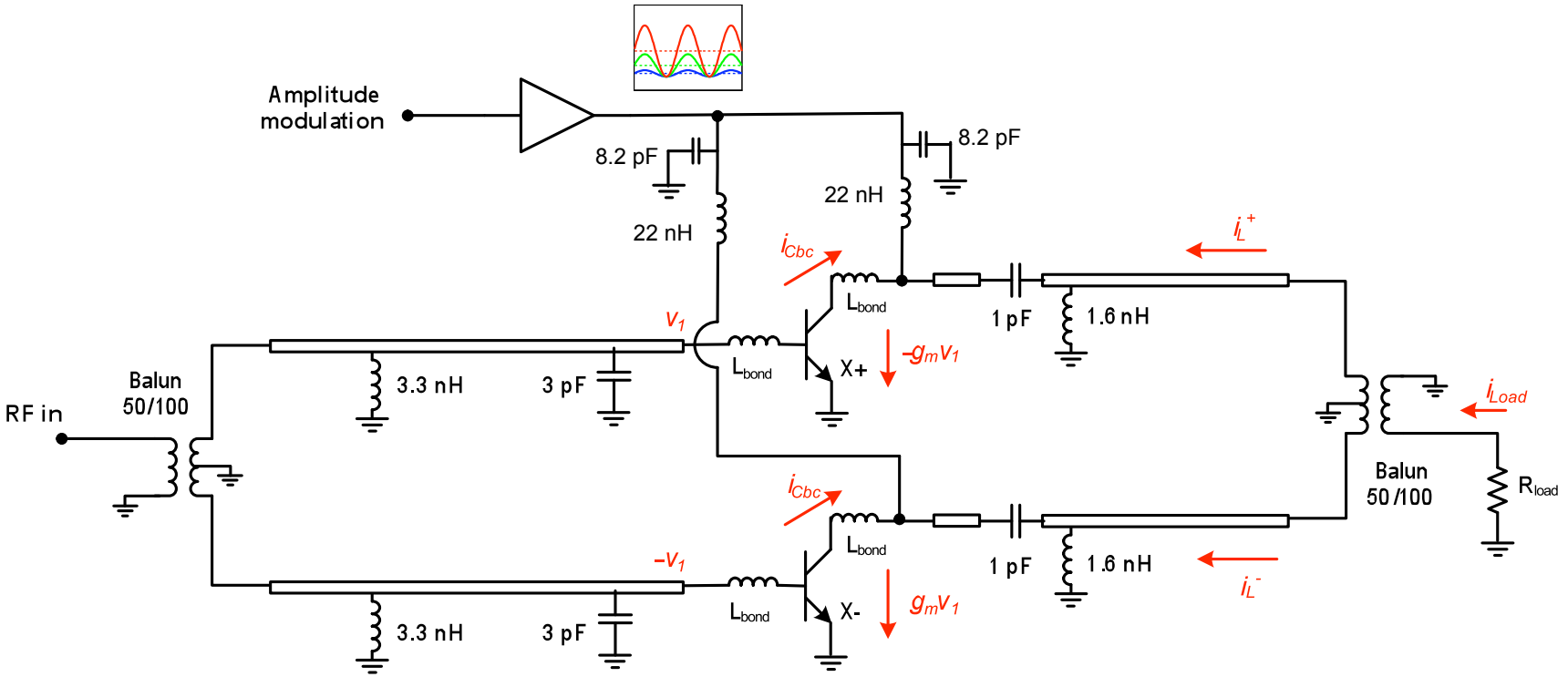

Figure 52: Schematic of the push-pull circuit for both HBT A and HBT B devices.

5.3.1 Push-Pull Implementation

To test the hypothesis of partial C_{bc} cancellation through push-pull, pairs of identical HBT A and HBT B devices are implemented on the same die to ensure good matching of device parameters for the push-pull system. These circuits are tuned using matching networks and boards similar to those used by their single-ended counterparts. Murata 2.5 GHz 50/100 Ω wideband balun transformers are used to convert between balanced and unbalanced signals. The circuits are tested with P_{in} of +19.5 dBm to ensure that individual devices in the push-pull structure are operating at gain compression levels close to those used in the single-ended tests. A photograph of a board and a die used for push-pull EER PA measurements is shown in Figure 53.

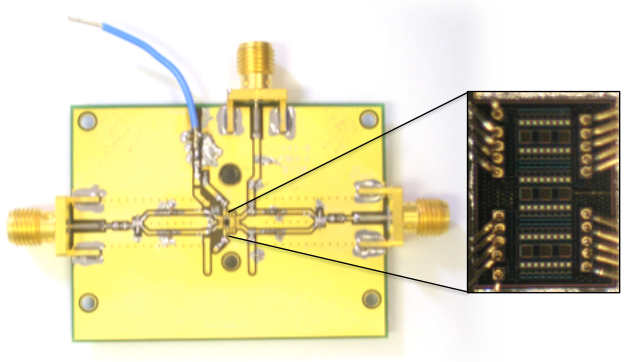

Figure 53: Board used for HBT A and HBT B push-pull PAs with HBT A die (HBT B looks identical).

While seemingly simple, push-pull EER PAs should be implemented with care to avoid stability problems. Odd-mode parametric oscillations often plague push-pull PA designs [5]. In addition EER PAs cannot use large decoupling capacitors on supply rails due to the fact that their collector or drain terminal is used for amplitude modulation. Therefore bypass capacitance has to be small enough not to interfere with base-band amplitude signals applied to the collector. The envelope amplitude signal can often have bandwidth several times larger than the modulated RF signal at the output of the PA. An attempt to combine EER and push-pull designs in one

RF PA should be justifiably expected to pose stability challenges to the designer.

It seems to be common wisdom that EER RF amplifiers are unconditionally stable due to significant compression [45]. While this might be true, EER amplifiers are not any more stable than conventional PAs, when large output power is required, which forces the EER PA to operate in the low compression environment without sufficient bypassing.

A technique developed by Almudena Suarez for stability analysis was successfully used to identify parametric oscillations in the push-pull PA [69]. Matching networks were then redesigned to provide high out-of-band rejection and quell parametric oscillation. In addition to matching network redesign, the frequency of the RF input signal had to be shifted from 2.5 GHz to 2.8 GHz for testing push-pull amplifiers. However it is believed that this small shift in frequency does not materially interfere with the results obtained from measuring phase distortion in push-pull EER RF PAs.

5.3.2 Results of Distortion Mitigation

As can be seen in Figure 54, phase rotation of first harmonic sidebands is significantly lower when the PA is used in push-pull configuration for both HBT A and HBT B devices. Milder phase rotation of 15° in single-ended HBT A device is reduced to merely 5° over the range of dynamic V_{cc} swing. Significant phase distortion of 30° in HBT B is reduced to only 10°. Even though phase rotation is cut in third for each case, first harmonic sidebands are still not exactly 180° out of phase from the carrier as would be expected if all distortion came from a nonlinear current source. This can be explained by the fact that not all signals due to nonlinear C_{bc} have been cancelled by the push-pull arrangement. However, the remaining phase deviation from 180° has a significantly lower dependence on supply voltage and therefore can be corrected in a static manner with a reasonable degree of accuracy. V_{cc}-dependent phase distortion in EER PAs would require linearization, in which phase correction would have to be

synchronized with amplitude correction in real-time. Flattening the phase response of an EER PA enables the use of linearization architectures where the phase and amplitude of the input signals are adjusted independently.

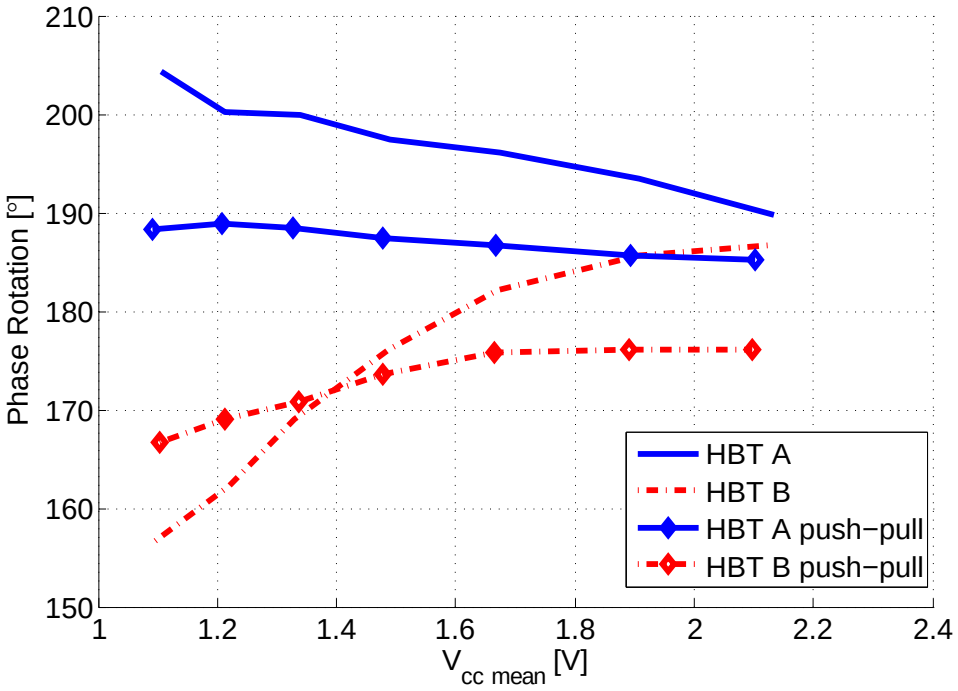

Figure 54: Measured phase rotation of first harmonic sidebands vs. V_{cc} in single-ended HBT A and HBT B, as well as in their push-pull configurations.

It is also worth noting that the push-pull configuration does not increase the level of first harmonic sidebands, as can be seen in Figure 55. In fact, the level of first harmonic sidebands in push-pull EER PAs is consistently 1-2 dB lower than in corresponding single-ended PAs. This fact makes the technique utilizing push-pull architecture more advantageous from the distortion mitigation standpoint than the one based on shorting second harmonic, described in Chapter 4.3.

Despite its design challenges push-pull architecture can be viewed as a practical method of reducing phase distortion, as well as adjacent channel emissions in EER RF power amplifiers.

In this chapter supply-dependent phase distortion was measured in GaAs HBT

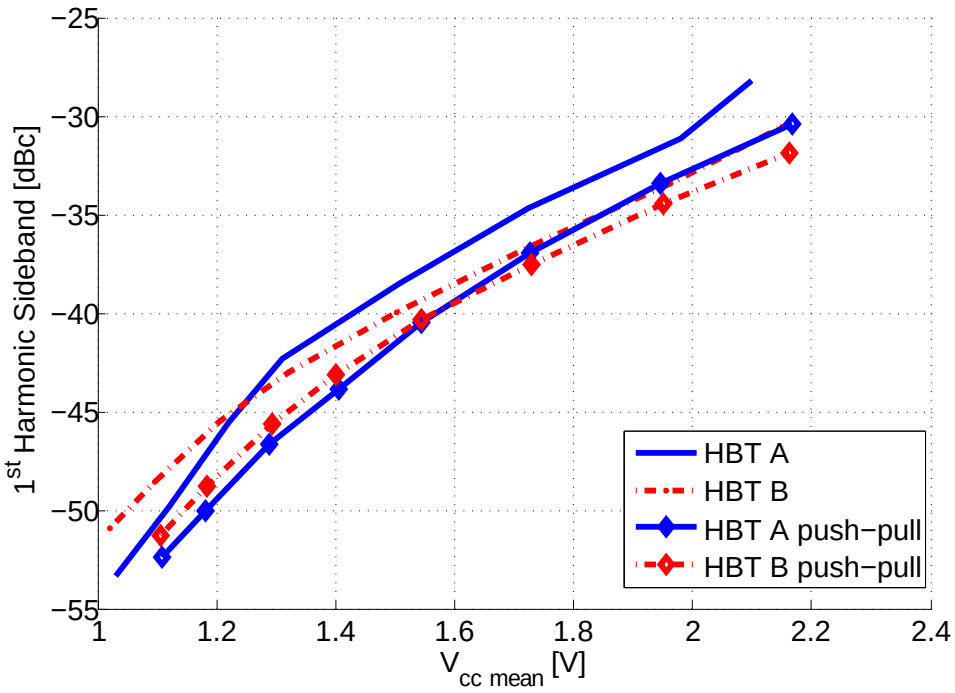

Figure 55: Measured level of first harmonic sidebands vs. V_{cc} in single-ended HBT A and HBT B as well as in their push-pull configurations.

EER RF power amplifiers. It has been experimentally shown that nonlinear base-collector capacitance is primarily responsible for this distortion. The dominant distortion mechanism in C_{bc} under varying V_{cc} operation has been traced to minority carrier injection occurring in forward-biased base-collector junction. Devices with a heavier-doped collector were outlined as preferred RF transistors in EER PAs as their minority carrier injection has been reported to be significantly lower than that of devices with a lightly-doped collector.

Push-pull configuration of EER RF PAs has been proposed as a simple technique to mitigate supply-dependent phase distortion, due to its ability to cancel odd-order voltage-dependent components of a nonlinear C_{bc}. Measurement of phase distortion in push-pull EER RF PAs revealed a 67% reduction in phase distortion and a 1-2dB reduction in levels of adjacent channel emissions compared to their single-ended counterparts.

CHAPTER VI

CONCLUSIONS AND FUTURE WORK

This chapter provides a summary of the research presented in the dissertation. The summary is followed by a discussion of possible applications of principles outlined in the thesis. The original contributions are further highlighted, followed by a brief discussion of suggestions for future research.

6.1 Summary

This dissertation presented a study of phase distortion in envelope elimination and restoration radio frequency power amplifiers. Specifically, supply-dependent phase of out-of-band distortion components was analyzed in detail.

To better understand out-of-band phase distortion, occurring in EER RF power amplifiers, phase distortion was analyzed in conventional power amplifiers. Specifically, a measurement system was developed that allowed measurement of phase rotation of intermodulation products. This phase rotation of IMD components with respect to each other was used as a basis for analysis of memory effects, occurring in conventional power amplifiers.

Phase and amplitude asymmetry data, collected with the measurement system, were used to construct memory effect signatures in the complex plane. A novel physically-based memory model was developed to interpret the memory effect signatures. The model enabled drawing a clear distinction between thermal and bias-related memory effects in RF power amplifiers. The knowledge about the origins of memory effects, and their prevalence in particular ranges of output power and frequency of the modulation signal, was used to predict improvements in linearization performance achieved in the transmission systems, employing different modulation

standards. Detailed knowledge of memory effects, occurring in a given RF power amplifier, makes it possible to design application-specific pre-distortion systems, which are likely to be much leaner than the traditional black-box approach.

The knowledge acquired in the process of analyzing phase distortion in conventional RF PAs was extended to the analysis of phase distortion in EER RF power amplifiers. Specifically, supply-dependent phase rotation of out-of-band distortion components with respect to the carrier was analyzed. Further investigation revealed the dependence of this rotation on second harmonic termination, as distortion signals were down-converted from the second harmonic band and added as vectors to the distortion components, generated by the third-order nonlinearity of the PA.

Voltage-dependent base-collector capacitance was found to be the dominant source of phase rotation in the HBT-based EER RF PAs. Large supply-dependent variation of base-collector capacitance in HBTs was traced to the minority carrier injection, occurring predominantly in HBT devices with lightly-doped collectors.

Detailed analysis of distortion origins enabled the development of simple mitigation techniques. Shorting the second harmonic reduced phase rotation, seen in an HFET-based handset EER PA in half. Because the distortion component due to the second harmonic was 90° to 270° out of phase, shorting the second harmonic increased the magnitude of the resultant distortion vector. However, careful design of second harmonic termination can decrease both the phase rotation and the magnitude of intermodulation products.

Lastly, push-pull EER architecture was proposed to reduce the distortion stemming from nonlinear base-collector capacitance. This architecture yielded 67% reduction in phase rotation and 1-2 dB improvement in the magnitude of the resultant intermodulation products. This technique was successfully tested and yielded similar results with two HBT-based EER amplifiers, originally exhibiting different levels of supply-dependent phase distortion.

6.2 Applications

Development of multimode, multiband EER PAs was the main motivation for this work. The findings, summarized in this dissertation, can be used to advance the development of RF transistors, specifically designed for EER operation. Specifically, the principles outlined in Chapter 5 can be used by device designers to minimize phase distortion in EER RF transistors by controlling nonlinear base-collector capacitance at low collector voltages. Also, distortion mitigation techniques, such as modified second harmonic termination and EER push-pull architecture, give circuit designers tools to develop EER systems with lower phase- and amplitude- out-of-band distortion.

Lower inherent distortion in the phase path of EER RF transistors can reduce the need, or completely eliminate, pre-distortion systems, currently used to achieve acceptable linearity for EER PAs. Reduction in the complexity of linearization systems, applied to EER PAs will significantly lower the cost and power consumption of envelope elimination and restoration transmitters, thus making them more suitable for use in handset applications. While this research was primarily targeting handset applications in the cellular band, it can be extended to encompass basestation solutions, and circuits, operating at higher RF frequencies.

6.3 Contributions

The key original contributions of this work are outlined below.

1. Attribution of measured memory effects in conventional power amplifiers to their physical origins.

    - Development of a system, comprised of standard RF test equipment, capable of accurately measuring memory effects in RF power amplifiers.
    - Development of a power amplifier model, based on the physical origins of

the memory effects.

- Using the knowledge about the origins of memory effects to predict PA behavior under pre-distortion linearization.

2. Identification of origins of phase distortion occurring in the EER RF power amplifiers.

   - Development of a system, comprised of standard RF test equipment, capable of measuring out-of-band phase distortion in EER RF PAs.
   - Design of a linear regulator, capable of driving the drain of handset EER RF PAs with minimal baseband distortion.
   - Attribution of phase rotation of out-of-band distortion components in EER RF power amplifiers to the signals mixed down from second harmonic frequency and a portion of base-collector capacitance.

3. Development of techniques for mitigating phase distortion in EER RF power amplifiers.

   - Shorting of the second harmonic to reduce its out-of-phase contribution to the total out-of-band distortion vectors.
   - Use of push-pull circuit architecture for EER RF PAs to cancel distortion, produced by linear dependence of base-collector capacitance on collector-base voltage.

6.4 Future Work

A number of research topics outlined in this section will facilitate the development and further adoption of multimode envelope elimination and restoration RF power amplifiers.

It has been determined that traditional AM-AM and AM-PM measurements do not adequately describe the transfer function of a memoryless EER PA. Therefore an addition of amplitude-to-phase distortion is necessary to make a full transfer function of the three-port memoryless device. Using these three metrics, a three-port behavioral model can be developed for EER RF PAs.

Current compact models do not adequately capture all the processes, occurring in RF transistors under low voltage supply operation [52]. Better modeling of RF transistor operations at low supply voltages and incorporation of empirical data into existing compact models will equip RF designers with the tools to efficiently realize EER RF power amplifiers. These EER design tools can be significantly enhanced by adapting the technique of attributing IMD distortion, developed by Aikio and Rahkonen, for the use with EER systems [1, 2]. The performance of EER systems, designed for lower phase distortion can be experimentally evaluated by using complex modulation signals. For completeness, supply-induced phase distortion should also be evaluated in envelope tracking amplifiers, where the amplitude of the phase signal is preserved during the cartesian-to-polar conversion.

APPENDIX A

RECURSIVE IMPLEMENTATION OF A BISECTION ALGORITHM IN MATLAB

```
function [minimum, minphase] = binaryphaseadjust(sig4, agesa, ...
phase_lower, phase_upper, tolerance)
%using bisection search for phase determination
%sig4, agesa — GPIB handles of signal generator and spectrum analyzer
%phase_lower, phase_upper — search boundaries
%tolerance — search for answers within this tolerance


dTolerance = tolerance;

phase(1) = phase_lower;
phase(2) = phase_upper;
mag_at_phase1 = magnitudeatphase(sig4, agesa, phase(1));
%find resultant IMD3 magnitude at a given phase setting
mag_at_phase2 = magnitudeatphase(sig4, agesa, phase(2));

phase_middle = (phase(2)—phase(1))./2+phase(1);
mag_at_phase_middle = magnitudeatphase(sig4, agesa, phase_middle );

  phase_first_quarter = (phase_middle — phase(1))/2+phase(1);
  phase_third_quarter = (phase(2) — phase_middle)/2+phase_middle;
  %check the lower half—point
  mag_at_first_quarter = magnitudeatphase(sig4, agesa, ...
  phase_first_quarter );
```

```
25    % get a new reading
26    %check the upper half-point
27    mag_at_third_quarter = magnitudeatphase(sig4, agesa, ...
28    phase_third_quarter );
29
30  phase(3) = phase_first_quarter;
31  phase(4) = phase_third_quarter;
32  phase(5) = phase_middle;
33
34  if ( phase(2) - phase(1) ≤ dTolerance )    %should we keep searching?
35     [minimum, A] = min([mag_at_phase1 mag_at_phase2 ...
36     mag_at_first_quarter mag_at_third_quarter mag_at_phase_middle]);
37     % break out of the recursion
38     minphase = phase(A);
39  elseif (mag_at_first_quarter≤mag_at_third_quarter)
40      minphase = phase_first_quarter;
41      minimum = magnitudeatphase(sig4, agesa, phase_first_quarter);
42  %recursively call this function for lower half
43  [minimum, minphase] = binaryphaseadjust(sig4, agesa, phase(1), ...
44  phase_middle, tolerance);
45  else
46  %recursively call this function for upper half
47      minphase = phase_third_quarter;
48      minimum = magnitudeatphase(sig4, agesa, phase_third_quarter);
49  [minimum, minphase] = binaryphaseadjust(sig4, agesa, phase_middle, ...
50  phase(2),tolerance );
51  end
52
53  %(c) Pavlo Fedorenko and Dan Savio 2005
```

APPENDIX B

SETUP FOR MEASURING PHASE DISTORTION IN EER RF POWER AMPLIFIERS

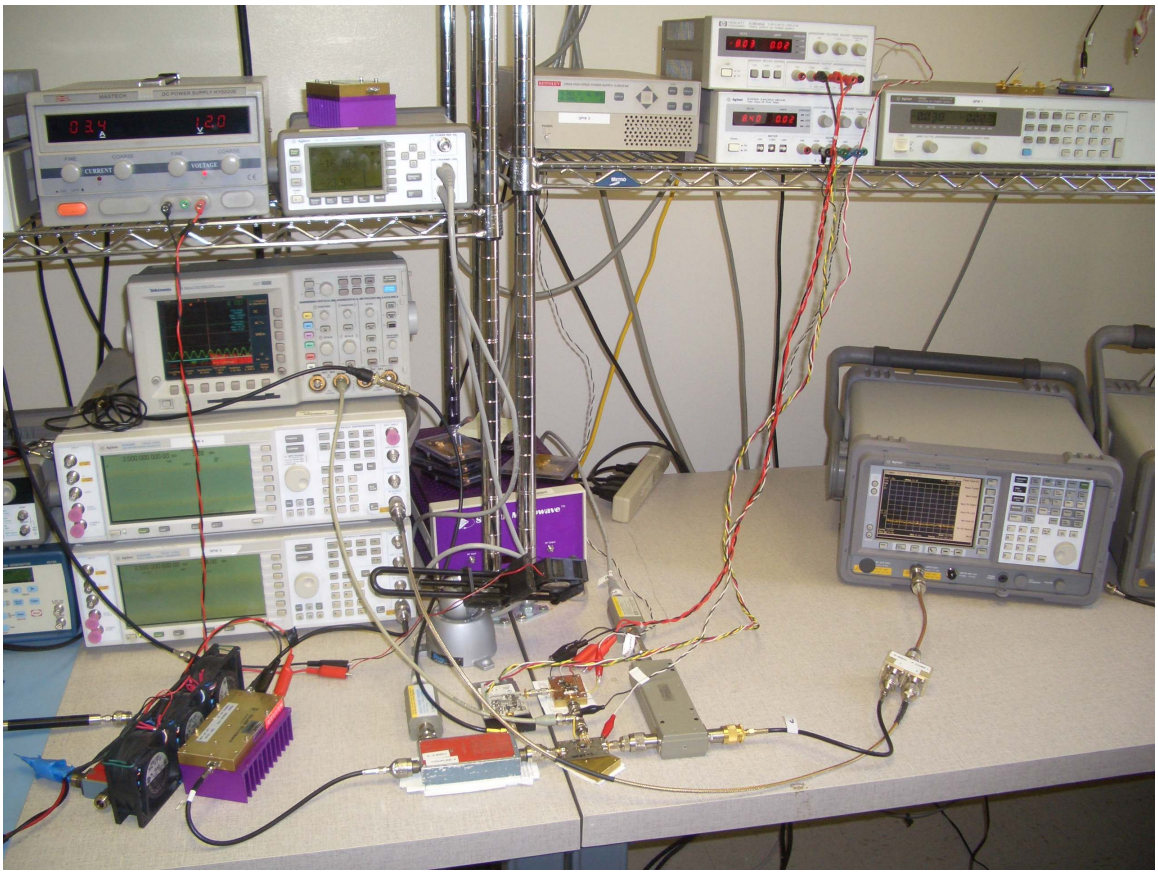

Figure 56: Measurement setup used to characterize the modulation transfer characteristic of an EER PA.

Bibliography

[1] Aikio, J. and Rahkonen, T., "Detailed analysis of IMD in an LDMOS RF power amplifier," in *Microwave Symposium Digest, 2005 IEEE MTT-S International*, p. 4 pp., 2005.

[2] Aikio, J. and Rahkonen, T., "Detailed distortion analysis technique based on simulated large-signal voltage and current spectra," *Microwave Theory and Techniques, IEEE Transactions on*, vol. 53, no. 10, pp. 3057–3066, 2005.

[3] Anadigics, "AWM6431 WiMAX 802.16 power amplifier," 2006. Datasheet.

[4] Anadigics, "AWM6423 WiMAX 802.16 power amplifier," 2008. Datasheet.

[5] Anakabe, A., Collantes, J. M., Portilla, J., Jugo, J., Mons, S., Mallet, A., and Lapierre, L., "Analysis of odd-mode parametric oscillations in HBT multi-stage power amplifiers," in *Gallium Arsenide Applications Symposium*, (Munich, Germany), Oct. 2003.

[6] Analog Devices, "AD8397 Rail-to-Rail, high output current amplifier," 2005. Datasheet.

[7] Axelsson, H., Bjrkn, P., de Bruin, P., Eriksson, S., and Persson, H., "GSM/EDGE continued evolution," *Ericsson Review*, vol. 1, 2006.

[8] Black, H. S., "Wave translation system," Dec. 1937. U.S. Patent 2102671.

[9] Black, H. S., "Translating system," Oct. 1928. U.S. Patent 1686792.

[10] Black, H. S., "Wave translation system," July 1935. U.S. Patent 2007172.

[11] Carvalho, N. D. and Pedro, J., "Large- and small-signal IMD behavior of microwave power amplifiers," *Microwave Theory and Techniques, IEEE Transactions on*, vol. 47, no. 12, pp. 2364–2374, 1999.

[12] Chen, J. H., *Wideband Dynamic Biasing of Power Amplifiers for Wireless Handheld Applications*. PhD, Georgia Institute of Technology, Aug. 2006.

[13] Chen, J. H. and Staudinger, J., "DCDC converter for power level tracking power amplifiers," Mar. 2007. U.S. Patent 7190150.

[14] Chen, J., Fedorenko, P., and Kenney, J., "A low voltage W-CDMA polar transmitter with digital envelope path gain compensation," *Microwave and Wireless Components Letters, IEEE*, vol. 16, no. 7, pp. 428–430, 2006.

[15] Chen, N. and Zhou, G., "Peak-to-average power ratio reduction in OFDM with blind selected pilot tone modulation," *Wireless Communications, IEEE Transactions on*, vol. 5, no. 8, pp. 2210–2216, 2006.

[16] Chen, P., Hsin, Y., and Asbeck, P., "Saturation charge storage measurements in GaInP/GaAs/GaAs and GaInP/GaAs/GaInP HBTs," in *Compound Semiconductors, 1997 IEEE International Symposium on*, pp. 443–446, 1998.

[17] Chireix, H., "High power outphasing modulation," *Proceedings of the IRE*, vol. 23, no. 11, pp. 1370–1392, 1935.

[18] Cripps, S. C., *RF Power Amplifiers for Wireless Communications, Second Edition*, pp. 285–334. Artech House Publishers, 2 ed., May 2006.

[19] Cripps, S. C., "Personal communication," 2008.

[20] Curtice, W., Pla, J., Bridges, D., Liang, T., and Shumate, E., "A new dynamic electro-thermal nonlinear model for silicon RF LDMOS FETs," in *Microwave Symposium Digest, 1999 IEEE MTT-S International*, vol. 2, pp. 419–422 vol.2, 1999.

[21] de Carvalho, N. B. and Pedro, J., "A comprehensive explanation of distortion sideband asymmetries," *Microwave Theory and Techniques, IEEE Transactions on*, vol. 50, no. 9, pp. 2090–2101, 2002.

[22] Doherty, W., "A new high efficiency power amplifier for modulated waves," *Proceedings of the IRE*, vol. 24, no. 9, pp. 1163–1182, 1936.

[23] Fager, C., Pedro, J., de Carvalho, N., Zirath, H., Fortes, F., and Rosario, M., "A comprehensive analysis of IMD behavior in RF CMOS power amplifiers," *Solid-State Circuits, IEEE Journal of*, vol. 39, no. 1, pp. 24–34, 2004.

[24] Faulkner, M. and Johansson, M., "Adaptive linearization using predistortion-experimental results," *Vehicular Technology, IEEE Transactions on*, vol. 43, no. 2, pp. 323–332, 1994.

[25] Fedorenko, P., Chen, J. H., and Kenney, J. S., "Bandwidth-specific memory ratio as a predictor of RF power amplifier predistortability," in *IEEE Topical Workshop on Power Amplifiers*, (Long Beach, CA), 2007.

[26] Fedorenko, P. and Kenney, J. S., "Measurement of relative phase and magnitude of third order IMD components for identification and characterization of RF power amplifier memory effects," in *IEEE Topical Workshop on Power Amplifiers*, (San Diego, CA), 2006.

[27] Fedorenko, P. and Kenney, J., "Analysis and suppression of memory effects in envelope elimination and restoration (EER) power amplifiers," in *Microwave Symposium, 2007. IEEE/MTT-S International*, pp. 1453–1456, 2007.

[28] Fedorenko, P., Savio, D., and Kenney, J. S., "Phase distortion mechanisms in polar modulators," in *Power Amplifier Symposium*, (Orlando, FL), 2008.

[29] Fedorenko, P., Paulsen, B., and Kenney, J. S., "Origins of phase distortion in GaAs HBT envelope elimination and restoration RF power ampliers," *To be submitted to Microwave Theory and Techniques, IEEE Transactions on*, 2009.

[30] Gray, P. R., Hurst, P. J., Lewis, S. H., and Meyer, R. G., *Analysis and Design of Analog Integrated Circuits*. Wiley, 4 ed., Feb. 2001.

[31] Grundlingh, J., Parker, K., and Rabjohn, G., "A high efficiency chireix out-phasing power amplifier for 5GHz WLAN applications," in *Microwave Symposium Digest, 2004 IEEE MTT-S International*, vol. 3, pp. 1535–1538 Vol.3, 2004.

[32] Hammi, O., Carichner, S., Vassilakis, B., and Ghannouchi, F., "Power amplifiers' model assessment and memory effects intensity quantification using memoryless Post-Compensation technique," *Microwave Theory and Techniques, IEEE Transactions on*, vol. 56, no. 12, pp. 3170–3179, 2008.

[33] Hietala, A. W., "Direct digital polar modulator," Dec. 2004. U.S. Patent 6834084.

[34] Hietala, A., "A quad-band 8PSK/GMSK polar transceiver," *Solid-State Circuits, IEEE Journal of*, vol. 41, no. 5, pp. 1133–1141, 2006.

[35] Jeon, Y., Kim, H., Kim, H., Ryu, G., Choi, J., Kim, K., Sung, S., and Oh, B., "A highly efficient CDMA power amplifier based on parallel amplification architecture," *Microwave and Wireless Components Letters, IEEE*, vol. 14, no. 9, pp. 401–403, 2004.

[36] Kahn, L., "Single-Sideband transmission by envelope elimination and restoration," *Proceedings of the IRE*, vol. 40, no. 7, pp. 803–806, 1952.

[37] Kenney, J. and Fedorenko, P., "Identification of RF power amplifier memory effect origins using Third-Order intermodulation distortion amplitude and phase asymmetry," in *Microwave Symposium Digest, 2006. IEEE MTT-S International*, pp. 1121–1124, 2006.

[38] Kimball, D., Jeong, J., Hsia, C., Draxler, P., Lanfranco, S., Nagy, W., Linthicum, K., Larson, L., and Asbeck, P., "High-Efficiency Envelope-Tracking W-CDMA Base-Station amplifier using GaN HFETs," *Microwave Theory and Techniques, IEEE Transactions on*, vol. 54, no. 11, pp. 3848–3856, 2006.

[39] Ku, H., McKinley, M., and Kenney, J., "Quantifying memory effects in RF power amplifiers," *Microwave Theory and Techniques, IEEE Transactions on*, vol. 50, no. 12, pp. 2843–2849, 2002.

[40] Ku, H. and Kenney, J., "Behavioral modeling of nonlinear RF power amplifiers considering memory effects," *Microwave Theory and Techniques, IEEE Transactions on*, vol. 51, no. 12, pp. 2495–2504, 2003.

[41] Lee, J., Kim, W., Kim, Y., Rho, T., and Kim, B., "Intermodulation mechanism and linearization of AlGaAs/GaAs HBTs," *Microwave Theory and Techniques, IEEE Transactions on*, vol. 45, no. 12, pp. 2065–2072, 1997.

[42] Liou, J., Lindholm, F., and Park, J., "Forward-voltage capacitance and thickness of p-n junction space-charge regions," *Electron Devices, IEEE Transactions on*, vol. 34, no. 7, pp. 1571–1579, 1987.

[43] Maas, S., Nelson, B., and Tait, D., "Intermodulation in heterojunction bipolar transistors," *Microwave Theory and Techniques, IEEE Transactions on*, vol. 40, no. 3, pp. 442–448, 1992.

[44] Martins, J., Cabral, P., Carvalho, N., and Pedro, J., "A metric for the quantification of memory effects in power amplifiers," *Microwave Theory and Techniques, IEEE Transactions on*, vol. 54, no. 12, pp. 4432–4439, 2006.

[45] McCune, E., "High-efficiency, multi-mode, multi-band terminal power amplifiers," *Microwave Magazine, IEEE*, vol. 6, no. 1, pp. 44–55, 2005.

[46] McCune, E., "Polar modulation and bipolar RF power devices," in *Bipolar/BiCMOS Circuits and Technology Meeting, 2005. Proceedings of the*, pp. 1–5, 2005.

[47] McCune, E., "Personal communication," 2007.

[48] McMacken, J., Nedeljkovic, S., Gering, J., and Halchin, D., "HBT modeling," *Microwave Magazine, IEEE*, vol. 9, no. 2, pp. 48–71, 2008.

[49] Moore, G., "Cramming more components onto integrated circuits," *Electronics Magazine*, vol. 38, pp. 114–117, Apr. 1965.

[50] Nam, J. and Kim, B., "The doherty power amplifier with On-Chip dynamic bias control circuit for handset application," *Microwave Theory and Techniques, IEEE Transactions on*, vol. 55, no. 4, pp. 633–642, 2007.

[51] Narendra, K., Anand, L., Sangaran, P., Anbalagan, S., and Boeck, G., "Impedance adjustment for constant efficiency power amplifier applying stage bypass method," in *Electronics, Circuits and Systems, 2007. ICECS 2007. 14th IEEE International Conference on*, pp. 266–269, 2007.

[52] Nielsen, T., Nedeljkovic, S., and Halchin, D., "Large-signal hybrid compact/behavioral HBT model for IIIV technology power amplifiers," in *Microwave Symposium Digest, 2008 IEEE MTT-S International*, pp. 483–486, 2008.

[53] Parker, A. and Rathmell, J., "Broad-band characterization of FET self-heating," *Microwave Theory and Techniques, IEEE Transactions on*, vol. 53, no. 7, pp. 2424–2429, 2005.

[54] Pedro, J., Garcia, J., and Cabral, P., "Nonlinear distortion analysis of polar transmitters," *Microwave Theory and Techniques, IEEE Transactions on*, vol. 55, no. 12, pp. 2757–2765, 2007.

[55] Raab, F., "Intermodulation distortion in kahn-technique transmitters," *Microwave Theory and Techniques, IEEE Transactions on*, vol. 44, no. 12, pp. 2273–2278, 1996.

[56] Raab, F., Asbeck, P., Cripps, S., Kenington, P., Popovic, Z., Pothecary, N., Sevic, J., and Sokal, N., "Power amplifiers and transmitters for RF and microwave," *Microwave Theory and Techniques, IEEE Transactions on*, vol. 50, no. 3, pp. 814–826, 2002.

[57] Reynaert, P. and Steyaert, M., "A 1.75-GHz polar modulated CMOS RF power amplifier for GSM-EDGE," *Solid-State Circuits, IEEE Journal of*, vol. 40, no. 12, pp. 2598–2608, 2005.

[58] RF Micro Devices, "RF3198 dual-band GSM900/DCS power amp module," 2006. Datasheet.

[59] RF Micro Devices, "RF3266 3V W-CDMA linear PA module," 2006. Datasheet.

[60] RF Micro Devices, "RF5198 3V W-CDMA linear power amplifier module," 2006. Datasheet.

[61] Sahu, B. and Rincon-Mora, G., "A high-efficiency linear RF power amplifier with a power-tracking dynamically adaptive buck-boost supply," *Microwave Theory and Techniques, IEEE Transactions on*, vol. 52, no. 1, pp. 112–120, 2004.

[62] Seidel, H., "Feed-forward amplifier," Oct. 1969. U.S. Patent 3471798.

[63] Seidel, H., "A feedforward experiment applied to an l-4 carrier system amplifier," *Communication Technology, IEEE Transactions on*, vol. 19, no. 3, pp. 320–325, 1971.

[64] Sevic, J., "Statistical characterization of RF power amplifier efficiency for CDMA wireless communication systems," in *Wireless Communications Conference, 1997., Proceedings*, pp. 110–113, 1997.

[65] Sevic, J., Burger, K., and Steer, M., "A novel envelope-termination load-pull method for ACPR optimization of RF/microwave power amplifiers," in *Microwave Symposium Digest, 1998 IEEE MTT-S International*, vol. 2, pp. 723–726 vol.2, 1998.

[66] Shirvani, A., Su, D., and Wooley, B., "A CMOS RF power amplifier with parallel amplification for efficient power control," *Solid-State Circuits, IEEE Journal of*, vol. 37, no. 6, pp. 684–693, 2002.

[67] Sowlati, T., Rozenblit, D., Pullela, R., Damgaard, M., McCarthy, E., Koh, D., Ripley, D., Balteanu, F., and Gheorghe, I., "Quad-band GSM/GPRS/EDGE polar loop transmitter," *Solid-State Circuits, IEEE Journal of*, vol. 39, no. 12, pp. 2179–2189, 2004.

[68] Staudinger, J., Gilsdorf, B., Newman, D., Norris, G., Sadowniczak, G., Sherman, R., and Quach, T., "High efficiency CDMA RF power amplifier using dynamic envelope tracking technique," in *Microwave Symposium Digest., 2000 IEEE MTT-S International*, vol. 2, pp. 873–876 vol.2, 2000.

[69] Suarez, A. and Quere, R., *Stability Analysis of Nonlinear Microwave Circuits*. Artech House Publishers, 2003.

[70] Suematsu, N., Iyama, Y., and Ishida, O., "Transfer characteristic of IM3 relative phase for a GaAs FET amplifier," *Microwave Theory and Techniques, IEEE Transactions on*, vol. 45, no. 12, pp. 2509–2514, 1997.

[71] Teeter, D., Spears, E., Bui, H., Jiang, H., and Widay, D., "Average current reduction in (W)CDMA power amplifiers," in *Radio Frequency Integrated Circuits (RFIC) Symposium, 2006 IEEE*, p. 4 pp., 2006.

[72] Triquint Semiconductor, "TQM 7M5004 GSM/EDGE multi-mode power amplifier module.," 2006. Datasheet.

[73] Vuolevi, J., Rahkonen, T., and Manninen, J., "Measurement technique for characterizing memory effects in RF power amplifiers," *Microwave Theory and Techniques, IEEE Transactions on*, vol. 49, no. 8, pp. 1383–1389, 2001.

[74] Vuolevi, J. and Rahkonen, T., *Distortion in RF Power Amplifiers*. Artech House Publishers, Feb. 2003.

[75] Wang, F., Ojo, A., Kimball, D., Asbeck, P., and Larson, L., "Envelope tracking power amplifier with pre-distortion linearization for WLAN 802.11g," in *Microwave Symposium Digest, 2004 IEEE MTT-S International*, vol. 3, pp. 1543–1546 Vol.3, 2004.

[76] Wang, F., Yang, A., Kimball, D., Larson, L., and Asbeck, P., "Design of wide-bandwidth envelope-tracking power amplifiers for OFDM applications," *Microwave Theory and Techniques, IEEE Transactions on*, vol. 53, no. 4, pp. 1244–1255, 2005.

[77] Williams, D., Leckey, J., and Tasker, P., "A study of the effect of envelope impedance on intermodulation asymmetry using a two-tone time domain measurement system," in *Microwave Symposium Digest, 2002 IEEE MTT-S International*, vol. 3, pp. 1841–1844, 2002.

[78] Woo, W. and Kenney, J., "A new envelope predistortion linearization architecture for handset power amplifiers," in *Radio and Wireless Conference, 2004 IEEE*, pp. 175–178, 2004.

[79] Zetex, "ZXM61N02F 20-V N-Channel enhancement mode MOSFET," 2004. Datasheet.

VITA

Pavlo Fedorenko was born in Zaporizhzhya, Ukraine in 1983. He received his BSEE degree with High Honors from Worcester Polytechnic Institute, Worcester, MA, in 2004. He also received MS in electrical and computer engineering and an MBA from Georgia Institute of Technology in 2006 and 2008 respectively. Throughout his studies Pavlo held a number of internships at RFMD and Analog Devices.

His research interests include design and analysis of RF, analog and mixed-signal circuits and systems, as well as broader technology commercialization and economic development.